Aalto University
School of Science

Erno Kemppainen

Coupled optical and electrical modeling of dye solar cells

Master's thesis submitted in partial fulfilment of the requirements for the degree of Master of Science in Technology in the Degree Programme in Engineering Physics and Mathematics.

Espoo, 12.3.2012

Supervisor: Professor Peter Lund
Instructor: D.Sc. (Tech.) Janne Halme

Aalto University School of Science	ABSTRACT OF THE MASTER'S THESIS
Author: Erno Kemppainen	
Title: Coupled optical and electrical modeling of dye solar cells	
Title in Finnish: Väriaineaurinkokennojen yhdistetty optinen ja sähköinen mallinnus	
Degree Programme: Degree Programme in Engineering Physics and Mathematics	
Major subject: Advanced energy systems	Minor subject: Engineering physics
Chair (code):Tfy-56	
Supervisor: Prof. Peter Lund	Instructor: D.Sc. (Tech.) Janne Halme

In the case of building-integrated photovoltaics (BIPVs) the appearance of the solar cells is a more significant concern than in most other solar cell applications. The appearance aspect includes the transparency of the cells. Dye solar cells (DSCs) have the advantage that their color can be tuned by the choice of dye and its amount, which also allows different levels of transparency. Lately one-dimensional photonic crystals (1DPCs) have been used in DSCs to enhance their light absorption. In addition to this they also affect the appearance of the DSC in question, by reflecting a selected range of wavelengths and allowing the rest of the incident light to be transmitted.

A simple optical model was used to simulate the effects of 1DPCs and the amount of dye in the photoelectrode (PE) of a DSC on the optical properties and appearance of DSCs. Additionally, the effects of different dyes were tested in the simulations. Estimates for the short-circuit current and efficiency in AM1.5G conditions were calculated.

In addition to performance, the color of the DSCs was also calculated. The calculation method was verified with photos of 1DPCs coupled with a PE and assembled DSCs. The employed calculation method for the color proved to be accurate enough. Most of the errors in results appear to be related to problems with homogeneity of the light used to illuminate the samples and the camera settings causing problems with over- and underexposure, so improving only computational accuracy would not essentially improve the accuracy of the results.

The particle and pore size in TiO_2 layers of 1DPC is significantly smaller than in the PE of the DSCs, which may reduce the efficiency of the DSCs by impeding the ion transport -based charge transfer in the electrolyte. The diffusion of the redox couple in the electrolyte was modeled to find a limiting value, where the diffusion would cause problems for the cell efficiency. The effect of the charge carrier concentrations at counter electrode (CE) on the IV curve was added to the electrical model of the PE to improve the accuracy of the efficiency estimates. Surprisingly, it turned out that voltage losses at CE would not have a significant effect on the efficiency of the DSCs, unless the 1DPC (or similar reflecting layer) would be relatively thick with very small pores. The lack of any effect on efficiency seems counter-intuitive, and would have to be verified with experiments and/or more detailed models that would also take into account the effects of the accumulation of positive charge carriers and the depletion of the negative ones in the PE due to slow diffusion through the 1DPC. Otherwise the estimates for cases with larger pore size appear realistic and could be relatively accurate estimates of the efficiency of the DSC configurations in question.

Date: 12.3.2012	Language: English	Number of pages: 7+83

Keywords: solar cell, color, RGB, photonic crystal, scattering layer, diffusion, limiting current density, overpotential

Aalto-yliopisto Perustieteiden korkeakoulu	DIPLOMITYÖN TIIVISTELMÄ
Tekijä: Erno Kemppainen	
Työn nimi: Väriaineurinkokennojen yhdistetty optinen ja sähköinen mallinnus	
Title in English: Coupled optical and electrical modeling of dye solar cells	
Tutkinto-ohjelma: Teknillisen fysiikan ja matematiikan tutkinto-ohjelma	
Pääaine: Energiatieteet	Sivuaine: Teknillinen fysiikka
Opetusyksikön (ent. professuuri) koodi: Tfy-56	
Työn valvoja: Prof. Peter Lund	Työn ohjaaja(t): TkT Janne Halme

Rakennuksiin integroitujen aurinkokennojen (building-integrated photovoltaics, BIPV) tapauksessa kennojen ulkonäkö on tärkeämpi tekijä kuin monien muiden aurinkokennosovelluksien tapauksessa. Myös aurinkokennojen läpinäkyvyys sisältyy huomioitaviin seikkoihin. Väriaineaurinkokennojen (dye solar cells, DSCs) etuna on, että niiden väriä ja läpinäkyvyyttä voidaan muuttaa väriainetta ja sen määrää vaihtamalla. Viime aikoina väriainekennoissa on käytetty yksiulotteisia fotonikiteitä tehostamaan valon keräystä. Niiden vaikutus valon keräykseen ja myös kennon ulkonäköön perustuu siihen, että fotonikiteet heijastavaat valoa kapealla aallonpituusalueella, kun muut aallonpitudet kulkevat fotonikiteen läpi heijastumatta.

Fotonikiteiden ja väriaineen määrän vaikutusta väriainekennojen optisille ominaisuuksille ja ulkonäölle simuloitiin yksinkertaisella optisella mallilla. Myös eri väriaineiden vaikutus laskettiin. Optisten ominaisuuksien perusteella laskettiin arviot kennojen oikosulkuvirrasta ja hyötysuhteesta AM1.5G-olosuhteissa.

Sähköisen suorituskyvyn lisäksi laskettiin myös kennojen väri. Näiden laskujen tuloksia verrattiin todellisten fotonikiteiden ja aurinkokennojen väriin tunnetuissa valaistusoloissa otetuissa valokuvissa. Käytetty laskentamentelmä osoittautui riittävän tarkaksi. Suurin osa havaituista virheistä oli todennäköisimmin seurausta valaistuksen epähomogeenisuudesta ja kameran asetusten tuottamasta yli- tai alivalottuneisuudesta kuvissa, joten vain laskentatarkkuuden parantaminen ei oleellisesti parantaisi tarkkuutta.

Fotonikiteiden TiO_2-kerrosten hiukkasten ja huokosten koko on huomattavasti pienempi kuin valoelektrodissa, mikä saattaa heikentää kennojen hyötysuhdetta hidastamalla varauksenkuljettajien diffuusiota fotonikiteen läpi. Diffusiota elektrolyytissä simuloitiin, jotta voitaisiin arvioida tämän ilmiön vaikutusta vastaelektrodin ylipotentiaalille ja sitä kautta kennon IV-käyrälle. Tulosten perusteella vaikuttaa yllättäen siltä, että heikentynyt diffuusio ei heikentäisi kennojen hyötysuhdetta vastaelektrodin jännitehäviöiden kautta lähes ollenkaan, ellei fotonikide (tai vastaava heijastava kerros) ole todella paksu ja sen huokoskoko erittäin pieni. Vaikutuksen pienuus on varsin epäintuitiivinen tulos, joten olisi syytä suorittaa tarkempia simulaatioita, joissa otetaan huomioon positiivisten varauksekuljettajien kerääntyminen ja negatiivisten vähentyminen elektrolyytissa valoelektrodin huokosissa hidastuneen diffuusion takia. Muuten tulokset vähiten diffuusiota rajoittavien kalvojen osalta vaikuttavat realistisilta arvioilta kyseisten väriainekennojen hyötysuhteesta.

Päivämäärä: 12.3.2012	Kieli: englanti	Sivumäärä: 7+83

Avainsanat: aurinkokenno, väri, RGB, fotonikide, sirottava kerros, diffuusio, rajavirrantiheys, ylipotentiaali

Acknowledgement

This work was carried at the New Energy Technologies group, Department of Applied Physics at the Aalto University School of Science. The work was done as a part of the Nordic-DSC –project, funded by Nordic Innovation Centre (NICe). The photonic crystal samples necessary for experiments were from other collaborators of this project, namely NLab Solar and Multifunctional Optical Materials Group of Institute of Materials Science of Seville (Instituto de Ciencia de Materiales de Sevilla, ICMS).

I wish to express my gratitude to both my supervisor professor Peter Lund and instructor D.Sc. (Tech.) Janne Halme for the opportunity of doing this work. This thesis has been a challenging, interesting and educational project. The help and feedback I have received have improved this thesis in many ways. I thank MSc Imran Asghar for his assistance in the photography of the samples. I also thank MSc Francisco Enrique Gálvez from ICMS for his help in developing the simulation code needed for calculations about charge carrier diffusion in the electrolyte.

Espoo, 12.3.2012

Erno Kemppainen

Contents

Abbreviations and symbols

These are lists of recurring abbreviations and symbols in this thesis. Abbreviations and symbols used only in one section of the text are not included here, but their meaning is explained, where they appear in the text.

Abbreviations

1DPC	one-dimensional photonic crystal
3MPN	3-methoxypropionitrile
AM	air mass
BAPV	building-applied photovoltaics
BIPV	building-integrated photovoltaics
CE	counter electrode
CIE	The International Commission on Illumination (Commission internationale de l'éclairage)
COL	(electron) collection
CT	charge transfer
D	dye, diffusion
DSC	dye solar cell
DSSC	dye-sensitized solar cell
El	electrolyte
FTO	fluorine doped tin oxide
HOMO	highest occupied molecular orbital
ITO	indium doped tin oxide
INJ	(electron) injection
IPCE	incident-photon-to-collected-electron efficiency
LH	light harvesting
LUMO	lowest unoccupied molecular orbital
OC	open circuit
PC	photonic crystal
PD	photodiode
PE	photoelectrode
PV	photovoltaics
REC	recombination
redox	reduction-oxidization
REG	(dye) regeneration
RGB	red, green, blue
SC	short circuit
SL	scattering layer
TCO	transparent conductive oxide

Symbols

C	concentration
d	thickness
D	diffusion coefficient
e^-	electron
g	spatial electron generation profile
$h\nu$	photon
i	current density
$I(\lambda)$	spectral irradiance
I^-	iodide ion
I_3^-	tri-iodide ion
L	electron diffusion length
M	mol/dm^3
n	electron concentration
p	optical mean path length
P	power density
q_e	elementary charge
R	reflectance, resistance
S	sensitizer
S^*	excited sensitizer
S^+	oxidized sensitizer
t	time
T	transmittance
V	voltage
α	light absorption coefficient
β	recombination reaction order, symmetry factor of CE redox reaction
ϵ	porosity of PE/1DPC/SL
ϵ_D	molar light absorption coefficient of dye
γ	constrictivity of PE/1DPC/SL
ϕ	photon flux
η	efficiency
λ	wavelength of light
τ	time constant (of a reaction)
τ^2	tortuosity of PE/1DPC/SL

1 Introduction

The global energy consumption has steadily increased and the typical scenarios predict its growth to continue, just the rate of growth varies from one scenario to another [1]. The peaking and especially the following decline of oil production are a widely known global concern for energy production, especially for transportation: In 2009 oil production supplied 32.8% of world total primary energy supply (and 41.3% of the total final consumption) [1]. However, only 5.1% of the electricity was produced with oil, whereas transports are responsible for 61.7% of the oil consumption and 93.5% of the energy demand of transports was supplied with oil products [1].

Another, probably not so widely recognised concern is the production rate of coal: At the end of 2000 it was estimated that the known coal reserves would last for 227 years at the production rate of the time [2]. Five years later the estimate had decreased to about 155 years and in 2011 the U.S. Energy Information Administration (EIA) estimated the known reserves to be enough for about 126 years [2, 3]. Chinese coal production and consumption are both about half of the global total amount [1]. The estimates of the Chinese reserves were 116, 52 and 41 years, correspondingly [2, 3]. It is important to notice that in general the cumulative production over this time period is small compared to the reductions in reserves, so the reserves must have been overestimated to begin with [4]. For the sake of comparison, the estimates of the global oil and gas reserves have been steady at 40 and 60 years from 2000 to 2005 [2]. Overall, it seems that the quality of the current data of coal reserves is poor, and coal production peak and the irreversible decline may occur sooner than previously thought [2, 4]. Considering that about 27% of the world primary energy supply and about 41% of the electricity were produced with coal or peat in 2009, an unexpected decline in the amount of the available coal could have serious effects on the energy prices and production [1].

It is obvious that there is a growing need for new methods in energy production, as the conventional easy fossil fuels will eventually run out, and their production rate will decrease relatively soon. The solar irradiation received on earth is many times larger than the current rate of energy consumption [5]. This abundance combined with the sustainability and environmental friendliness of photovoltaic (PV) technology makes the solar cells an excellent candidate for large scale energy production. Solar cells require some raw materials, and actually deplete mineral ores more than for example fossil fuels, but generally have a smaller impact on environment than more conventional technologies [6].

1.1 Building-Integrated Photovoltaics

Compared to many other energy sources, PVs have the advantage of being able to produce electricity near the point of use. This means significantly reduced power transfer and distribution costs and losses [7]. The idea behind building-integrated photovoltaics (BIPVs) and building-applied photovoltaics (BAPVs) is using this possibility and utilizing buildings as platforms for solar cells [7]. The difference between BIPVs and BAPVs is that the BAPVs are designed according to the pre-existing structure of the building, whereas the structure

of the building is designed with an eye to the BIPVs. A typical example of BAPVs are the solar panel racks mounted on the roof of a building, whereas BIPVs could act as the protecting roof material and cover larger fraction of the available area for the benefit of power generation and architectural aspects. Additional benefits of both BAPVs and BIPVs include the lack of a need for additional acquisitions, fencing, road building and major support structures for the PV modules that centralized PV plants would require [7]. The building already provides these with little or no additional cost. Additionally BIPVs can also protect the building from the weather and replace other conventional materials. Rigid PV devices can be used in most façade applications and may actually be a better option than their flexible counterparts, especially when the panels are intended to act as a protecting coating for the building. On the other hand, flexible solar cells enable architectural possibilities that would be impossible to realize with rigid PV modules.

Figure 1: The Co-operative Insurance (CIS) tower in Manchester, England (left), the roof of the Vatican Paolo VI audience hall (center), the winner of the 2008 European solar prize and the Matterhorn glacier paradise restaurant & shop (right), the winner of 2010 European solar prize [8, 9, 10, 11].

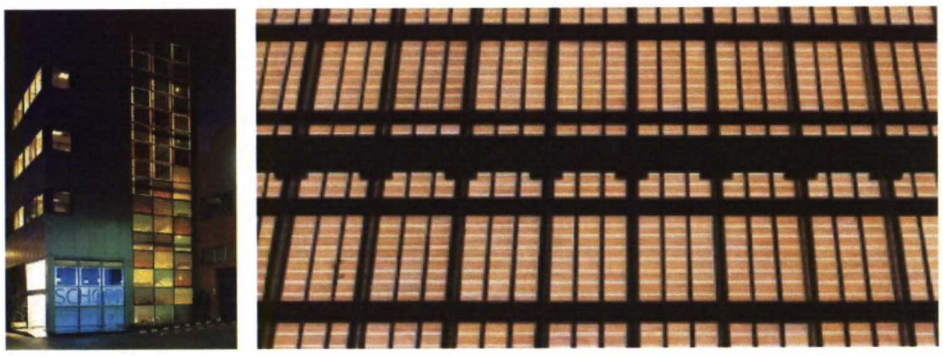

Figure 2: The façade of the headquarters of Schott Iberica in Barcelona (left) and a caption of the windows of the CSIRO (The Commonwealth Scientific and Industrial Research Organisation) Energy Centre in Newcastle, New South Wales, Australia [9]. Note that the bottom of the façade of the Schott Iberica headquarters consists of coloured glass and the top half is made of PV modules.

The whole PV market is at the moment dominated by crystalline silicon (Si) that covers almost 90% of the market [9, 12]. Thin-film Si technologies cover about half of the remaining fraction so that technologies not based on Si had a market share of about 5% in 2008 [12]. Considering this, it is not surprising that a large fraction of the BAPV and BIPV installations are Si-based and therefore their color is mostly either blue or black, such as the examples in figure 1: In the case of CIS tower and Paolo VI audience hall the solar panels have been added, when the building has been renovated, and only in the case of the restaurant in Matterhorn the panels have been originally designed as a part of the building. Different thin-film technologies offer the additional possibility of using other colors than black or blue, as illustrated in figure 2: The top of the façade of Schott Iberica consists of amorphous silicon (a-Si) solar cells and the windows of the CSIRO energy centre are made of dye solar cells (DSCs) [9].

In some BIPV applications the transparency of the solar panels may be an important criterion. There are three categories of semi-transparent PV devices: matrix, process-induced and intrinsic semi-transparency. Matrix semi-transparency refers to solar panels that have an alternating structure of opaque solar cells and transparent gaps.Process-induced semi-transparency is achieved by removing parts of the semiconductor substrate by laser cutting. This creates void portions that allow light to pass through. The third category, intrinsic semi-transparency is based on the properties of the materials of the solar cell itself: They enable making solar cells so thin that some portion of light is transmitted through them.The advantage of the last category, compared to the former two, is that it does not require any additional processes after the solar cell has been manufactured. [9, 13]

There are several factors that can affect the final decision about the type of PV modules used in buildings. Naturally the modules must produce electricity at some power, or there is no real gain compared to for example coloured glass or other façade materials that are almost certainly cheaper than solar cells. It seems likely that in many cases the architects would like to choose the color of the solar cells to fit the design of the building and surroundings, not vice versa, so different thin-film technologies appear a likely candidate to take over a large fraction of the BIPV/BAPV market. The color and appearance of the solar panels are a combination of the reflected and transmitted light that an observer sees. Therefore it is possible that the appearance of a solar panel viewed from the inside of the building is completely different compared to the view from the outside. During daytime the reflected or transmitted sunlight is most likely the factor that determines most of the appearance of the solar panels. After sunset the reflected and transmitted light from e.g. street lights and lights inside the building play a more significant role in the appearance of the solar cells.

In addition to affecting the appearance of the solar cells, the reflected and especially transmitted light affect the energy balance of the building: High transmittance of e.g. windows and skylights allows large amounts of energy to be transmitted and heat the air inside the building, and also reduces the amount of electrical power that can be generated with the PV modules [14, 15, 16]. In hot climates this is means high cooling loads and low power from the solar cells. Correspondingly, reducing the transmittance decreases the cooling load, but increases the lighting electricity consumption [14, 15, 16]. This is com-

pensated by the increased electrical power of the solar cells, and especially with proper lighting control it may be possible to actually reduce the total consumption of electricity by replacing the glass in windows etc. by PV modules with suitably low transparency [14]. In addition to the appearance and energy balance the transmittance spectrum of the solar cells also affects the living and working comfort via the color of the transmitted light. It is not hard to imagine that only a wrong color of the window can make living and/or working less comfortable compared to a clear window. The optimal design parameters of the BIPVs depend on several other parameters, including the fraction of façade area covered by windows, the facing direction of the façade and naturally the local climate [14]. The performance of the cells is also affected by how urban or rural the surrounding area is [17]. Therefore detailed analysis of the building and its requirements is needed for good results.

1.2 Dye solar cells as BIPV technology

The latest version of DSCs was invented in 1991 by Michael Grätzel and Brian O'Regan[18]. This was the first DSC to produce enough power for practical applications, but not the first attempt to make a functional DSC [19]. The main advantages of DSCs include low energy and relatively low material purity requirements in manufacturing compared to conventional PV technologies. Additionally, DSCs can be manufactured on flexible substrates, which enables them to be used in applications, where rigid solar cells are at disadvantage or entirely unusable. This also makes it possible to manufacture DSCs with roll to roll methods. DSCs can be made on glass substrates, as most of the laboratory samples are made, so the potential for flexibility will not limit the applications of DSCs.

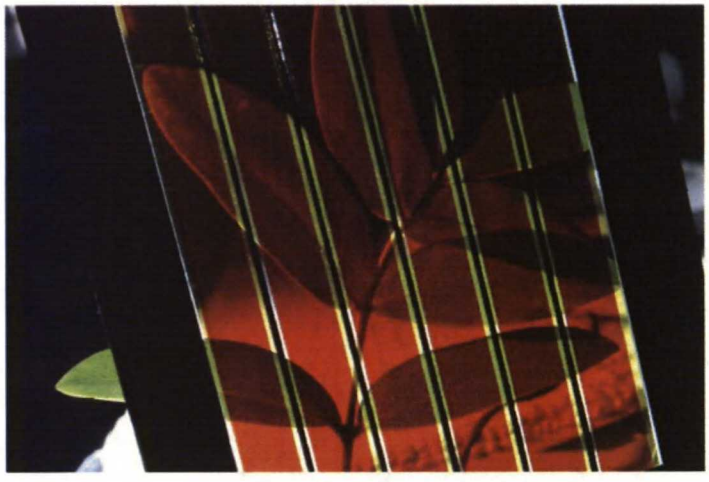

Figure 3: Illustration of the transparency of DSCs: The shapes and the lightness/darkness of colors is visible, but the color of the transmitted light is strongly affected by the color of the DSC. Photo from [20].

1.3 One-dimensional photonic crystal DSCs

Considering the design aspect of BIPVs and BAPVs, DSCs have the advantage of coming in several different colors, not just black and blue.This increases the design options, but there may be some trade-offs in the efficiency, because of the performance differences between the dyes that are needed for the different colors. Recently, the color palette of DSCs has gained a new degree of freedom from photonic crystals [21, 22, 23, 24]. The idea behind the use of photonic crystals is to reflect a selected wavelength range of light back to dyed TiO_2 film to enhance photocurrent, while the rest of the light is transmitted normally. Compared to light scattering layers, which is the conventional option for enhancing light absorption by back reflection of light, the total amount of reflected light is smaller, but the transparency is preserved. The photonic crystals are Bragg reflectors, whose high reflectance is based on constructive and destructive interference of light caused by their periodical structure [24, 25, 26]. The original idea in using them in DSCs was to enhance the photocurrent and thus the efficiency of the cell [21, 22, 23]. The problem with many of them was, that the photonic crystal encumbered the diffusion of charge carriers in electrolyte so much that the efficiency of the DSCs decreased even when the short circuit current clearly increased [22, 23]. This problem appears to have been solved by using one-dimensional photonic crystals (1DPCs, also known as distributed Bragg reflectors) [23, 25].

The main challenge with 1DPCs in DSCs is achieving high reflectance without impeding the diffusion through the stack too much. 1DPCs are based on combination of material layers of proper thicknesses and refractive indices. Increasing the thickness of the stack improves the reflectance, but also impedes the diffusion through it [26]. Increasing the porosity will improve the diffusion properties, but reduces the difference of the effective refractive indices in the stack, which changes the reflectance [24, 27, 28]. With too large porosities the refractive indices in the stack begin converging towards the refractive index of the medium inside the pores and the reflectance is reduced [28]. Compensating this by adding more layers to the stack would be counter-productive for diffusion. Fortunately the problem can be reduced by adding polyethylene glycol (PEG) to the nanoparticle solutions used to make the 1DPCs, which increases the porosity without reducing the reflectance too much [28].

1.4 Objectives

The optical properties of the DSCs affect the available architectural options (color etc.), energy balance of the buildings and the efficiency of the DSCs in ways that are sometimes indirect and complicated, so it is important to be able to characterize all these properties accurately. DSCs have been modeled from several different approaches [29, 30, 31, 32, 33]. In BIPV applications it is important to know the optical properties of the solar cells used in order to determine the appearance of the cells and the transmitted energy that will heat the building. So far the optical aspects of DSCs have been slightly overlooked in many models, including the overall most complex ones [29, 32, 33]. This is understandable, since for their purposes a properly chosen monochromatic illumination has been sufficiently

accurate approximation of sunlight [29]. However, without a more detailed optical model it is impossible to model the appearance of the DSCs or the effects of different dyes or any other optical component, whose effects are wavelength-dependent similarly to 1DPCs.

Apparently there is some interest towards this topic, since calculations about the performance, transparency and appearance have been done for organic solar cells [34]. However, in that case the color and the connection between cell performance and color is no discussed in detail. Also, it appears that the calculations about the color were not verified in any way [34]. The aim of this work is to develop tools to combine optical and electrical modeling in such way that one model could predict the optical properties of an assembled DSC, its appearance in controlled test conditions and its electrical performance with good accuracy. This includes also the verification of the color calculations with DSC samples. The approach of the model is similar to the model presented in [32]. It is meant to describe the steady state operation of the DSC with a reasonable accuracy, utilizing measured transmittance, reflectance and absorptance spectra of different DSC components as optical data. These are then linked with optical and electrical model to calculate the optical properties of an assembled DSC and its appearance and electrical performance in known lighting conditions. Ultimately, with experimentally verified data, such model could be a valuable tool used to tailor DSCs according to given requirements about appearance, transparency and efficiency.

The modeling of the optical properties is concentrated on the effects of different dyes and reflecting layers on the properties of DSCs. This task is done in two parts: In the first one, the focus is in the optical properties and appearance of the DSCs, and the optical model is used as a basis for calculating the color of DSCs with different dyes, dye concentrations and photonic crystals. The efficiency of the cells is also estimated, but more as an upper limit than accurate estimate. The color and efficiency aspects are combined in an example scenario, where certain transparency is required from solar cells, and the properties of different DSC designs are adjusted to fit this criterion. The available performance and appearance (color) choices are limited by the designs fulfilling the transparency criterion. The choice of starting point could be different, but in BIPV applications the brightness and intensity of the transmitted light are important factors that may be overlooked, if they are not explicitly considered as design parameters. However, the calculations about the color of the DSCs with different components and dyes are ultimately useful only, if and when it is possible to somehow control the optical properties of the assembled DSC. Otherwise they are mostly speculation without a way to realize the theoretical possibilities. Therefore one relatively simple and straightforward method is tested for controlling the amount of dye in the TiO_2 film of the DSC.

In the second part voltage losses caused by charge transfer at CE and diffusion of I^- and I_3^- in electrolyte are taken into account in the model and the aim is to give more accurate predictions about the performance of the DSCs. The optical properties of the DSCs can be modified, but are not the central part of the simulation, and the appearance aspect is ignored.

This thesis is divided into three sections. The first of them is an introduction to structure and working principles of DSCs. Following that are the simulations about the optical properties of DSCs: basic optical model of DSC, theory related to calculating color of an irradiation spectrum and calculating the maximum performance of a DSC based on its optical properties. Simulation procedure, some calculations and experimantal verification are also included. The third main section is centered on modeling the transport of I^- and I_3^- in electrolyte by diffusion in different DSC configurations, and adding the charge transfer and diffusion losses to the electrical model.

2 Overview on dye solar cells

2.1 The structure and materials of dye solar cells

Dye solar cells (DSCs, also dye-sensitized solar cells DSSCs or Grätzel cell) have been a topic of great interest ever since O'Regan and Grätzel managed to make one, whose efficiency was high enough for practical applications [18]. Since then several different materials and compounds have been studied in different cell components, but the DSCs with highest efficiencies still greatly resemble the original Grätzel cell [35].

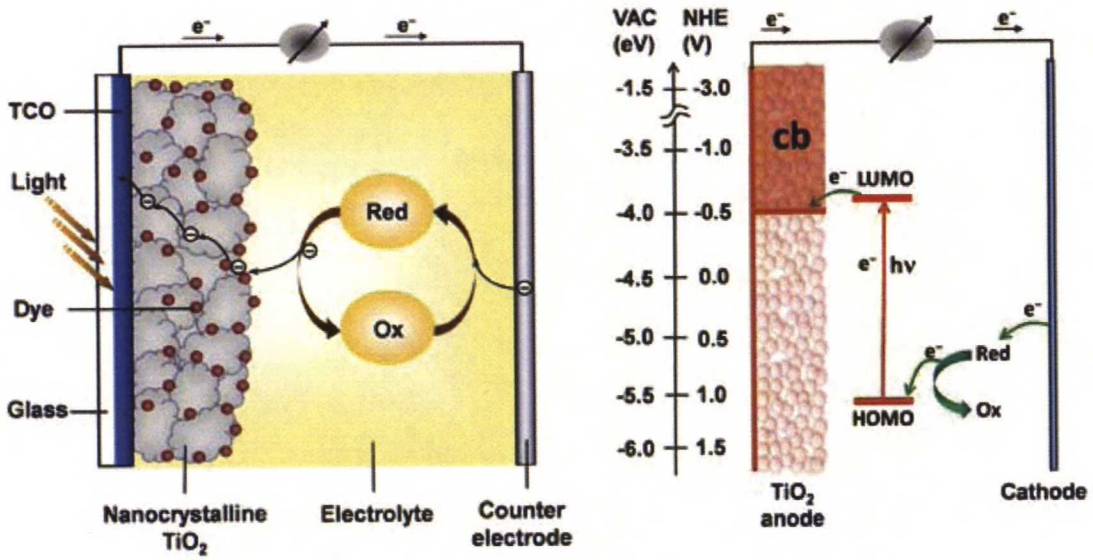

Figure 4: Typical structure and materials of DSCs and an illustration of charge transport and typical HOMO, LUMO and conduction band (cb in figure) energy levels. Figure from [36].

The substrate for both electrodes is typically a glass (or also plastic) sheet coated with transparent conducting material, most common ones being fluorine-doped tin oxide (FTO) and indium-tin oxide (ITO). They are both also referred as transparent conductive oxide (TCO) [18, 19, 37, 38, 39]. The glass substrates are also one of the most significant

limitations for mass production. The highest efficiencies and otherwise best DSCs are based on TCO glass substrates, but in mass production the size of the available glass sheets would set limitations to module size and also production rate. Plastics and thin metal sheets would be more suitable for mass production, but their problems lie in the efficiency and stability issues.

The photoactive electrode (photoelectrode, PE) of most DSCs today consists of TiO_2 nanoparticles that form a mesoporous layer with high surface area, where a monolayer of sensitizer/dye has adsorbed [18, 19, 37, 38, 39, 40]. TiO_2 is by far the most common material for the PE, but alternative materials, such as ZnO, SnO_2 and Nb_2O_5 have been studied [37]. In addition to changing the main material of the PE, different morphologies and additive materials have been studied [37]. One usual theme in these studies are different nanotube structures that could act as conducting wires inside the film [41, 42, 43, 44, 45, 46, 47].

Despite there being several thousands of dyes that have been studied, the most typical and ones yielding highest efficiencies are still ruthenium (Ru) complexes, similarly to the first Grätzel cell [18, 37, 39, 40]. Ru-based dyes have very wide absorption spectrum that enables absorbing high amount of photons and thus high photocurrents, which is one reason, why many DSCs with high efficiencies have been sensitized with them [37]. Ru-dyes are also electrochemically stable [37]. Still, alternatives to them are being actively studied. For example organic dyes have the advantage of easier design and synthesis processes and higher absorptivity than Ru complexes [37, 48, 49, 50, 51, 52]. This would enable high light harvesting efficiencies with thinner TiO_2 films than with Ru dyes, which in turn would decrease the average distance between electron excitation and the PE substrate and hence improve electron collection. However, the problem with many organic dyes is their narrow absorption spectrum, but this problem has been reduced and the best organic dyes yield efficiencies fully comparable to best Ru dye based DSCs [37, 48, 49, 50, 51, 52]. In addition to alternative dyes, using two or more dyes in the same DSC has been attempted successfully [53, 54]. This method could enable manufacturing thin film DSCs that absorb light efficiently at wide spectral range, but would apparently require that the dyes adsorb on the TiO_2 in different locations to fully utilize the potential of the method [53, 54].

The counter electrode (CE) of DSCs is typically made by coating the TCO film of the substrate with a thin film of platinum (Pt) acting as a catalyst to the reduction reaction of the redox couple of the electrolyte [19, 37, 38, 39, 40]. (Note that there are also p-type DSCs, where the redox couple is oxidized at the CE and reduced in PE [37].) There are alternatives to Pt CEs, but it is a stable material that yields high efficiencies, so less research is centred into studying them than for example alternative dyes and electrolytes [37]. The obvious drawback of Pt is its price, even if the required amounts are small.

The space between PE and CE, and also the pores of PE, is filled with electrolyte. The electrolyte of the "original" Grätzel cell was liquid, which is still a common solution [18, 37, 38]. The most efficient DSCs have a liquid electrolyte based on acetonitrile (CH_3CN, ACN) because of its extremely low viscosity (0.34 mPa·s; lower than water, 0.89 mPa·s) and high diffusion coefficient for the most common redox couple of iodide and tri-iodide (I^- and I_3^-) [37, 35]. Another electrolyte solvent worth mentioning is 3-methoxypropionitrile (3-MPN) that is the solvent used in most studies related to DSC stability [37]. In addition

to liquid solvents, also ionic liquids, gel and polymer electrolytes and hole conductors are being studied [37]. Their inherent properties should give them thermal stability and reduce problems with sealing and electrolyte leaking out of cells [37]. The (quasi-)solid electrolyte would also enable faster mass production of DSCs than liquid electrolytes, at least in principle.

Quite similarly to Ru complexes still dominating the DSC research, the redox couple of I^- and I_3^- is still the standard in DSCs despite large amount of research focused on alternative redox couples and electrolytes [18, 19, 37, 39, 40]. The combination of Ru-based dye and I^-/I_3^- redox couple is so common that at times they are used almost synonymously to dye and redox couple without referring to alternatives, when describing the DSC structure [19, 38, 39, 40]. The highest certified efficiencies have still been achieved with the conventional I^-/I_3^- couple, but high (uncertified) efficiencies have been recently achieved with e.g. cobalt-based (Co) redox couples [35, 55, 56]. Remarkably the efficiency with Co-based redox couples has in some cases been higher than when I^-/I_3^- was used with the same DSC components [56, 57]. This could very well mean that it is possible to achieve higher efficiencies than what has already been achieved, but it would require more than improving the dye of the DSCs.

2.2 Working principle of DSCs

The purpose of DSCs is to convert the power of solar irradiation into electric power. This process can be divided into several phases that all set their own requirements for the materials used in DSCs.

The first step in the energy conversion is the absorption of photons, or light harvesting. The fraction of photons absorbed by the dye is called the light harvesting efficiency ($\eta_{\mathrm{LH}}(\lambda)$). This efficiency depends on the thickness of the PE film, dye adsorbed on it and the concentration of the dye. The optical losses caused by the PE substrate and electrolyte in the pores also contribute to it. Light harvesting efficiency also depends on the illumination direction (through PE or CE). After absorbing a photon the electron is excited over the HOMO-LUMO gap of the dye (sensitizer, S):

$$S + h\nu \rightarrow S^* \tag{1}$$

The LUMO level of the dye should be higher than the conduction band of TiO_2 to enable efficient electron injection:

$$S^* \rightarrow S^+ + e^-_{\mathrm{TiO_2}} \tag{2}$$

It is generally accepted that electron injection is very fast process, even if the exact mechanism of the injection is under debate [37]. Electron injection also competes with the decay of the excited state by luminescence, thermal decay to ground or quenching [39]. The quenching process means a situation, where iodide reduces an excited dye molecule (and becomes an iodine radical) [58]:

$$S^* + I^- \rightarrow S^- + I^\cdot \tag{3}$$

The reduced dye can either inject an electron into TiO_2 film or react with I_3^-, creating I and $I_2^{-\cdot}$ [58]. Quenching may play a role in DSCs with very high I concentrations (> 5 M) that appear in e.g. ionic liquid electrolytes. When the concentration I is sufficiently low, increasing it will increase the photocurrent by reducing mass transport problems [59]. However, when I concentration becomes too high, the photocurrent and efficiency begin to decrease [58, 59]. Transient measurements suggest that the reaction with I_3^- is the dominant reaction after dye reduction [58, 59]. Therefore quenching would not help electron injection, but competes against it.

The efficiency of electron injection is denoted with $\eta_{\mathrm{INJ}}(\lambda)$. Similarly to light harvesting efficiency, it announces the fraction of excited electrons successfully injected into the conduction band of TiO_2. Generally its dependence on the wavelength of the light is quite weak, but the electron injection into TiO_2 is slower, and less efficient, from some electron states than from others [60]. In worst case it may even be possible that conduction band of TiO_2 is at higher potential than the LUMO level of the dye, impeding the electron injection especially, when the wavelength of the photon is relatively long [37].

The injected electrons are transported through the mesoporous TiO_2 film to the electric contact. The conductivity of the film is low and the small size of the particles prevents an internal electric field from being born [37]. When current is extracted from the cell, the PE substrate acts as a sink and creates a gradient in electron concentration, which causes diffusive electron transport [39]. (See also section 3.1.4.) The collection efficiency of the electrons, $\eta_{\mathrm{COL}}(\lambda)$, is typically quite high, because the recombination time constant of electrons with I_3^- is longer than the transport time of the electrons in the TiO_2 [37].

The dye cations (S^+) have to be reduced to enable continuous energy conversion. This happens, when the dye cation reacts with the reductant of the redox couple. In the case of I^-/I_3^- the oxidized sensitizer (reactions (1) and (2)) is generally considered to be reduced simply according to:

$$2S^+ + 3I^- \rightarrow 2S + I_3^- \tag{4}$$

However, the reduction of I_3^- is most likely a sequence of several reactions, the exact process most likely happening according to the following sequence: [37, 61]

$$S^+ + I^- \rightarrow (S \cdots I) \tag{5a}$$
$$(S \cdots I) + I^- \rightarrow (S \cdots I_2^{-\cdot}) \tag{5b}$$
$$(S \cdots I_2^{-\cdot}) \rightarrow S + I_2^{-\cdot} \tag{5c}$$
$$2I_2^{-\cdot} \rightarrow I_3^- + I^- \tag{5d}$$

The cation binds an I^- ion into itself and is reduced into I. Thereafter another I^- ion comes into contact with I and they form a diiodide (I_2^-) radical that comes loose from the dye molecule. Finally, two such radicals react with each other forming I^- and I_3^-. [37, 61, 58]

If the dye cations cannot be reduced fast enough, they recombine with electrons in the conduction band of TiO_2 [61]. The fraction of injected electrons not lost to recombination with dye cations is also known as regeneration efficiency, $\eta_{\mathrm{REG}}(\lambda)$.

The redox reaction of I^- and I_3^- is a two electron transfer reaction at CE: [37]

$$I_3^- + 2e^- \rightarrow 3I^- \tag{6}$$

This too consists of partial reactions:

$$I_3^- \leftrightarrow I_2 + I^- \tag{7a}$$
$$I_2 \leftrightarrow 2I \tag{7b}$$
$$(I + e^- \leftrightarrow I^-) \times 2 \tag{7c}$$

Incident-photon-to-collected-electron–efficiency (IPCE), $\eta_{\mathrm{IPCE}}(\lambda)$, is the probability that a photon of wavelength λ excites an electron that is successfully injected into the conduction band of TiO_2 and into the external electric circuit at the electric contact. With the efficiencies of the sub-processes IPCE is described as the probability that an electron is excited, injected and collected without recombining with dye cations or I_3^- :

$$\eta_{\mathrm{IPCE}}(\lambda) = \eta_{\mathrm{LH}}(\lambda)\,\eta_{\mathrm{INJ}}(\lambda)\,\eta_{\mathrm{REG}}(\lambda)\,\eta_{\mathrm{COL}}(\lambda) \tag{8}$$

As IPCE tells the ratio of successfully collected electrons to incident photons for each wavelength, the short circuit current of the DSC ($i_{\mathrm{SC,TiO_2}}$) can be expressed as

$$i_{\mathrm{SC,TiO_2}} = q_e \int_{\lambda_{\min}}^{\lambda_{\max}} \phi(\lambda)\,\eta_{\mathrm{IPCE}}(\lambda)\,\mathrm{d}\lambda \tag{9}$$

The elementary charge is denoted with q_e and the photon flux spectrum with $\phi(\lambda)$. The integration is done over the wavelength range, where both $\eta_{\mathrm{IPCE}}(\lambda)$ and $\phi(\lambda)$ have nonzero values.

3 Optical modeling of DSCs

3.1 Photocurrent generation in DSCs

3.1.1 Optical model of DSCs

The optical properties of the DSCs are defined by the materials used in them. Considering the requirements for the optical model of the DSCs, the important question is, how much the optical properties of the DSC are affected by interactions between the components. If the effect is small, it should be possible to model the DSCs by combining the properties of the components. In the opposite case the interactions affect the properties of the DSCs enough to require modeling of the interactions and their effect on the energy levels of the

components. The approach in the following model was to assume that the components would not affect each other's properties, except for TiO_2 and dyes.

Efficient light harvesting requires at least one of the electrode substrates to be transparent. The PE substrate is the better option, because it avoids the optical losses that occur in the catalyst layer and in the electrolyte, when DSCs are illuminated through CE. Laboratory samples typically have both PE and CE substrate made of some transparent material, unless some opaque material is being studied, so the losses typically are not too large. For example the transmittance of a typical TCO-coated glass substrate is between 80% and 90% for most of the utilizable wavelengths.

When a DSC is illuminated from the PE side, the light hits the PE substrate first (glass-TCO combination in figure 4). Typically most of the light is transmitted and only a small fraction is reflected. The transmitted light then comes into the TiO_2 layer. Some of the light is again scattered and reflected. Some wavelength-dependent fraction is absorbed by the dye molecules, and at short wavelengths (less than 400 nm) also TiO_2 absorbs light. The aim is for the dye to absorb as much light as possible, so typically significant portions of light are transmitted only at the long wavelengths that the dye cannot absorb or absorbs only weakly. Additionally, the electrolyte in the pores of the TiO_2 layer absorbs light (figure 20) and thus causes optical losses, even if they are not very significant.

When a DSC is illuminated through its CE, the optical losses are typically higher than in the case of PE illumination, but the PE film absorbs the same fraction of the incident light transmitted to TiO_2 film regardless of the illumination direction. It is the spatial concentration profile of the excited electrons that depends on the illumination direction: When the light comes to the DSC through the PE, the electron concentration is highest near the substrate and is reduced as the distance increases. In the case of CE illumination the situation is reversed. Electron collection losses then cause a smaller fraction of the free electrons being collected, when the DSC is illuminated from the CE side. This implies that as long as the optical losses in PE substrate are not higher than in CE and electrolyte, the cells should be illuminated through PE to achieve the highest possible efficiency.

When the small contribution of back-reflections from CE substrate (figures 5 and 20, or PE in the case of CE side illumination) is not taken into account, the light harvesting efficiencies for the PE and CE illuminations are [62, 32]:

$$\eta_{\mathrm{LH,PE}}(\lambda) = T_{\mathrm{TCO}}(\lambda)\,(1 - R_{\mathrm{PE}}(\lambda))\frac{\alpha_{\mathrm{D}}(\lambda)}{\alpha(\lambda)}(1 - e^{-\alpha(\lambda)d}) \tag{10a}$$

$$\eta_{\mathrm{LH,CE}}(\lambda) = T_{\mathrm{CE}}(\lambda)\,T_{\mathrm{El}}(\lambda)\,(1 - R_{\mathrm{PE}}(\lambda))\frac{\alpha_{\mathrm{D}}(\lambda)}{\alpha(\lambda)}(1 - e^{-\alpha(\lambda)d}) \tag{10b}$$

These expressions assume that the light absorption occurs according to the Beer-Lambert law. Also, if there are any other structures in the DSC that scatter or reflect light, the equations must be adjusted accordingly. (See section 3.1.2 and equation (14)) The transmittance of the PE substrate (usually TCO glass) is denoted as T_{TCO}, R_{PE} is the fraction of light that the TiO_2 film reflects and the transmittance of CE is T_{CE}. The electrolyte usually does not scatter light and is hence assumed to absorb light according to the Beer-Lambert law:

$$T_{\mathrm{El}}(\lambda) = e^{-\alpha_{\mathrm{El}}(\lambda)\, d_{\mathrm{El}}} \tag{11}$$

The absorption coefficient of the electrolyte is dominated by I_3^-, and affects only the shortest wavelengths. (See figure 20.)The electrolyte in the pores of the PE film also contributes to light absorption so that all light absorbed within PE film is not absorbed by TiO_2 or dye:

$$\alpha(\lambda) = \alpha_{\mathrm{D}}(\lambda) + p\,\epsilon\,\alpha_{\mathrm{El}}(\lambda) \tag{12}$$

The fraction of absorbed photons that can be transformed into photocurrent is marked with $\alpha_{\mathrm{D}}(\lambda)$. The optical mean path length is described by p, whose value is assumed to be 1.5, unless otherwise stated. The porosity of the TiO_2 film is given by ϵ, whose value is typically around 0.5. It is also readily visible that the light absorption is strongly affected by the exact dye used in the DSC and the thickness of the TiO_2 film. In addition to the choice of the dye, the dye concentration in the film has a strong effect on the absorptivity (α_{D}), even if that is not explicitly stated in previous equations. Typically the absorptivity is (approximately) linearly affected by the dye and its concentration:

$$\alpha_{\mathrm{D}}(\lambda) = C_{\mathrm{D}}\,\epsilon_{\mathrm{D}}(\lambda), \tag{13}$$

where C_{D} is the concentration of the dye and ϵ_{D} is the molar absorptivity of the dye in question. Note that the molar absorptivity of dye molecules adsorbed on TiO_2 may differ from the ones free in solvent [48, 49, 50]. This was taken into account in the calculations by using $\alpha_{\mathrm{D}}(\lambda)$ measured from dyed TiO_2 films. (See figure 18.)

3.1.2 Photonic crystals in DSCs

The efficiency of the DSCs can be improved by enhancing the electrical or optical properties of the cell. Adding a light-reflecting layer behind the TiO_2 film will improve the light harvesting efficiency by reflecting back some of the light that would normally be transmitted through the PE film and then lost [21, 22, 23, 24]. In the sense of enhancing light harvesting this method is similar to increasing the thickness of the TiO_2 layer, but has the additional benefit of keeping the electron excitation on average closer to PE substrate. The highest efficiencies can be achieved with a scattering layer that reflects most of the light at all wavelengths of the visible light range and turns the DSC opaque [21]. Conserving the transparency requires a smaller portion of the incident light to be reflected. One way to achieve this is to use a film that reflects light at only a narrow wavelength range and allows the rest to be transmitted normally [23].

The reflecting layer can be either coupled with the TiO_2 film or it can be placed on CE. The CE itself can also act as a reflecting layer: The reflectance of Pt depends on the deposition method, but e.g. FTO glass with sputtered Pt can reflect 15–20% of the incident light, depending on the wavelength [63]. Metal CEs with sputtered Pt can reflect 30–60% of incident light, depending on the wavelength and metal [63]. (See also figure 5.) The main advantage of reflectors coupled with TiO_2 is that the optical losses due to absorption

in the electrolyte between the back reflection and the PE film are minimized. However, if the reflecting layer is too thick or not porous enough, the hindrance to diffusion can offset the performance increase gained in light absorption [22, 23]. Possible chemical interactions inside the DSCs also set them limitations that may no apply to reflectors on the outer surface of the CE.

The structure of a photonic crystal can be periodical in one, two or three dimensions [22, 23, 64, 65]. An example of the structure of a one-dimensional photonic crystal (1DPC) is shown in figure 6. Of the available options at least one- and three-dimensional structures have been tested in DSCs and both have been shown to increase short circuit current [22, 23]. So far only 1DPCs have been thin and porous enough that the diffusion losses have not caused the DSC with photonic crystal to have a lower efficiency that otherwise similar DSC without one [22, 23]. (See also sections 4.1.1, 4.1.2 and 4.3.)

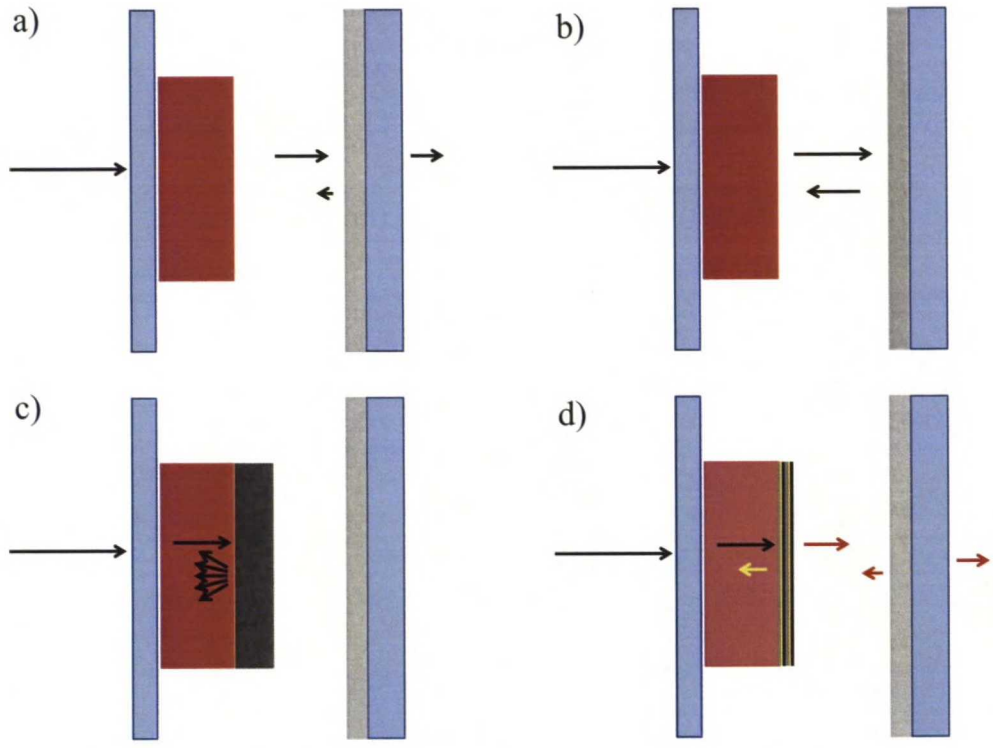

Figure 5: Scheme of reflections in different DSC. a) normal DSC, where Pt on CE reflects some of the light transmitted through PE and electrolyte. b) Highly reflecting CE that transmits little or no light. c) PE coupled with a porous scattering layer that reflects a large fraction of all wavelengths of visible light. d) PE coupled with a porous 1DPC that reflects a selected wavelength range and allows the rest to be transmitted.

Typical reflecting layer coupled with the TiO_2 film is thin, porous and consists of nanoparticles. The physical mechanism behind the reflection is not always the same: Scattering layers are based on light scattering from particles, whose diameter is comparable to

the wavelength of the light [66]. Scattering from such particles depends only weakly from the wavelength of light, so these scattering layers typically reflect all wavelengths quite equally and turn the DSC opaque [66]. (See also figure 42.) Photonic crystals are Bragg reflectors, so the high reflectance is based on constructive interference and periodic structure (figure 6) that modifies the phase of the light so that the intensity of the reflected light is maximized at a selected wavelength range [21, 24, 27]. Other wavelengths are affected only little, so the semi transparency of the DSC is preserved [21, 24, 27]. Because the physical basis of the reflection is interference from a periodic structure, the incident angle of light affects the reflectance spectrum. Due to the porous structure, also the composition of the electrolyte affects the reflectance spectrum [24, 26, 27].

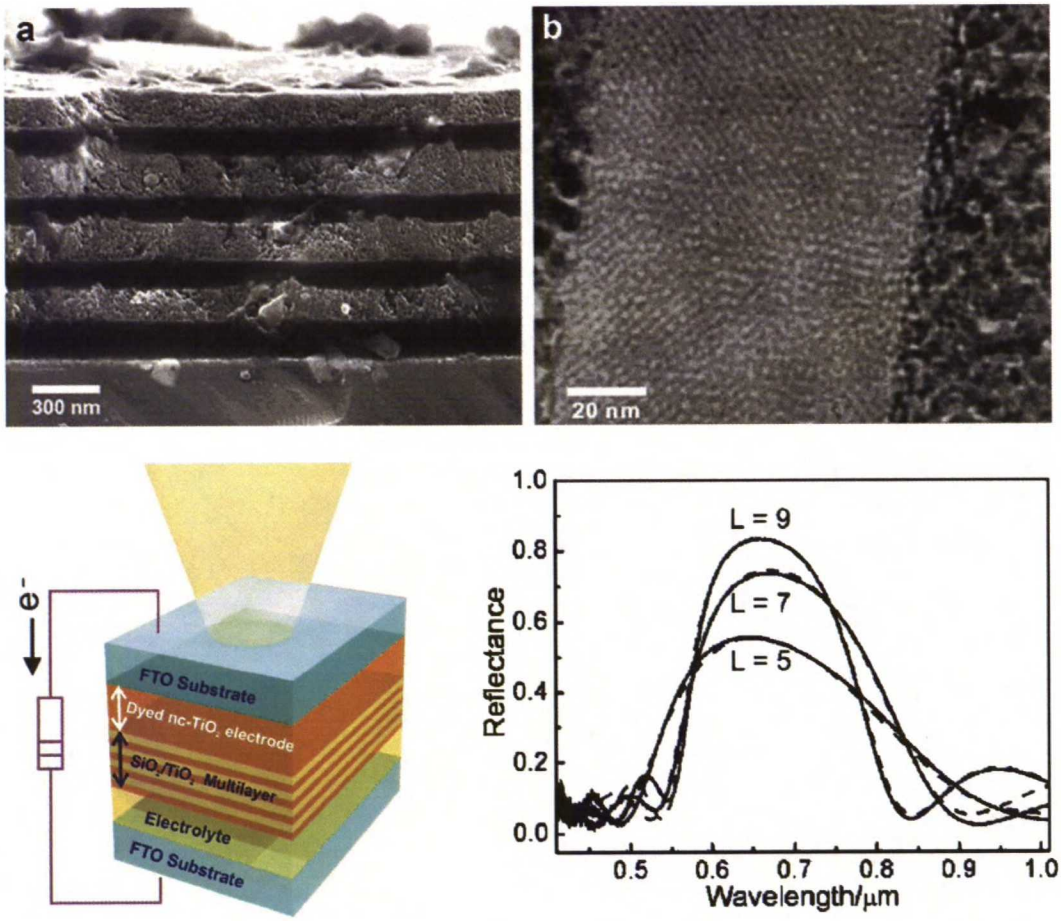

Figure 6: Top row: a) FESEM (field emission scanning electron microscope) image of an eight-layered Bragg reflector made of TiO_2 and SiO_2; dark gray: TiO_2, light gray: SiO_2, substrate: silicon. (b) TEM (transmission electron microscope) image of the same system showing two mesophases with different pore size [27]. Bottom row: Schema of a DSC with 1DPC coupled with the PE and an example of a reflectance spectrum of a 1DPC as a function of the number of layers in the stack (L) [23, 26].

Assuming that the photonic crystal in DSC is directly coupled with the TiO_2 film, the light harvesting efficiency will change from the case without a coupled reflector (equation (10)) to

$$\eta_{\mathrm{LH,PE}} = T_{\mathrm{TCO}}(1 - R_{\mathrm{PE}})\frac{\alpha_{\mathrm{D}}}{\alpha}(1 - e^{-\alpha d})(1 + e^{-\alpha d}R_{\mathrm{PC}}(1 - R_{\mathrm{PE}})) \tag{14a}$$

$$\eta_{\mathrm{LH,CE}} = T_{\mathrm{CE}}T_{\mathrm{El}}T_{\mathrm{PC}}(1 - R_{\mathrm{PE}})\frac{\alpha_{\mathrm{D}}}{\alpha}(1 - e^{-\alpha d}) \tag{14b}$$

A photonic crystal enhances the light absorption from one direction by reflecting (R_{PC}) as large portion of the transmitted light as possible. It also reduces the light harvesting efficiency of CE illumination, because it reflects some of the light before it can be absorbed. The incident angle of the light affects the reflectance spectrum and has to be taken into account in the calculations. For the sake of simplicity, the light is assumed to be at normal incidence to the DSC (and 1DPC) in all later calculations. The measurements were also conducted so that the light would be as close to normal incidence as possible.

3.1.3 Total transmittance and reflectance of the DSCs

The color of the DSCs is a combination of light transmitted through the cell, light reflected from the cell and response of the eye to their combined spectrum. Using the simple optical model and ignoring multiple reflections inside the cell, the total transmittance of a DSC can be expressed as

$$T_{\mathrm{DSC}} = T_{\mathrm{TCO}}(1 - R_{\mathrm{PE}})e^{-\alpha d}T_{\mathrm{PC}}T_{\mathrm{El}}T_{\mathrm{CE}} \tag{15}$$

Similarly, the total reflectances for illumination from the PE and CE side of the DSC are:

$$\begin{aligned} R_{\mathrm{DSC,\,PE}} =& R_{\mathrm{TCO}} + T_{\mathrm{TCO}}^2 R_{\mathrm{PE}} + \left(T_{\mathrm{TCO}}\left(1 - R_{\mathrm{PE}}\right)e^{-\alpha d}\right)^2 R_{\mathrm{PC}} \\ &+ \left(T_{\mathrm{TCO}}\left(1 - R_{\mathrm{PE}}\right)e^{-\alpha d}T_{\mathrm{PC}}T_{\mathrm{El}}\right)^2 R_{\mathrm{CE}} \end{aligned} \tag{16a}$$

$$\begin{aligned} R_{\mathrm{DSC,\,CE}} =& R_{\mathrm{CE}} + \left(T_{\mathrm{CE}}T_{\mathrm{El}}\right)^2 R_{\mathrm{PC}} + \left(T_{\mathrm{CE}}T_{\mathrm{El}}T_{\mathrm{PC}}\right)^2 R_{\mathrm{PE}} \\ &+ \left(T_{\mathrm{CE}}T_{\mathrm{El}}T_{\mathrm{PC}}\left(1 - R_{\mathrm{PE}}\right)e^{-\alpha d}\right)^2 R_{\mathrm{TCO}} \end{aligned} \tag{16b}$$

These expressions give the transmittance and reflectance spectra of a DSC in a general case, when multiple reflections can be neglected. With small modifications these can be applied to special cases of DSCs, the most important "special" case being a normal DSC without a back reflector coupled with PE. This case can be calculated simply by inserting $T_{\mathrm{PC}} = 1$ and $R_{\mathrm{PC}} = 0$. Another special case relevant for this thesis is an undyed PE film coupled with 1DPC and without the other components. (More of that in section 3.3.2.)

However, the given expressions (equations (15) and (16)) give only the reflectance and transmittance spectra of the DSCs. The reflected or transmitted irradiance (photon flux) spectrum is calculated by multiplying the transmittance or reflectance with the spectrum of the light source:

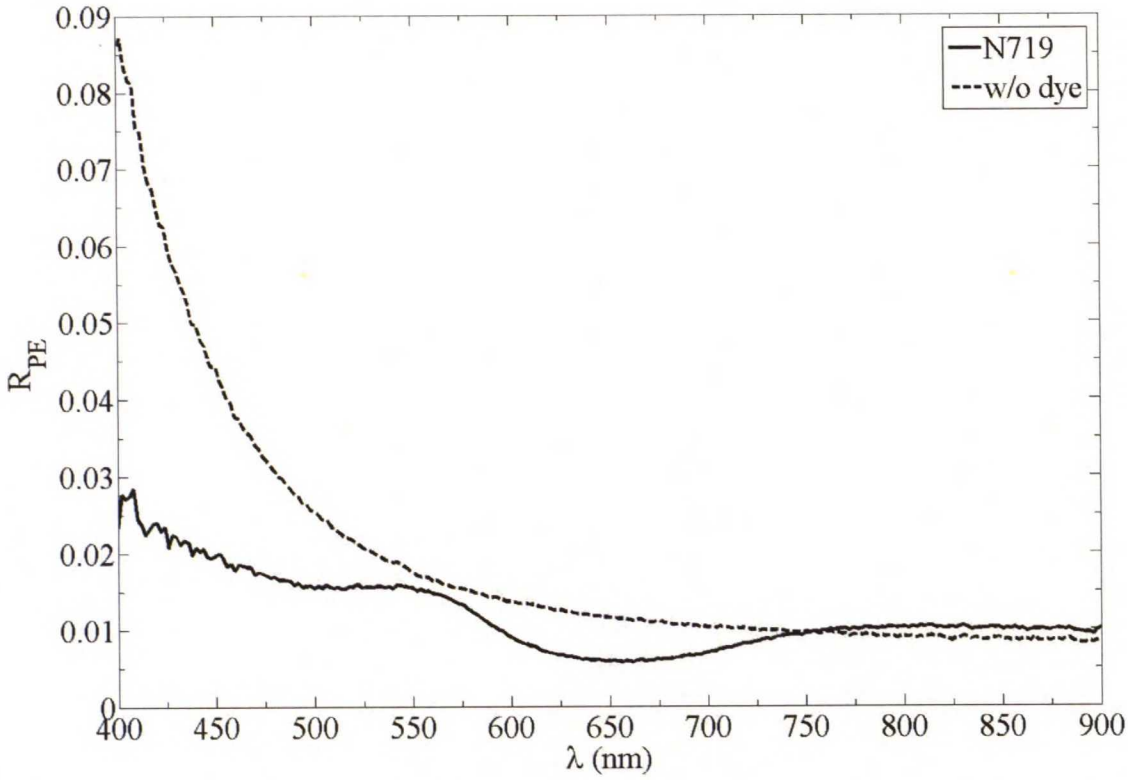

Figure 7: The reflectance of approximately equally thick TiO_2 films: one dyed with N719 and one without dye. Both spectra were used in calculations, N719 with all dyed films and undyed with films without dye.

$$I_T(\lambda) = I_0(\lambda)\, T_{\mathrm{DSC}}(\lambda) \tag{17}$$

This information was then used together with the spectrum of the light source ($I_0(\lambda)$) to calculate the color of the DSCs (or optical samples).

All the coefficients in previous equations were determined experimentally from components identical to ones used in DSCs or approximated by using existing data about similar, but slightly different components. Due to equipment limitations, only the transmission coefficients could be determined accurately. In the case of reflectance old data and/or some approximations had to be used: The reflectance of the TiO_2 film was assumed to be unaffected by the dye used and its concentration in the film. This may not be quite true, because the reflectance originates from the TiO_2-air/electrolyte interfaces that are located on both the surface of the film and its bulk. Therefore the amount of light absorbed and the absorption spectrum are likely to have some effect on the reflectance – as well as the thickness of the film. Unfortunately the data used was from a film thicker than the ones used in the experiments, so this introduces one additional error source to calculations. However, as figure 7 shows, the reflectance of a dyed TiO_2 should be small enough that small variations caused by the film thickness and dye used are not significant for the total

reflectance. The pores of the film were filled with 3MPN, so the different optical properties of TiO_2-air and TiO_2-solvent interfaces should not have any additional effect on the accuracy of the calculations.

3.1.4 Electron transfer in TiO_2 film

Solar cells are basically light absorbing diodes, or inverse LEDs. This analogue is of course most directly applicable to solid-state (crystalline) solar cells due to similar structure and materials, but even DSCs appear to act like diodes that absorb light to produce current. The main difference between DSCs and solid-state solar cells is the electron transfer mechanisms: In solid-state solar cells the diffusion of the majority charge carriers (electrons in N-type and holes in P-type semiconductors) creates a depletion zone in the P-N junction, where there is a net negative charge in the P-type and positive charge in the N-type material. This creates an electric field that accelerates electrons from P-N junction towards N-side, where they will be collected. A large portion of the photocurrent comes from electrons excited in the N-type material or in the depletion zone, but electrons excited in the P-type materials may also diffuse into N-side and be collected.

In DSCs the charge separation occurs by interfacial charge transfer kinetics and electron diffusion in TiO_2 is the charge transport mechanism. There are few different ways to present the continuation equation of the electron concentration that differ from each other in the way the exponent (reaction order) of the electron concentration is shown [29, 32, 67, 68].

$$\frac{\partial n_c}{\partial t} = D_0 \frac{\partial^2 n_c}{\partial x^2} - \frac{n_c^\beta - n_0^\beta}{\tau} + g(x) - N_{t,0} \left\langle \frac{\partial f}{\partial t} \right\rangle \tag{18}$$

The concentration of free electrons is n_c, and term n_0^β/τ corresponds to thermal electron generation in equilibrium in the dark. The similarity to n_c term is based on the assumption that the recombination mechanisms under illumination and in the dark are the same, so the thermal generation in the dark, $g_T(x)$, can be written with the dark recombination. The electron injection rate is given by g(x), and D_0 is the diffusion coefficient of free electrons, τ is the inverse of the rate constant for the electron transfer from TiO_2 to I_3^- ($k_r = 1/\tau$). The reaction order with respect to free electron concentration, β, has mostly been considered to be 1 making the continuation equation linear, but lately it has been shown that simulations with $\beta < 1$ can predict phenomena that occur in real DSCs, but linear model cannot predict [19, 31, 32, 39, 40, 67, 68]. The last term on the right hand size describes the trapping and detrapping of the conduction band electrons. In steady-state operation this term equals to zero.

When the continuation equation is assumed to be linear with respect to free electron concentration, it is possible to express the collection efficiency analytically, if Beer-Lambert law applies (or the electron generation profile is constant) [31, 32, 62]. In general case the generation profile tells the amount of electrons injected into TiO_2 per unit volume (excited by photons of wavelength λ). Regardless of the actual form of the generation profile, light harvesting efficiency in general can be defined as is the total amount of excited electrons divided by the photon flux:

$$\eta_{\mathrm{LH}}(\lambda) = \frac{\int_0^{d_{\mathrm{PE}}} g(x,\lambda)\,\mathrm{d}x}{\phi(\lambda)\,\eta_{\mathrm{INJ}}(\lambda)} \tag{19}$$

The photon flux is given by $\phi(\lambda)$ and $\eta_{\mathrm{INJ}}(\lambda)$ is the injection efficiency. If Beer-Lambert law applies, $g(x,\lambda)$ is exponentially decaying (with respect to x) and the light harvesting efficiencies are given by equation (10). When back reflectors are applied to this, the light harvesting efficiencies change as equation (14) states.

The continuation equation is solved by applying a voltage-dependent boundary condition at the PE substrate and a reflecting boundary condition at the opposite edge: [32]

$$n(x=0) = n_0 e^{\frac{E_F(x=0)-E_{\mathrm{redox}}(x=d)}{mk_BT}} = n_0 e^{-\frac{q_e V_{\mathrm{TiO_2}}}{mk_BT}} \tag{20a}$$

$$\left.\frac{\partial n}{\partial x}\right|_{x=d} = 0 \tag{20b}$$

The ideality factor m is an empirical constant that can be related to β as $m = 1/\beta$ [32]. In practise this means that approximate solution for equation (18) is derived by accounting for the nonideality in the boundary conditions (equation (20)) instead of the continuation equation. One physical interpretation of this approximation is that 1/m corresponds to an electron activity coefficient that represents interaction of the conduction band electrons with ions in the surrounding electrolyte [69].

The solution for steady-state electron collection efficiency is calculated at the short circuit conditions, i.e. $V_{\mathrm{TiO_2}}$=0 in equation (20a). Collection efficiency for illumination through both PE and CE are calculated from these boundary conditions, but by using different electron generation profiles. Electron lifetime (τ) and diffusion coefficient (D) are assumed to be independent of x and n(x). The extraction of electrons at short circuit conditions at the substrate contact is fast enough to keep the excess electron concentration at the contact close to dark equilibrium value. [62]

There are explicit expressions for the collection efficiencies, when the electron generation is exponential (or constant) [31, 32, 62]. However, in general case the collection efficiency is calculated from:

$$\eta_{\mathrm{COL}} = \frac{\int_0^d g(x)\,\eta_{\mathrm{COL},\delta}(x)\,\mathrm{d}x}{\int_0^d g(x)\,\mathrm{d}x} \tag{21}$$

The spatial collection efficiency, $\eta_{\mathrm{COL},\delta}$, is given by

$$\eta_{\mathrm{COL},\delta}(x) = \frac{\cosh\left(\frac{d-x}{L}\right)}{\cosh\left(\frac{d}{L}\right)} \tag{22}$$

The electron diffusion length is defined as $L = \sqrt{D\tau}$. As the spatial collection efficiency shows, the collection efficiency depends also on the thickness of the TiO_2 film, d. The thinner the film is, the higher the spatial collection efficiency at distance x. This can be understood as the generated electron having less space to move and thus having on average higher probability to diffuse into PE contact before it is lost to recombination.

The current density produced by a DSC at the substrate contact is defined as

$$i_{\mathrm{CELL}} = q_e D \left.\frac{\mathrm{d}n}{\mathrm{d}x}\right|_{x=0} \tag{23}$$

In real DSCs the direct electron recombination through PE substrate would have to be taken into account, but here it is neglected, i.e. $i_{\mathrm{CELL}} = i_{\mathrm{TiO_2}}$ (equation (9)). After a little reformulation, the solution for current density can be expressed as [31, 32]

$$i_{\mathrm{CELL}}\left(V_{\mathrm{TiO_2}}\right) = i_{\mathrm{SC,TiO_2}} - i_{\mathrm{REC},0}\frac{L}{d}\tanh\left(\frac{d}{L}\right)\left(e^{-\frac{q_e V_{\mathrm{TiO_2}}}{mk_BT}} - 1\right) \tag{24}$$

When recombination kinetics are first order with respect to electron concentration ($\beta = 1$ in equation (18)), the recombination current density in PE film of thickness d with uniform electron concentration n, i.e. in open circuit is [32]

$$i_{\mathrm{REC}} = q_e dk\left(n - n_0\right) = q_e d\frac{n - n_0}{\tau} \tag{25}$$

The rate constant of the first order recombination reaction is k. As can be seen, it is defined as $k = 1/\tau$.

The voltage of the PE can be solved from equation (24) as a function of the current density. This form is also more convenient, when other DSC components are taken into account in the model: Their effect on the IV curve can be expressed as voltage losses (overpotentials) that depend on the current density, and the final voltage is the sum of PE voltage and the voltage losses. The solution for PE voltage as a function of current density is

$$V_{\mathrm{TiO_2}}\left(i_{\mathrm{CELL}}\right) = -\frac{mk_BT}{q_e}\ln\left(\frac{d}{L}\coth\left(\frac{d}{L}\right)\cdot\frac{i_{\mathrm{SC,TiO_2}} - i_{\mathrm{CELL}}}{i_{\mathrm{REC},0}} + 1\right) \tag{26}$$

And thus the open circuit voltage is:

$$V_{\mathrm{OC}} = V_{\mathrm{TiO_2}}\left(i_{\mathrm{CELL}} = 0\right) = -\frac{mk_BT}{q_e}\ln\left(\frac{d}{L}\coth\left(\frac{d}{L}\right)\cdot\frac{i_{\mathrm{SC,TiO_2}}}{i_{\mathrm{REC},0}} + 1\right) \tag{27}$$

The factor $L/d\cdot\tanh\left(d/L\right) = L/\left(d\cdot\coth\left(d/L\right)\right)$ equals to the collection efficiency of a uniform, flat electron generation profile ($g\left(x\right)$ = constant in equation (21)). Typically, at least when the cell is illuminated from the PE side, the electron generation is biased towards the PE contact and the collection efficiency is higher than for constant generation profile. In such case the open circuit voltage decreases slightly, when diffusion coefficient increases.

However, if the electron generation is biased so that the collection efficiency is lower than in the case of constant generation profile, the open circuit voltage will slightly increase with diffusion coefficient. These phenomena are caused by the the relationship between i_{SC,TiO_2} and collection efficiency.

3.2 Color stimulus and its reproduction

3.2.1 Human visual system

The color of an object is strongly related to the irradiation spectrum reflected from or transmitted through it, but is not quite the same thing. The color of a surface is a combination of the irradiance, coming into eye from the surface, the surrounding illumination conditions and the response of the cone cells of the eye. White surface, for example, ideally reflects some constant fraction of light at all wavelengths, but so does also a neutral gray surface. The only difference is the higher irradiance from white surface. This difference is easily viewable by comparing for example illuminated sections of a white wall to ones in shadow. The opposite also applies: A normally gray surface may appear bright white, when its position is such that the reflected irradiance is higher than the irradiance coming to eye from other surfaces. (See figure 8.) The surrounding lighting conditions also affect the color of an object by affecting the response of the eye [70]. This can be demonstrated by comparing the apparent brightness of e.g. the headlights of cars in dark and during daytime, or streetlights in dark and in the morning before they turn off.

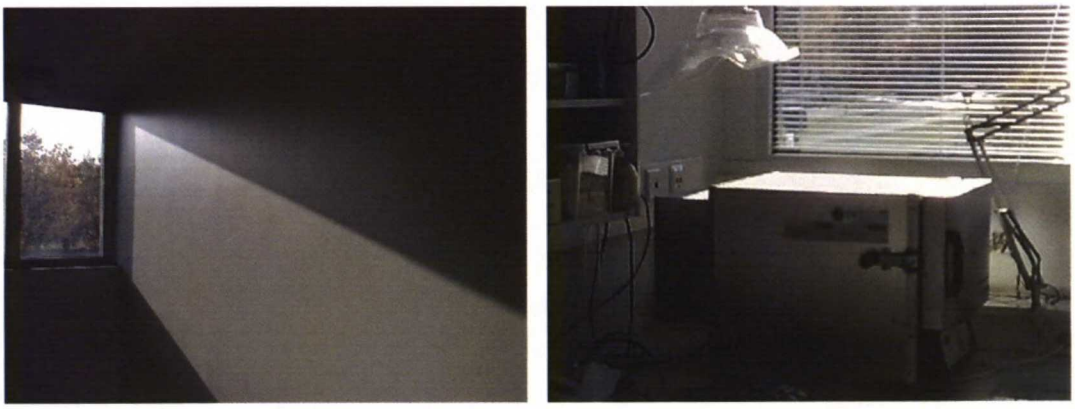

Figure 8: Examples of the effect of illumination intensity on color: The wall in the photo on the left is painted uniform white and the top of the oven in the photo on the right is the same gray metal as the sides. However, the brightest spot on the wall and the top of the oven both appear almost the same white/light grey.

The state of adaptation of the eye is tuned according to the overall light intensity, but the response is not immediate, which at times may affect the color experience. The colors may be poorly visible, when coming from brightly illuminated conditions, e.g. bright sunlight, to a space with low intensity illumination. Human vision can adapt to wide range

of intensity levels – over seven decades of dynamic range in total. For the lowest two decades of this, the rod cells are employed. Because there is only one type of rod cell, night vision cannot differentiate colors. The adaptation to light intensity is controlled by total retinal illumination, which is closely related to the overall intensity of "white" in the field of vision. About one decade of adaptation is affected by the iris; the rest is due to a photochemical process that involves the visual pigment substance in the photoreceptor cells. At any particular state of adaptation human vision can distinguish different luminance levels down to about one percent of peak white. Roughly speaking, luminance levels below this level appear black, and different levels below this threshold cannot be distinguished from each others. [70]

Adaptation to surrounding lighting conditions means that there is no "universal white" that could be used regardless of the light source; the luminance of the reference white must be comparable to the luminance of the light source. If the irradiation spectrum of the overall lighting is uniform enough, the eye adapts to see it as white and defines other colors wit respect to it. Unfortunately this only increases the complexity of calculating the color of an object: It is possible that some object appears more or less different in some conditions compared to its color in different conditions, which should be calculated somehow. With the proper choice of white spectrum this should be possible, but the problem is only transferred to the choice of white.

Comparison of calculated colors with photos taken in controlled conditions is more or less the only method to verify or falsify the accuracy of the calculations. The problem with photos is that cameras do not always make the adjustments to lighting automatically, or similarly to human visual system, so the colors may appear different to how people would experience them in same conditions.

Most people have a trichromatic color vision, meaning that they have three kinds of cone cells in their eyes that each has a spectral response different from the others. Color blindness means a situation, where there are only two kinds of cone cells in the eye. In addition, there are reports of people with four or more different cone types, giving them tetrachromatic vision [72]. Due to the underlying genetics, such vision is at least significantly more common among women than men (if not exclusive to women) [72].

The conventional understanding of human vision states that the three cone cells in the eye respond to different wavelengths of visible light so, that by comparing the strengths of the signals from different cells, the brain can deduce the color of the light hitting some part of the retina [73]. The relative sensitivity of the cones to different wavelengths is shown in figure 9. The maximum sensitivity of M cones is the highest followed by the L cones. Because they both are quite sensitive to wavelengths around 550 nm, human eye is most sensitive to those wavelengths [73]. The responses of M and L cones are remarkably similar. This is due to the corresponding genes having a common origin and either of them being a relatively recently mutated duplicate of the other [74]. Both are located in the X-chromosome one after the other and have remarkably similar DNA content [74].

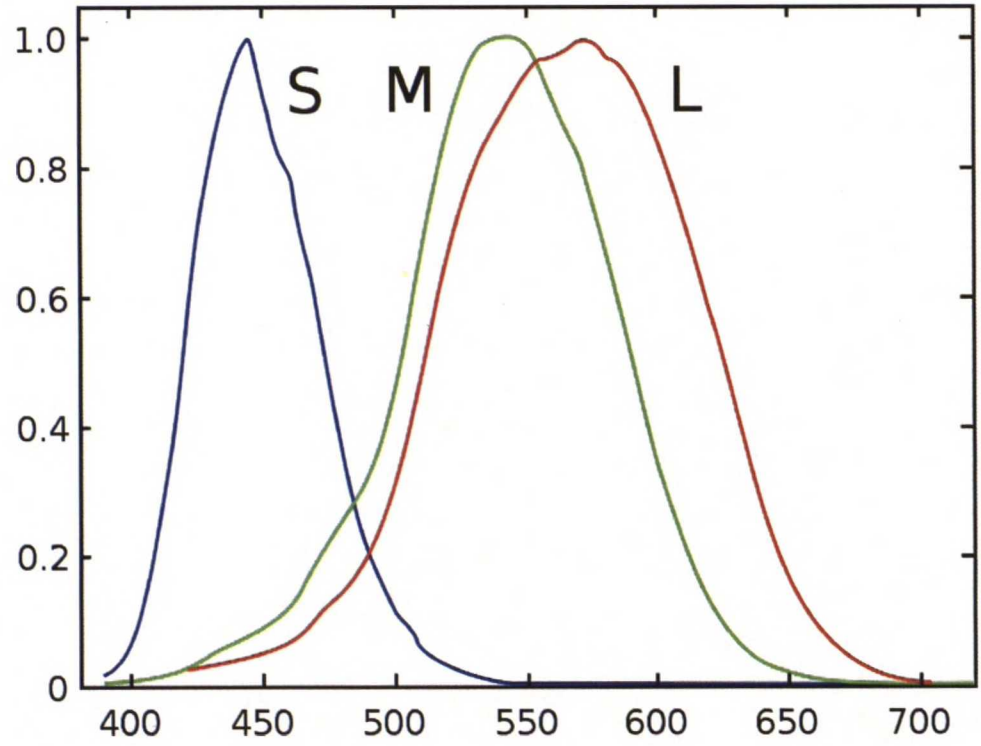

Figure 9: The relative responsivity of human S, M and L cone cells in wavelength range of visible light. Note that the lack of response in near ultraviolet and near infrared regions is caused by the lens absorbing those wavelengths. Figure from Wikipedia [71]

3.2.2 Color spaces and Grassmann's laws

The theory of trichromatic vision and three different cones (Young–Helmholtz theory) dates back to 1850. Later, in the early 20th century, experiments were conducted, where subjects were supposed to match a test color by combining three primary colors. In those experiments the primary color were chosen to be some shade of blue, green and red. These experiments were later used as a basis for the standards of color reproduction.

One very important result, and an implicit assumption in color systems, are the Grassmann's laws. They are empirical results that can basically be summarized as the colors, as seen by humans, being linear combinations of the responses of cone cells to irradiation stimulus. This applies only when the retinal illumination level is not high enough to cause photobleaching in cone cells. Also the rod cells influence the vision in the peripheral regions of the eye, and the color sensations may not be strictly trichromatic anymore. [75]

Based on Grassmann's laws and the trichromacity of the typical human photopic vision (vision in well-lit conditions, i.e. color vision), all colors can basically be considered as vectors in three-dimensional vector space. Therefore symmetry, transitivity, proportionality and additivity apply to all color stimuli that are within the linear range of human vision. Because of this, the total "length" of these component vectors can be calculated as a sum

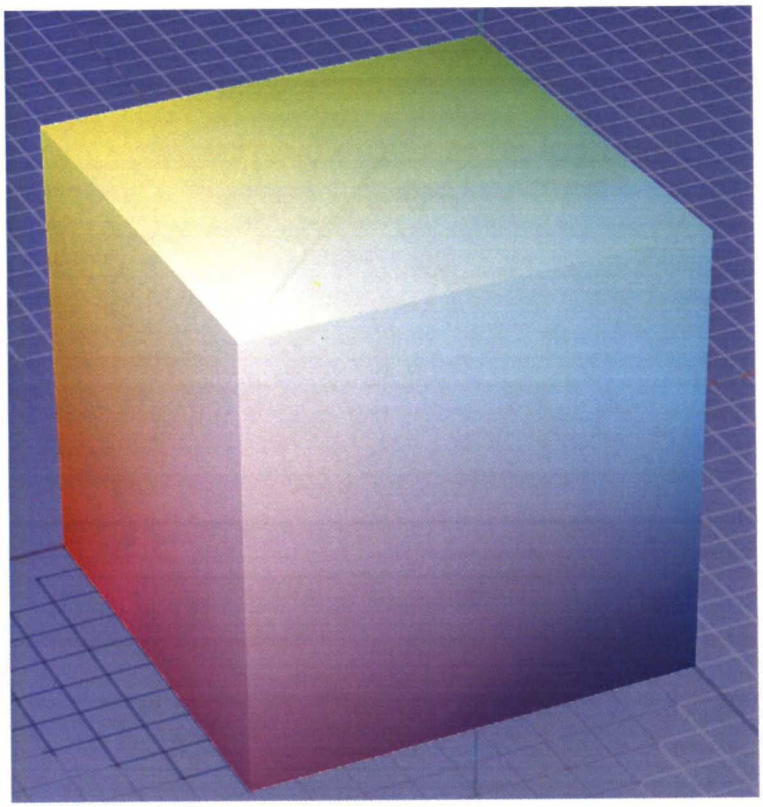

Figure 10: The RGB color model represented as a cube. The origin of the space, black, is behind the cube and not visible. Similarly, each point inside the cube corresponds to some color that is not visible on the surface. Note that the cube does not contain all colors that human eye can see. Figure from Wikipedia [76].

of the stimuli caused by the monochromatic light components of a light source over all wavelegnths of a spectrum, i.e. as an inner product integral of the spectrum and a response function corresponding to the vector:

$$R_C = \int_0^\infty I(\lambda)\, \overline{c}(\lambda)\, \mathrm{d}\lambda \tag{28}$$

The irradiation spectrum of the light is $I(\lambda)$ and $\overline{c}(\lambda)$ is the color matching function for coordinate R_C and basis vector $\boldsymbol{C}$. The total vector component is then $R_C \boldsymbol{C}$ and the location in the color space is the sum of such vectors. (See figure 10 for an illustration of three-dimensional color space.) The color matching function depends on the so-called primary color corresponding to it. Typically a primary color is a light source with a narrow irradiation spectrum, and there is one color matching function for each primary color of any color space. The product of irradiation spectrum and color matching funtion is integrated over the spectral range, where both have non-zero values. This is equal to the inner product of the functions in question (both have only real values), so the color

coordinate values can be considered as the projection of an infinite-dimensional spectrum to finite-dimensional Hilbert space (three-dimensional in the case of the standard color spaces). In that sense the color spaces are not vector spaces, but (real) Hilbert spaces, but can be treated with the vector analogy: If the normalized irradiation spectrum of primary j is $I_{\mathrm{j}}(\lambda)$ (analogous to vector $\boldsymbol{C}$) and the number of primaries is N, then $I_{\mathrm{RE}}(\lambda)$ is the reproducible irradiation spectrum that induces a stimulus as close as possible to the stimulus of the original irradiation spectrum $I(\lambda)$ with the given primaries. Whether the stimuli are identical or more or less different, depends on the original spectrum and the spectra of the primaries.

$$I_{\mathrm{RE}}(\lambda) = \sum_{j=1}^{N} R_j I_j(\lambda) \tag{29}$$

3.2.3 Calculating the coordinates in color spaces

In 1931 the Commission Internationale de l'Éclairage (CIE) established standards for color representation that were based on the physiological perception of light. The result was a set of three color matching functions that were derived from experiments, where the primary colors were three monochromatic light sources (435.8 nm, 546.1 nm and 700 nm). The average amounts of the monochromatic primaries needed to reproduce the stimulus of monochromatic light of wavelength λ are represented as functions $\overline{r}(\lambda)$ (700 nm), $\overline{g}(\lambda)$ (546.1 nm) and $\overline{b}(\lambda)$ (435.8 nm) (figure 11). Because the reproduction of a color is done by adding emission spectra together, the RGB system is an additive color system. Negative values at wavelength λ mean that the stimulus of that wavelength could not be reproduced with the used primaries, and the color matching had to be done by adding a correct amount (the absolute value of the function) of the correct primary color (function with the negative value) to the monochromatic test light. In wider sense the negative values of the functions mean that only a certain portion of all colors visible to human eye can be reproduced with the given primaries.

Thereafter several slightly different RGB spaces, each with more or less different primaries and thus reproducible color space, have been developed for different purposes and requirements. Nowadays the most common RGB spaces seem to be Adobe RGB and sRGB, the latter consisting of slightly smaller amount of colors, especially green and cyan shades. Still, sRGB is typically the standard or default color space in most typical applications, so it was also used in this work. However, regardless of the color space standard used to calculate the color coordinates, the final reproducible color space is always determined by the physical primaries of the display equipment used.

The color matching functions of the first RGB space were normalized so that

$$\int_0^\infty \overline{r}(\lambda)\,\mathrm{d}\lambda = \int_0^\infty \overline{g}(\lambda)\,\mathrm{d}\lambda = \int_0^\infty \overline{b}(\lambda)\,\mathrm{d}\lambda \tag{30}$$

In addition to coordinates R, G and B calculated according to equation (28), the chromacity coordinates r and g of the colors were also defined through R, G and B:

$$r = \frac{R}{R+G+B} \tag{31a}$$

$$g = \frac{G}{R+G+B} \tag{31b}$$

It is possible to define and calculate also the value of b similarly, but it makes no difference, since r and g are known and $r + g + b = 1$ by definition. (See also figure 12.)

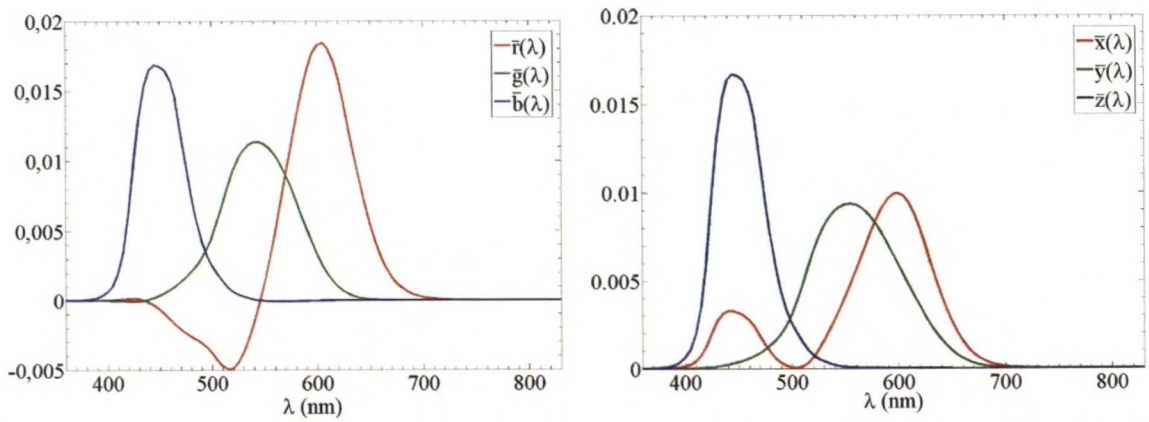

Figure 11: The CIE1931 RGB and XYZ color matching functions scaled so that integrals (30) and (35) are equal to unity in all cases.

After the RGB space was developed, a number of people of the commission wanted to develop a new color space that would be related to the RGB space through a linear transformation. The new color space would be defined by color matching functions $\overline{x}(\lambda)$, $\overline{y}(\lambda)$ and $\overline{z}(\lambda)$. The basis of the new color space was the assumption that Grasmann's laws would be valid. In addition to this, the new color space would have the following properties: [78]

1. At that time, the computations were done by hand or slide rule, so the new functions would have only positive values to simplify calculations.

2. The new function $\overline{y}(\lambda)$ would be equal to the photopic luminosity efficiency function $V(\lambda)$ for the CIE standard photopic observer. It was not guaranteed that the function could be constructed exactly as linear combination of the RGB color matching functions. However, this might be expected due to the near-linear nature of human sight. The reason for this requirement was again computational simplicity.

3. It was required that $x = y = z = 1/3$ for a constant white spectrum (equal irradiance at all wavelengths). (Defined from X, Y and Z similarly to r, g and b in equation (31). Note that this equality holds for also r, g and b of the CIE RGB space.)

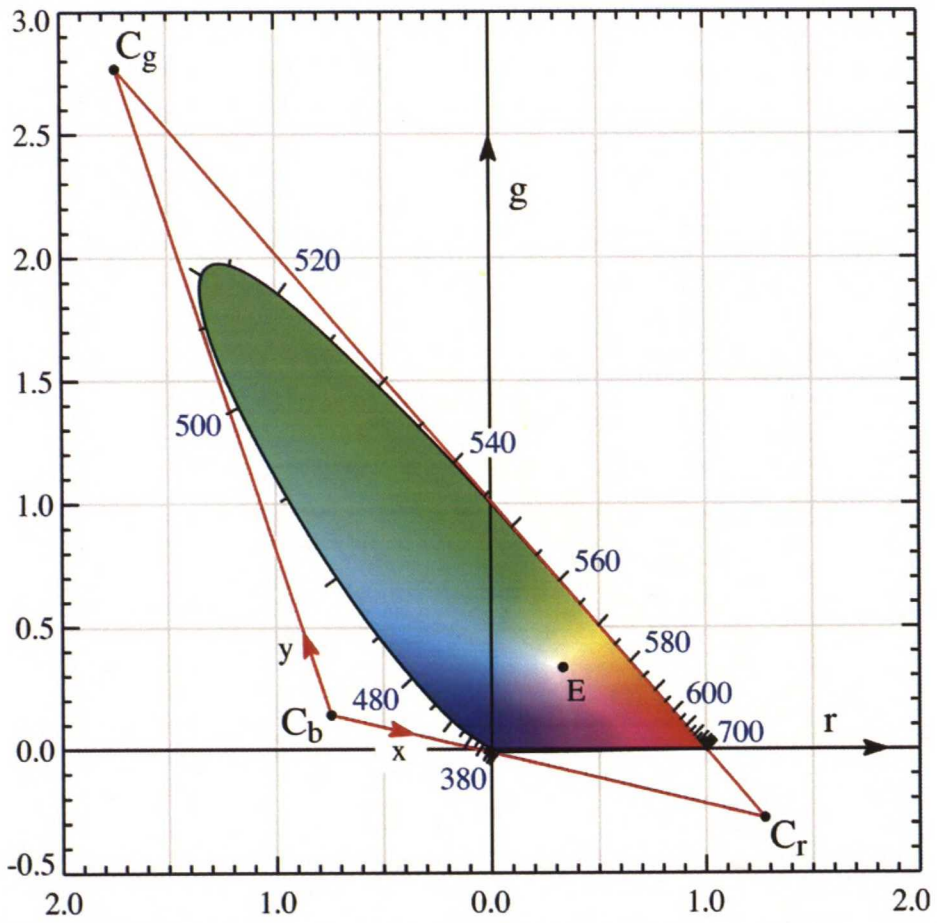

Figure 12: The CIE1931 chromacity space showing the triangles specifying the CIE XYZ and CIE RGB spaces. The triangle C_b, C_g, C_r equals to points (x,y) = (0,0), (0,1), (1,0). The points inside triangle (r,g)=(0,0), (0,1), (1,0) are the chromacities possible to reproduce using CIE RGB space. Point E is the chromacity of a constanct white spectrum; (1/3, 1/3) in both spaces, even if it may not appear to be so in the case of (x,y). Figure from Wikipedia [77].

4. Due to the definition of chromacity and the requirement of the positive values of x and y, it can be seen that the gamut of all colors will be inside the triangle (0,0), (1,0) and (0,1) (figures 14 and 12). It was required that the gamut would fill the space as completely as possible.

5. It was found out that function $\overline{z}(\lambda)$ could be set to zero at wavelengths above 660 nm and the results would still be within experimental errors. Again, for computational simplicity, this was specified to be the case.

The resulting linear transformation was:

$$\begin{bmatrix} X \\ Y \\ Z \end{bmatrix} = \begin{bmatrix} 0.49 & 0.31 & 0.20 \\ 0.17697 & 0.81240 & 0.01063 \\ 0.00 & 0.01 & 0.99 \end{bmatrix} \begin{bmatrix} R \\ G \\ B \end{bmatrix} \tag{32}$$

Similarly, the known XYZ coordinates can be transformed into RGB coordinates by multiplying with the inverse matrix of the transformation matrix. This is by no means a universal transformation to all RGB spaces and a different transformation matrix has to be used in each case. For the CIE XYZ and sRGB the transformation is [79] (See also figure 13.)

$$\begin{bmatrix} R \\ G \\ B \end{bmatrix} = \begin{bmatrix} 3.2406 & -1.3572 & -0.4986 \\ -0.9689 & 1.8758 & 0.0415 \\ 0.0557 & -0.2040 & 1.0570 \end{bmatrix} \begin{bmatrix} X \\ Y \\ Z \end{bmatrix} \tag{33}$$

The fact that the white point of sRGB and CIE XYZ/RGB color spaces is not the same, is visible in the sums of the rows of the transformation matrix; none of them equals to unity, so the chromacity of the white point of CIE XYZ/RGB spaces is not perfectly white in sRGB space, and vice versa. The white point of sRGB space is the standard illuminant D65 that is a simulated solar spectrum that approximately corresponds to midday solar irradiation in Western/Northern Europe and its color temperature is 6504 K.

The effect of different white points becomes apparent, when the coordinate values are normalized. Without normalization it would be practically impossible to determine the intensity or brightness of any color, i.e. to know whether a color is dark gray or white. Therefore a white point is used to define the coordinate values corresponding to the brightest visible colors. For example the final R-coordinate, R_{fin}, is:

$$R_{\text{fin}} = S\frac{R}{R_{\text{W}}} \tag{34}$$

The R-coordinate corresponding to the color stimulus is R and the coordinate corresponding to the spectrum of white point is R_{W}. It is possible that $R_{\text{fin}} < 0$ or $R_{\text{fin}} > 1$ (when $S = 1$). In those cases the final value is set to be equal to either 0 or 1, depending on the case. The normalization to scale [0, 1] can be further scaled with constant S, if desired or needed. Because the final coordinate value depends on the white point, different white points will yield different chromacities for the same irradiation spectrum. (See also equations (31) and (38).) Otherwise the white point has no effect on the calculations done before normalization.

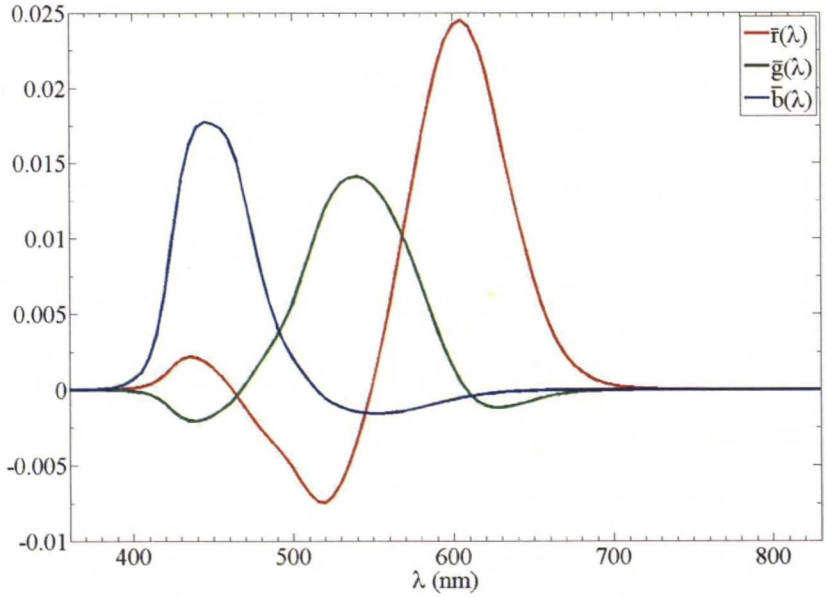

Figure 13: The color matching functions of sRGB color space calculated according to equation (33) from CIE $\overline{x}\,\overline{y}\,\overline{z}$ color matching functions in figure 11.

Due to the linearity of the integrand and integral, the linear transformation can be used as such directly to both coordinates (e.g. X) and color matching functions (e.g. $\overline{x}\,(\lambda)$) Because the sum of the coefficients on each row of the matrix of transformation from CIE RGB to CIE XYZ (equation (32)) is equal to one, it can readily be seen that:

$$\int_0^\infty \overline{x}\,(\lambda)\,\mathrm{d}\lambda = \int_0^\infty \overline{y}\,(\lambda)\,\mathrm{d}\lambda = \int_0^\infty \overline{z}\,(\lambda)\,\mathrm{d}\lambda \tag{35}$$

Chromacity coordinates x and y (and z) are defined similarly to r and g (equations (31)), and both chromacity spaces are shown in figure 12. The white regions in the figure correspond to imaginary colors that cannot be produced with any physical light spectrum that would consist of visible light. This illustrates that the primaries of the XYZ space are purely mathematical constructions, even if they are in a way based on physical primaries. Similarly to the white area, the colors, for which $r < 0$, $g < 0$ or $r + g > 1$ i.e. $b < 0$ are impossible to reproduce with the used RGB primaries. (See also figure 14 for comparison with sRGB space.)

Almost all monitors and graphic system produce the final image in some variation of the RGB system, because some physical light source has to be used in the end and RGB systems have the advantage of being the first and the most widespread standard. (Printed colors are produced in subtractive color systems, because inks absorb light. One common example of such systems is CMYK (cyan magenta yellow key) space.) With different intensities, a relatively large fraction of visible colors can be reproduced quite accurately (to trichromatic vision), but there are colors impossible to reproduce with such system, as in any finite-dimensional color space with physical light sources as primaries. The vastness

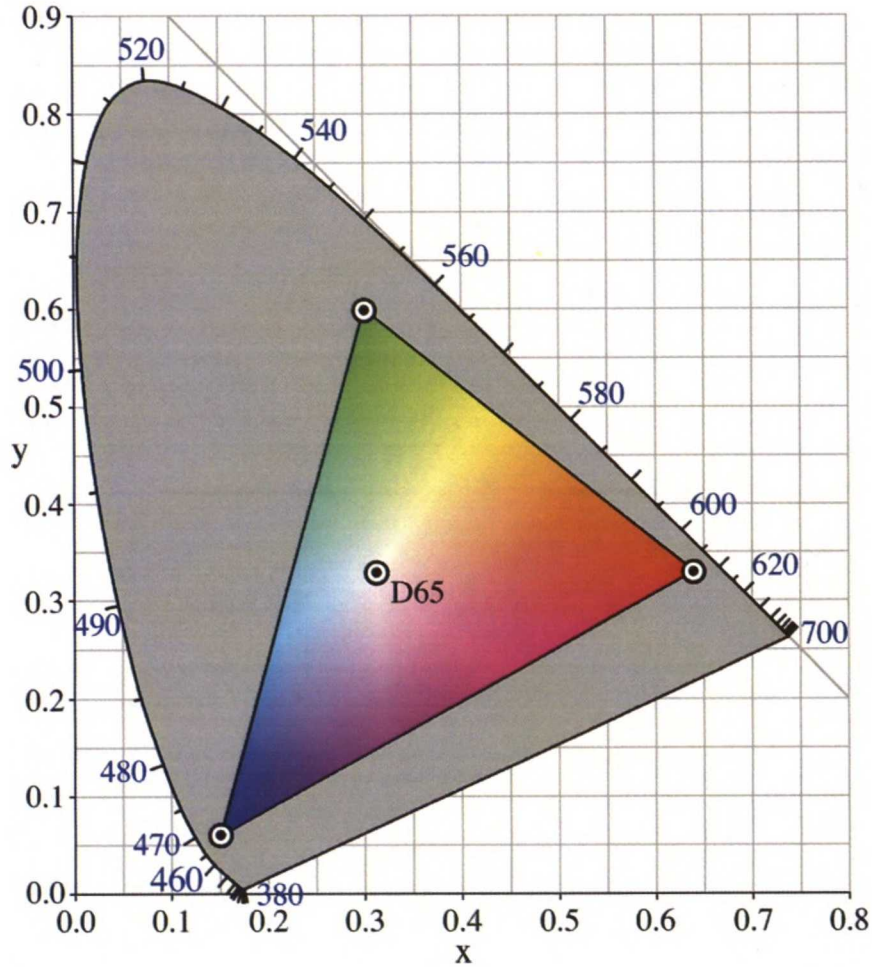

Figure 14: The area of visible light (gamut, gray) in CIE1931 xy-coordinates (see equations (31) and (32)) and sRGB-space (colored triangle) with the location of D65 standard illuminant spectrum (the white point of sRGB space). The monochromatic light sources (wavelength in nm) form the perimeter of the colors visible to human eye. Picture taken from Wikipedia [76].

of the reproducible color space depends on the choice of the primary colors: For example, the primary colors of the sRGB space are not monochromatic, so no monochromatic color (or a narrow wavelength distribution) is reproducible in sRGB space. This can be seen in the values of the response function of sRGB space: At any given wavelength at least one of the response functions has a negative value (figure 13), corresponding to negative intensity of the primary light source in question, which is physically impossible to realize. The monochromatic colors closest to some reproducible color are in the deep blue and yellow to red parts of spectrum, where the monochromatic perimeter is closest to the triangle of reproducible colors. (See figure 14.) This is not very serious limitation, but relatively small

amount of shades of cyan and green may limit the image quality in some situations. Also, all discrepancies between color space standard used to calculate the colors and the color space of the device showing the colors, will distort the colors due to the differences between assumed and real primaries.

3.2.4 Non-linearity of brightness in human vision

In general, the way humans experience the brightness of colors is nonlinear. Therefore it makes no sense to use linear scaling (equation (28)), when the accuracy is limited, as is the case in using integers to describe the colors. People could not distinguish between several consecutive bright color shades, so the color resolution in light areas would be unnecessarily high. On the other hand, there would be visible color bands in the dark areas of the pictures due to too low color resolution. Instead, it makes more sense to encode the colors approximately linearly with respect to the perceived (and assumed) brightness sensation. Within the luminance range that vision has adapted to, there is a certain discrimination threshold [70]. It has been found that for a wide range of luminances the discrimination threshold is about one percent difference in the luminance of adjacent color patches [70]. This means that discrimination capability of eye is nearly logarithmic as a function of luminance near the discrimination threshold [70]. However, it has been found that over a wider range of luminances, a power function is a better approximation of perceived brightness than logarithmic function [70]. Several different functions have been used to describe the relationship between the perceived lightness of a color and its luminance and there is no agreement on one function for all purposes, but they all have the same basic shape (that also the γ encoding function in figure 15 has). In 1976 CIE standardized the L^* function, which is a power function of the luminance modified by introducing a linear segment near black [70, 80]:

$$L^* = 116\, f\left(Y/Y_W\right) - 16 \tag{36a}$$

$$f(x) = \begin{cases} x^{\frac{1}{3}}, & \text{if } x > \left(\frac{6}{29}\right)^3 \\ \frac{1}{3}\left(\frac{29}{6}\right)^2 x + \frac{4}{29}, & \text{otherwise} \end{cases} \tag{36b}$$

This is also one of the basis functions of the CIE $L^*a^*b^*$ color space that has been developed to describe the way human vision system perceives colors. The value of function L^* describes the apparent brightness of the colors, and Y and Y_W are the luminance (Y-coordinate in XYZ space) of the color and the white point, respectively. This color system was not used in this work, because the colors would have had to be transformed into some RGB space in any case. Therefore, it did not make sense to add an additional intermediate step to calculations, when the step would not have given out any additional information.

Digital cameras record light using electrical sensors that typically respond to light intensity linearly. However, in the process of compressing the raw data to conventional RGB format, they encode the linear data according to a power function (equation (38)) or a function of similar shape. In particular, almost all standard RGB spaces and file formats

encode the intensities of the primary colors of the photographic reproduction non-linearly (gamma-compression). The historical reason for such practise is the characteristics of the electron gun of a cathode ray tube (CRT) device: The intensity of the light produced at the face of the screen (I) is proportional to the voltage input (V) to power 5/2 [70]:

$$I \approx A \cdot V^{2.5} \tag{37}$$

Factor A is a constant that depends on the exact characteristics of the device. Therefore, when image data is represented in values directly proportional to voltage, the original data that is linear with respect to intensity must be encoded with a power function, where $\gamma = 2/5 = 0.4$ in order to reproduce the original intensities:

$$C' = S\left(\frac{C}{C_{\mathrm{W}}}\right)^{\gamma} \tag{38}$$

Except for the exponent γ this procedure is identical to the normalization of the linear color coordinates (equation(34)): C corresponds to the color coordinate of the irradiation spectrum, whose color is being calculated, C_W is the coordinate of the white point and S is a scaling constant. The most typical values of S are 1 (decimal floating point values) and 255 (eight bit integers). Correspondingly, it should be possible to calculate the linear coordinate values, if the encoding (γ) is sufficiently well known:

$$\frac{C}{C_{\mathrm{W}}} = \left(\frac{C'}{S}\right)^{1/\gamma} \tag{39}$$

As mentioned before, the luminance is the inner product of the irradiance spectrum of the light source and function $\overline{y}$ defined by CIE, and thus proportional to the intensity of the light source. It is not readily visible, but L^* (equation (36)) is nearly equal to gamma encoding with $\gamma \approx 0.4$ [70]. (See figure 15.) Best overall fit is achieved with $\gamma = 0.42$ [70]. Yet, for example $\gamma = 0.40$ is a better fit when the light intensity is more than 20% of the peak white. No value of γ fits the function L^* exactly and the difference and its location (intensity) depends on the value of γ.

The characteristics of human vision and CRT devices mean that a voltage-based scale is also (approximately) linearly proportional to how bright human vision perceives the color. This convenient coincidence was probably one of the most significant reasons for encoding the colors approximately according to equation (38) with γ around 0.40 to 0.45. The combination of the characteristics of human vision and the historical vestige from CRT monitors with the use of integers in color systems means that the color coordinate values are typically gamma encoded values. In other words, value 0.5 does not correspond to $C/C_W = 0.5$ in equation (39), but to $C' = 0.5$ ($S = 1$) in equation (38). (See also figure 15: In the case of gamma encoding x–axis represents C/C_W and y–axis C', and vice versa with decoding.) Therefore a proper gamma encoding must be applied to the linear RGB coordinates calculated from linear spectral optical data, to create a realistic representation of color on the computer screen or printed media, or to compare the calculated RGB-values with RGB-values stored by a digital camera in an image file.

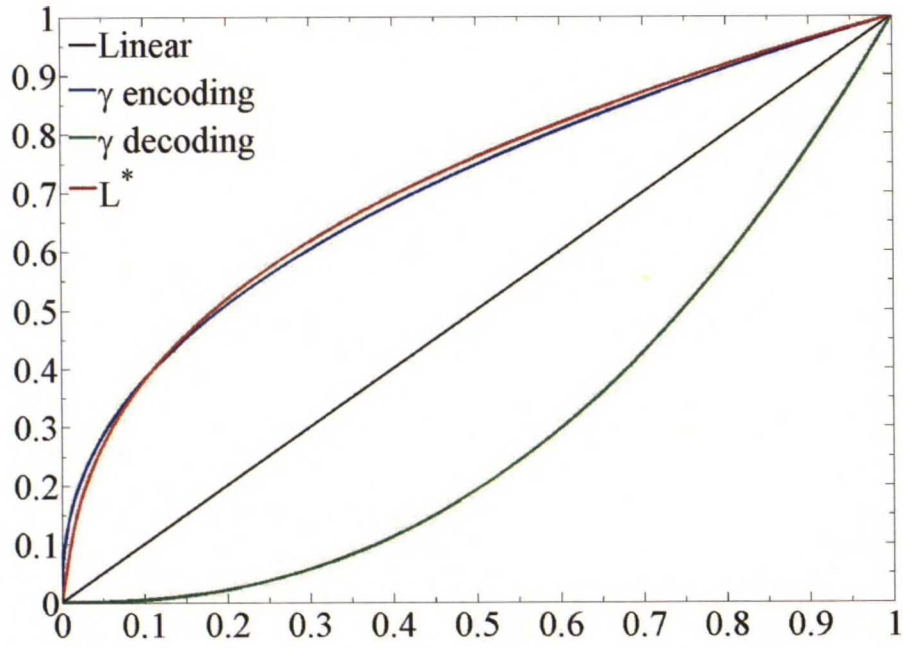

Figure 15: Encoding and decoding for $\gamma = 0.42$ and CIE L^* function (equation (36) normalized to 0–1). In this case $S = C_W = 1$ in equations (38) and (39). Linear encoding corresponds to XYZ and RGB values that are linearly dependent on the light intensity.

3.3 Experiments

The experiments were done to compare the calculations and predictions about the optical properties and appearance of the DSCs to real DSC samples. The most important measurements in this were the transmittance measurements of the DSC components and assembled DSCs and photos taken of the DSC samples. Also, the irradiance spectrum of the light source in the photos was measured to improve the accuracy of the calculations about the color the photographed samples. The IPCE spectrum of the assembled DSCs was also measured.

The transmittance and IPCE spectra were both measured with the same equipment, whose main function is the IPCE measurements (PV Measurements Inc., model QEX7). The wavelength interval in these measurements was 5 nm and, according to the manual of the equipment, the width of the wavelength distribution was 4 nm with the slits that were used in the monochromator in the measurements. The IPCE spectra were measured with the DC method (only monochromatic beam, no bias light). The reflectance spectra of all components, except for 1DPCs are from earlier measurements done with LI-COR 1800 spectroradiometer (licor) and an integrating sphere. The irradiance spectra of the light sources in the photos were also measured with licor. The wavelength interval in these measurements was 1 nm.

3.3.1 Optical samples

Three groups of 1DPCs with distinctively different optical properties were used in experiments. They were indexed according to their origin: Samples S1 & 2 and S3 & 4 were made in Instituto de Ciencia de Materiales de Sevilla (ICMS). Samples N1 – N10 were made by NLab Solar in Sweden. All 1DPCs were coupled with TiO_2 films, so their properties could not be measured directly. However, the TiO_2 films used as their substrates were screen printed at the same time with other TiO_2 films, so the effect of the 1DPCs on the total transmittance and reflectance could be calculated using the screen printed TiO_2 films. The transmittance spectra of the available screen printed TiO_2 films were practically identical to each other, so it could safely be assumed that the film under the 1DPC would also have similar optical properties. The screen printed PEs were all given a number (1–30) to identify them from each other. When referring to a sample as only PE, a "PE" is typically added in front of the sample number, e.g. PEN7 or PE19. When referring to an assembled DSC, prefix "DSC" is used, e.g. DSCN7, DSC19. If there is no prefix in front of the sample number (e.g. in figures), the sample in question is only a PE with no other DSC components.

3.3.2 Transmittance and reflectance of the solar cell materials and components

The transmittance of the 1DPCs was calculated from measured transmittance spectra of a PE without 1DPC (TCO, PE) and the PE coupled with the 1DPC in question (TCO, PE, 1DPC):

$$T_{PC} = \frac{T_{TCO,\,PE,\,1DPC}}{T_{TCO,\,PE}} \tag{40}$$

The transmittances in the fraction correspond to equation (15) with $T_{El} = T_{CE} = 1$ and $T_{TCO}(1 - R_{PE})e^{-\alpha d}$ equal to the transmittance of the TCO-TiO_2 combination without a 1DPC. If the properties of the TCO substrate and TiO_2 film are similar in both cases, the result should tell, how the 1DPC affects the transmittance of the PE. Since all TiO_2 films were screen printed similarly on similar TCO glasses, this assumption should be quite accurate. The reflectance of the 1DPCs was assumed to be $R_{PC} = 1 - T_{PC}$, so that the total reflectance of the PEs with 1DPC could be calculated from equation (16) by inserting $T_{El} = T_{CE} = 1$ and $R_{CE} = 0$.

The transmittance of all 1DPCs was measured from a dry sample, where the medium in the pores of the film was air (figure 16). In a complete DSC the pores are filled with electrolyte, whose refractive index differs from air. Therefore the reflectance and transmittance of the 1DPCs in DSC are different from those measured from dry 1DPCs in air. This was taken into account by measuring the transmittance of one 1DPC (sample N3) doused with 3MPN (the solvent of the electrolyte) and comparing the results to spectrum measured from the same sample without 3MPN. All samples were not measured with 3MPN, because it was not known, whether the dousing with 3MPN could affect dye adsorption or other properties of the PE. The reflectance spectra that were measured from dry samples

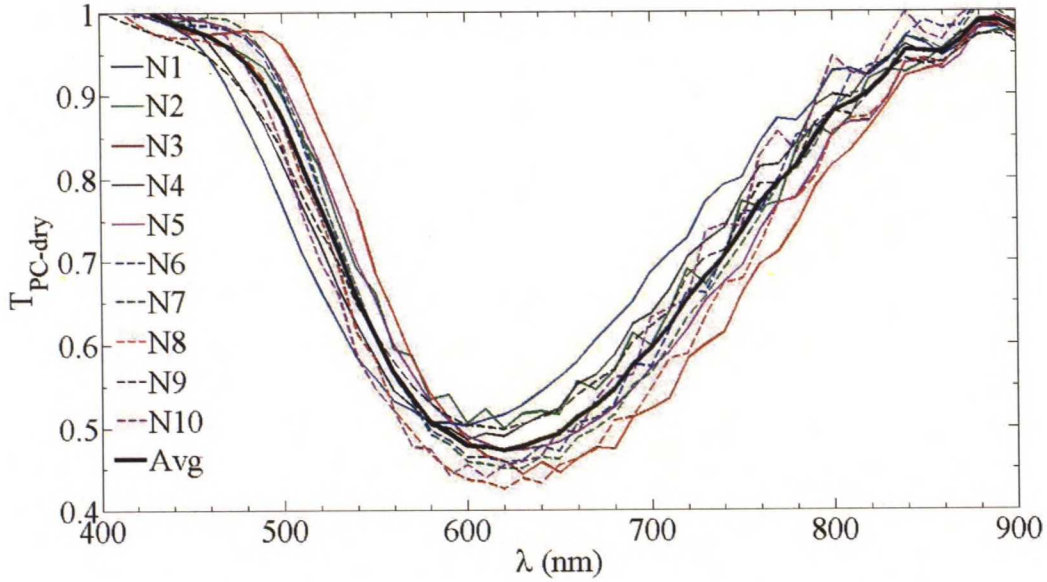

Figure 16: The transmittance of the dry N-1DPC films

were then corrected for calculations with electrolyte: The reflectance peak was shifted by the wavelength difference in the reflectance peaks of wet and dry sample. The reflectance spectrum was then multiplied with the ratio of the peak reflectances of wet and dry samples. In the case of samples similar to the one that was measured also with 3MPN (N1–N10) this should be a relatively good approximation, but there would quite likely be some errors caused by this method, when applied to different 1DPCs (S1–S4).

The reflectance peak turned out to be shifted to longer wavelengths by 80 nm and the peak reflectance was about 84.7% of the reflectance of the dry 1DPC. Reflectances and transmittances that seemed non-physical ($R, T < 0$ or $R, T > 1$) were set to be equal to either zero or one, depending on the case. However, it is possible to increase the transmittance of any sample by adding thin layers of material with proper refractive index and thickness, which would then appear as $T > 1$ for the added layers. This has occurred with similar samples and there is no reason, why it could not have occurred also with the samples used here [23]. Because the relationship between the wavelengths with increased transmittance and the properties of the 1DPC in question was not known and because the increase in transmittance has previously occurred at longer wavelengths, this detail was omitted from the calculations [23]. Also, the reflectance peak at wavelengths around 350 nm may be caused by the combination of TiO_2 layers in 1DPC absorbing light and the transmittance of the samples being low due to also substrate glass absorbing those wavelengths. Because of the assumption $T + R = 1$ used to calculate the reflectance of the 1DPC layer, the light absorbed by 1DPC would appear as increased reflectance.

The reflection from the visible surface of the film and air/solvent/electrolyte may be different in the cases of TiO_2 and 1DPC, because the 1DPCs consist of alternating layers of SiO_2 and TiO_2 [23, 26]. It is also possible that the reflection is quite similar, if the

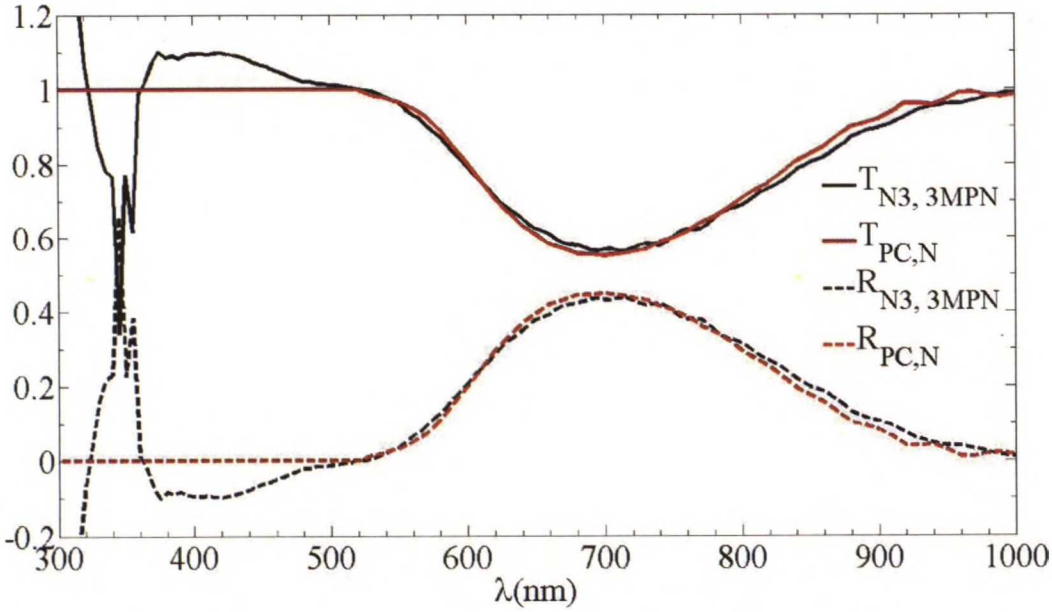

Figure 17: The measured reflectance and transmittance of wet 1DPC sample N3 and the fits for the reflectance and transmittance of the average of N-1DPCs.

interfacial layer consists of TiO_2 particles [23, 26]. Unfortunately the surface layer was not known certainly, but the reflectivity of the 1DPCs is so large that small variations in this should not have significant effects on the results.

The calculated transmittance of wet sample N3 and the calculated fit for the average of the N-1DPCs are shown in figure 17. Comparison with figure 16 shows that the fit for the average transmittance will likely predict most of the 1DPCs relatively well, but there may be some problems with 1DPCs, whose reflectance peak differs most from the average – peak value, wavelength of the peak or both.

The absorption coefficient spectra of the dyes used in experiments were measured from dyed TiO_2 films. The transmittance of the films was measured before and after dyeing and the absorption coefficient was then calculated from the ratio of the transmittances adjusted with the change in the reflectance of the PE, when dyed (figure 7 and equation (15)). In addition to this, the absorption coefficient of the used organic dyes was measured in 3MPN to see, if there would be any difference to literature values measured in ethanol solution. The measured spectra turned out to be identical to literature values, so the solvent of the dye solution did not seem to affect the light absorption in this case. (See figure 18.)

The transmittances of TCO glass and CE were measured directly from a correct glass substrate dampened with 3MPN and covered with a cover glass slide. The reflectance at the interface of the cover glass and air was taken into account to calculate the transmittance of only the sample in contact with 3MPN from the measured total transmittance. The reflectance could not be calculated from this data, but comparing the transmittance data to earlier measured data showed both sets to be similar enough that old data for reflectance (figure 20) could be used. Also, because the reflectance of the DSCs could not be measured

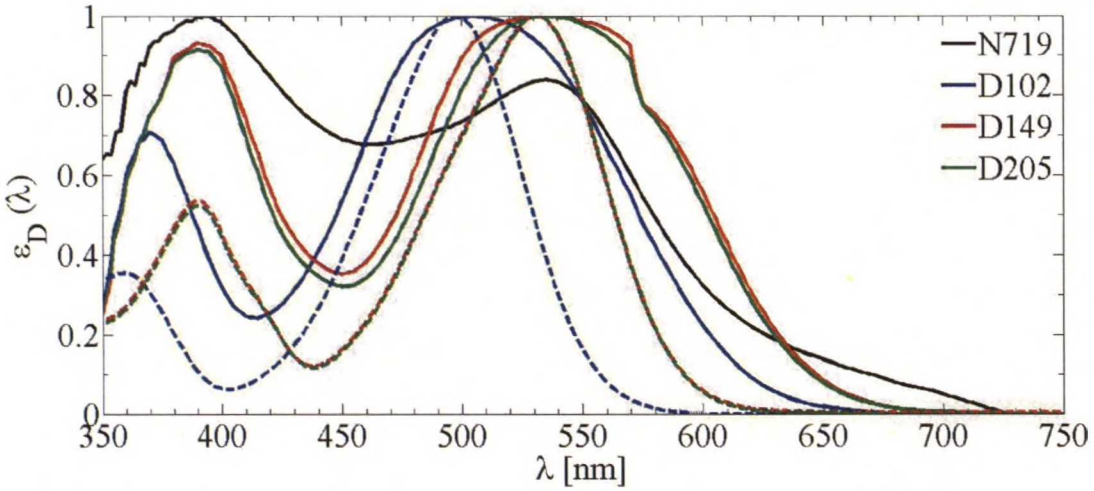

Figure 18: The relative molar absorption coefficients of the dyes adsorbed on TiO_2 and wetted with 3MPN (solid) and in 3MPN solution (dash). In the case of N719 data about absorption in solution was not needed.

as accurately as the transmittance, it was considered more important to be able to calculate the transmittance accurately than to have all optical data about a cell component from same measurements.

In the case of electrolyte the absorption coefficient had to be calculated in order to have the necessary information for the transmittance of the electrolyte (equation (11)) and the total absorption coefficient of the PE (equation (12)). This was done by measuring the transmittance of two samples, both consisting of two microscope glasses and sealant. One was filled with electrolyte and the other with 3MPN. The distance between the glasses was known with adequate accuracy and was same in both cases, so $\alpha_{El}(\lambda)$ (figure 20) could be calculated directly from the ratio of the transmittances of the samples.

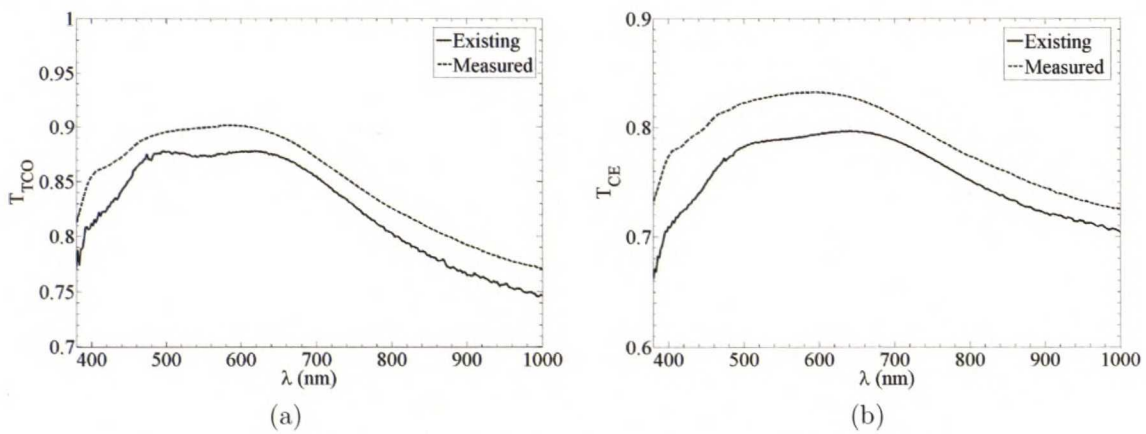

Figure 19: The pre-existing and measured transmittance data of a) TCO and b) CE substrates. The differences between TCO and CE are caused by a thin Pt coating on the TCO in the case of CE.

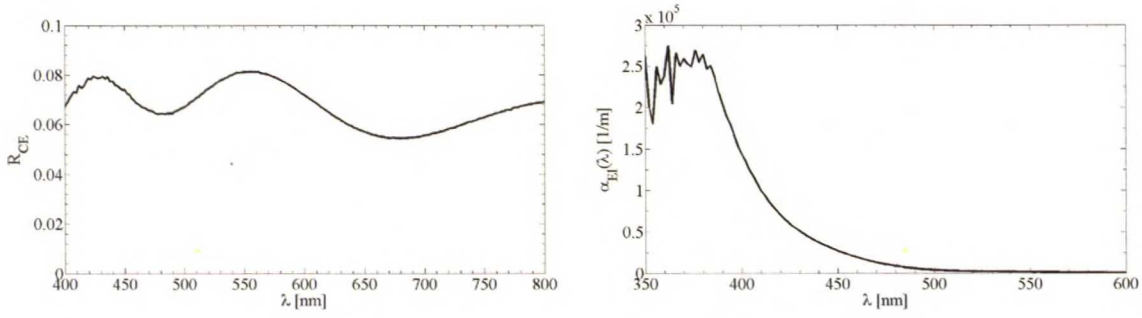

(a) (b)

Figure 20: a) Reflectance spectrum of the CE. b) The absorption coefficient of the electrolyte corresponding to 50 mM I_3^- concentration.

3.3.3 Calculating the performance and color of DSCs with given transparency

When the transmittance of the solar cells depends on the wavelength of the light, its transparency is not unambiguous, but can be defined according to either light intensity or the brightness of the light. The brightness of the light is not a physically clear concept, and may depend on the viewer, but the L^*-function (equation (36)) of the CIE $L^*a^*b^*$ is considered to describe the apparent brightness of light sources. For simplicity, the brightness transparency was defined according to the luminance of the transmitted light, i.e. the Y coordinate in the XYZ space.

The luminance transparency of a DSC was defined as the fraction of the transmitted and incident luminance:

$$T_{\text{eye}} = \frac{\int_0^\infty I_0(\lambda)\, T_{\text{DSC}}(\lambda)\, \overline{y}(\lambda)\, \mathrm{d}\lambda}{\int_0^\infty I_0(\lambda)\, \overline{y}(\lambda)\, \mathrm{d}\lambda} \tag{41}$$

Function $\overline{y}(\lambda)$ is the color matching function corresponding to the Y coordinate in XYZ color space, but also the standard luminosity function of photopic vision. This definition is identical to the definition of the transmittance perception of the human eye that has been used before in the calculations about the organic solar cells [34]. The apparent brightness of the transmitted light would be given by equation (36). As figure 15 shows, values as low as 0.2 would appear relatively bright and anything over 0.3 would probably be sufficiently bright for most lighting requirements in daytime. The transparency depends also on the shape the irradiance spectrum $I_0(\lambda)$. Air-mass 1.5G (AM1.5G.) spectrum was used in all transparency calculations due to its status as the standard spectrum for operating conditions of solar cells. Generally, any spectrum representing the illumination conditions can be used.

Alternatively, the transmittance can be defined as the fraction of transmitted light intensity. Because optical data outside wavelength range 300 nm–1000 nm was not available,

it was decided to limit the definition to be the transmitted portion of the energy contained by the visible light and the shortest wavelengths of the near infrared:

$$T_{\mathrm{E}} = \frac{\int_{380\,\mathrm{nm}}^{900\,\mathrm{nm}} I_0(\lambda)\, T_{\mathrm{DSC}}(\lambda)\, \mathrm{d}\lambda}{\int_{380\,\mathrm{nm}}^{900\,\mathrm{nm}} I_0(\lambda)\, \mathrm{d}\lambda} \tag{42}$$

In the case of wavelength-independent transmittance (matrix transparency with glass and opaque solar cells) luminance transparency and intensity transparency of a PV panel are equal to each other. Otherwise there is no analytic relation between the luminance and intensity transparencies that could be calculated with sensible effort.

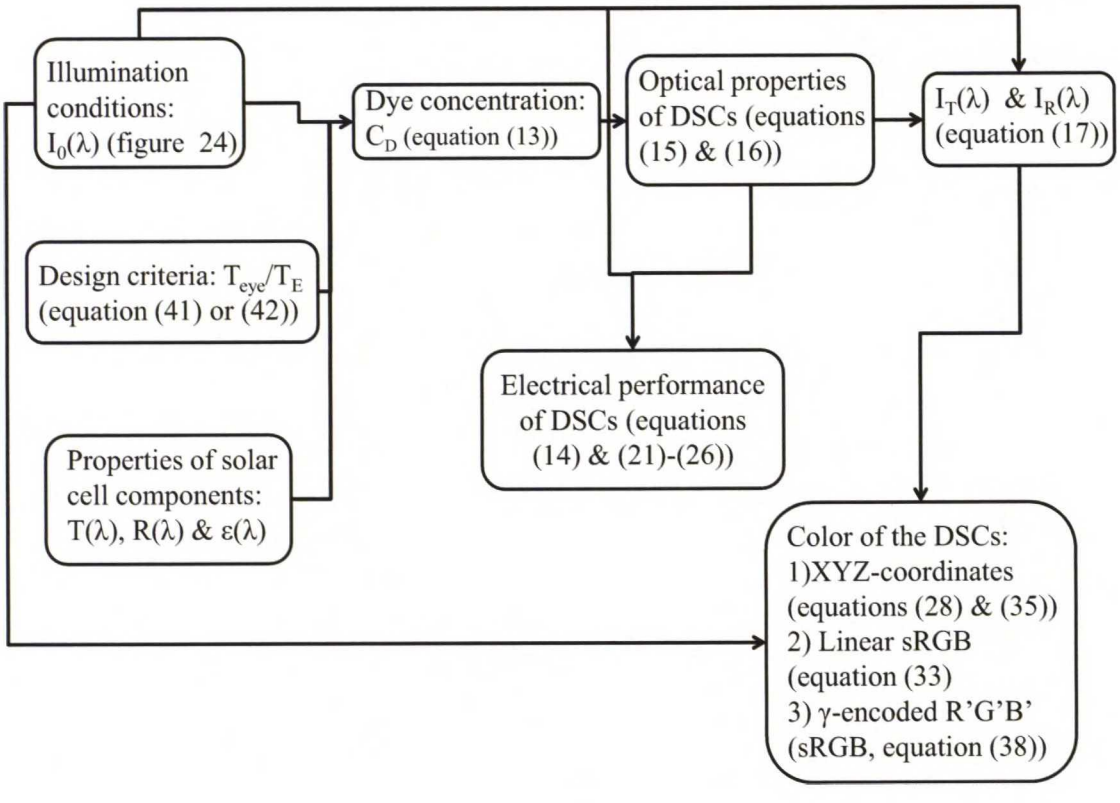

Figure 21: The calculations about the color of the samples and DSCs

The starting point of the calculations was a preset transparency (T_{eye}, equation (41)). The concentration of the dye was adjusted to change the absorption coefficient of the dye (and PE film) so that the transmittance spectrum of the complete DSC matched the transparency requirement. The optical properties of other components were kept constant at the measured values. In practise this calculation order corresponds to a case, where the light transmitted through for example a window or a skylight must be bright enough and/or contain some amount of energy. The options that do not fulfil the requirements are

ignored, and the final choice is made between DSCs with varying appearance and efficiency, but similar transparency.

The transmitted color was calculated assuming that there would be only one light source facing the PE of the DSC, and the color of the DSC would be determined by the transmitted light. The real life situation corresponding to these conditions is that the cell is placed as a window and viewed from the inside of a dark room, so no light is reflected from the surface of the cell facing the viewer. The reflected spectrum in turn was calculated assuming that there would be no light sources behind the cell and thus only the reflected light affects the color of the cell. This corresponds to viewing the cell from outdoors at bright daylight with no light source or only comparatively dim light behind the cell. In façade applications, the spectrum is likely to be a combination of some transmitted and reflected spectrum.

In the different DSC compositions the properties causing variations were the 1DPC, dye and the concentration of the dye. In all 1DPC-dye combinations the concentration of the dye was the factor that determined the final properties of the DSC. The effect of the concentration on the absorption coefficient was assumed to be linear according to equations (12) and (13). Therefore it was not necessary to know the exact value of $\alpha_D(\lambda)$ calculated from a TiO_2 film, but the relative spectrum was sufficient, and concentration term (C_D in equation (13)) signified the maximum value of the absorption coefficient instead of the actual concentration. The upper limit for the transparency of the DSC, obtained with an undyed TiO_2 film, is given by the other components of the cell. The case without a 1DPC was also calculated.

When the optical properties of the DSCs were known, calculating their color was a relatively simple and straightforward process. (See figure 21.) The only complication was the normalization of the linear RGB values. The white point of sRGB space is the D65 standard illuminant, which could of course be used as the light source and white point in most calculations. However, as the calculations were compared to photos taken in real life conditions, using the solar spectrum measured at the conditions where the photos were taken would enable more accurate results. Hence, a measured solar spectrum was used as the white point in the case of 1DPC samples. In the case of DSCs the white point was the irradiation spectrum of the halogen lamps used as the light source, when taking the photos. The spectrum of sunlight was close enough to white and D65 (figure 24) that it could be used as such to normalize the RGB values, especially because the eyes define white according to it. The spectrum of the lamps is a bit questionable choice, but since their light appeared white to naked eye, it was considered to be a good enough white point. Small variations from white in overall illumination do not typically show in the colors that people see. In addition to these issues with white point, the exact encoding of sRGB space is not a power function, but a piecewise defined function. However, $\gamma = 1/2.2 \approx 0.455$ (equation (38)) fits this function very accurately, and was thus used [79]. The encoding process was done separately for each component.

In addition to the components of the DSC, the irradiance spectrum also affects the transparency of the DSCs (equations (41) and (42)). As the incident irradiance spectrum most likely is the spectrum of solar irradiation, this effect may not not always be noticed,

but at times it may require small adjustments to be made to the dye concentrations or transparency values.

3.3.4 Simulation parameters

This section includes a list of simulation parameters and variables that were needed for the calculations, the values used and the reason for using those values. The parameters related only to electrolyte diffusion are presented and discussed in section 4.2.2.

The electron injection and regeneration efficiencies were assumed to be 100%, because the purpose of the calculations was to give an upper limit to the power the DSCs could possibly generate, with the exception that electron collection losses were accounted for by an electron diffusion length of 20 μm (compared to film thickness of 5.3 μm). Because the effects of diffusion were not included in these calculations, it did not really make sense to even attempt to make "realistic" calculations about the true efficiency of the configurations. The difference in the potential of the different designs could be seen already in the maximum photocurrent that could be extracted from the cells.

Table 1: The simulation parameters in the calculations about the optical properties and color of DSCs with different dyes.

Parameter	Symbol	Value	Estimation
TiO_2 film thickness	d, d_{TiO_2}	5.3 μm	Profilometer
1DPC thickness	d_{1DPC}	0.6 μm (if included in the DSC configuration)	Profilometer
Bulk electrolyte thickness	d_{El}	25 μm $-d_{TiO_2} - d_{1DPC}$	Assumption
Transmittance of the PE substrate	T_{TCO}	Figure 19	Measured
Transmittance of the CE (with Pt)	T_{CE}	Figure 19	Measured
Reflectance of the TiO_2 film	R_{PE}	Figure 7	Measured
Reflectance of the 1DPC	R_{PC}	Figures 17 (Ns, wet) and 26 (dry)	Measured
Reflectance of the CE	R_{CE}	Figure 20	Measured
Absorption coefficient of the electrolyte	α_{El}	Figure 20	Measured
Absorption coefficient of the dyes in TiO_2 film	ϵ_D	Figure 18	Measured
Electron diffusion length	L	20 μm	Assumption
Exchange current density of the electron recombination recombination	$i_{REC,0}$	$4.20 \cdot 10^{-4}$ A/m^2	[32]
Electron injection efficiency	η_{Inj}	1	Assumption
Dye regeneration efficiency	η_{Reg}	1	Assumption
Ideality factor	m	2.1	[32]
Ambient Temperature	T	293.15 K	Assumption
Incident photon flux	$\phi(\lambda)$	AM1.5G; 1000 W/m^2	Assumption

3.3.5 Experimental verification of the colors

The calculations about transmitted color were verified by placing the samples so that they were illuminated only by light that was reflected from white paper. In the case of 1DPCs the reflected light was sunlight that was transmitted through a glass window, but in the case of DSCs halogen lamps had to be used due to date and weather. These spectra together with D65 and AM1.5G are shown in figure 24. Originally also the DSCs were photographed in sunlight, but those photos were overexposed, and therefore could not be used in accurate comparisons with calculations, so new ones had to be taken later. Due to this delay between cell assembly and photos, small increase in transmittance could be seen by comparing the spectra measured immediately after assembling the cell (figures 28, 31, 33 and 34) and at

the time the final photos were taken (not shown). However, the differences were typically at most a couple of percents, which would not affect the color significantly. Only in the case of DSCs 22 and 23 there were larger differences around 650 nm, but even then the relative difference was less than 10%. Considering function $\overline{r}(\lambda)$ in figure 13, this should affect R only little.

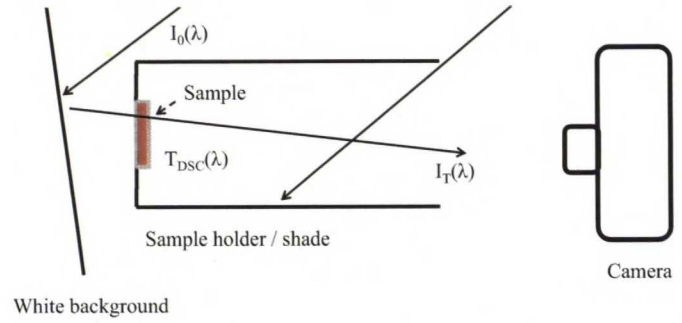

Figure 22: The cross section of the arrangement for photos. The solid arrows illustrate the light propagation.

The samples were inside a box made of black cardboard, whose bottom had an opening, through which light could pass unrestricted. The samples were attached to the bottom so that they covered this opening. The box was placed at a small distance from the white surface so that the light passing through the opening would have relatively high intensity. (See figures 22 and 23.) The walls of the box were aligned so that they would prevent all but practically horizontally propagating light from reaching the sample, because the inside walls reflected almost no light. In the case of DSCs the halogen lamps were the only light source in the room, where the photos were taken, so possible reflections from the surface of the DSCs should be negligible.

The sunlight used with 1DPCs had passed through a glass window, so it is likely that some of the light had been reflected away or absorbed by the glass. The reflection is most likely almost independent of the wavelength, but the absorption should affect only near UV and the shortest wavelengths of the visible light, so the relative spectrum was slightly different from both D65 and AM1.5G. The spectrum of the direct sunlight is not visible in figure 24, but it was measured and used to calculate the reflectance of the white cardboard (figure 25), which expectedly turned out to be almost constant across the visible light range. Therefore the relative spectrum of the reflected light represents the differences between standard spectra and the measured spectrum quite well. The spectrum of the reflected sunlight is the average of two spectra with slightly different intensities, but practically identical shape.

The photos turned out to be slightly underexposed with both 1DPCs and DSCs, which posed no serious problems: It was relatively easy to scale values again so that $T = 1$ would correspond to something less than 1 (or 255) without loosing too much information, because the RGB values of $T = 1$ were known. In the case of overexposure, information about the brightest colors were lost, and with that the exact knowledge of what transmittance

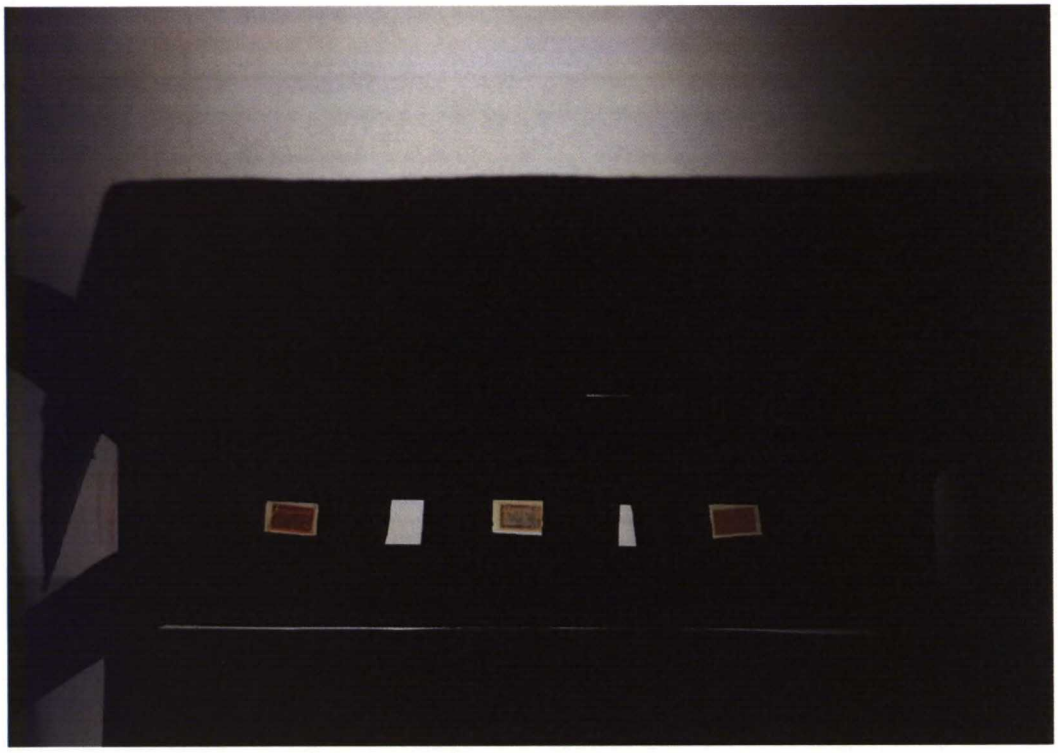

Figure 23: Example of the photos taken of the DSCs. From left to right DSCN10, DSCN2 and DSC27.

corresponds to what RGB values. Results from overexposed photos were therefore omitted.

The photos were taken with Olympus E-620 camera in raw format. The color balancing was done with X-Rite color checker passport: The white balancing was done first by taking a photo of a large, uniform gray area in the color checker that was supposed to reflect 18% of all incident wavelengths. This was confirmed by a quick and simple measurement, where the irradiance reflected from white cardboard and the color checker were compared to each other (figure 25). After white balancing the other coloured squares in the color checker were photographed, and these photos were used later to correct the color balance in the photos and to determine the color of the samples in the final pictures. The software used for this purpose was Adobe Photoshop Lightroom 3.

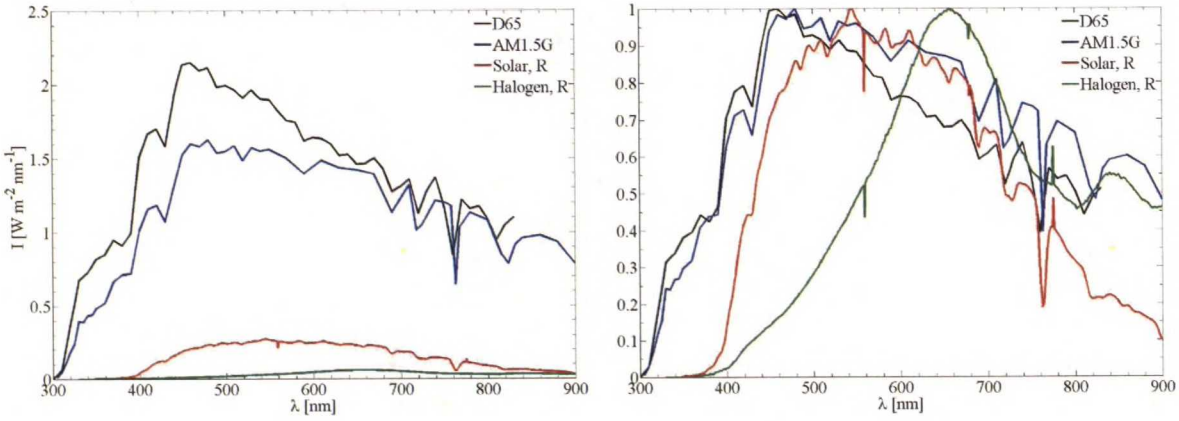

Figure 24: The irradiance and normalized irradiance spectra used in calculations: D65 standard illuminant, AM1.5G, irradiation spectrum of sunlight transmitted through a window and reflected from white, glossy cardboard (average) and the irradiance of halogen lamps reflected from white paper. The relative irradiation spectrum of D65 is not hard to find, but apparently the total intensity of the spectrum is not defined, or it is very hard to find. The best approximation that could be found was normalized to have the same spectral irradiation as AM0 spectrum at 560 nm [81].

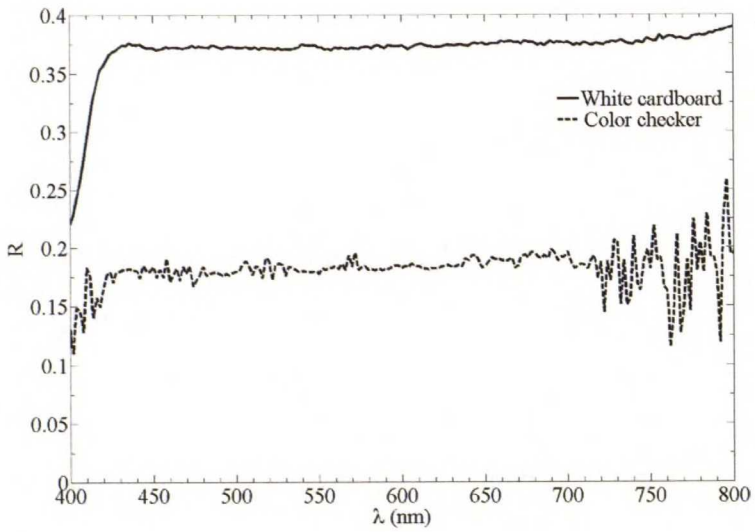

Figure 25: The reflectance spectrum of the white cardboard and the color checker (18% gray) used for white balancing. The irregularities at longest wavelength are most likely due to inaccuracies in the measurement. (Variations in lighting conditions, different sizes of color checker and white cardboard, etc.)

3.4 Results and discussion

The accuracy of the results is self-evidently one of the most important evaluation criteria for any simulation model. The calculations carried out about the optical properties and color are no exception in that regard. The evaluation can be divided into three parts:

- The accuracy of the color calculated for a transmittance/reflectance spectrum
- The accuracy of the transmittance spectrum calculated from the optical data of the component materials
- The combination of the two: the accuracy of the color calculated for a calculated transmittance/reflectance spectrum

The first part of the evaluation was done with dry 1DPC samples, because their transmittance spectrum could be measured simply and accurately. Also, the transmitted light would have a distinctive color that could be used for visual comparison. The second and third part were evaluated more or less together with complete DSCs, because the final goal was to be able to accurately predict the properties of the DSCs from the properties of their components and materials.

3.4.1 Color characterization of photonic crystal samples

The first evaluation criterion of the calculation method was the accuracy of predicting the color of 1DPC samples and plain TiO_2 in illumination conditions described in section 3.3.3. The transmittance spectrum of each sample was measured, so the accuracy of the results would reflect the accuracy of the calculations about the color of an irradiance spectrum in known illumination conditions. The first calculations were quite close to photos taken, but only by luck: Because the samples were relatively transparent, the linear encoding did not produce too large errors. (See figures 15, 26 and 27. Transmittance in figure 26 is comparable to x–axis in figure 15.) When gamma encoding was added to calculations, the results became more accurate (figure 27).

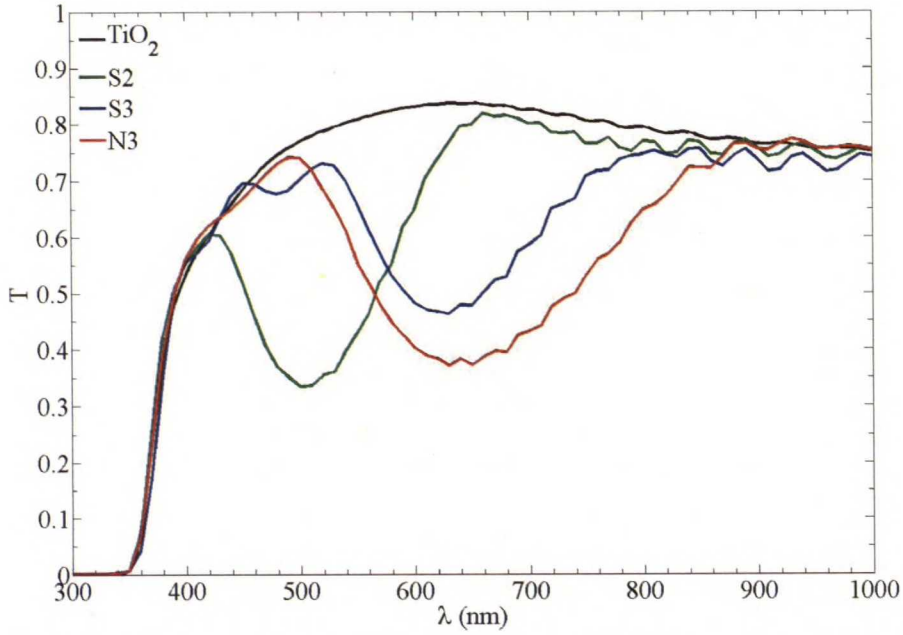

Figure 26: The transmittance spectra of TiO_2 film and 1DPC samples used in calculations. (Complete, dry PEs, not just the 1DPC film.)

Table 2: The RGB values of the samples in the photo (figure 27) and the gamma encoded RGB values with and without the correction for the observed background brightness, in order (R, G, B). Note that the calculated colors of 1DPCs shown in figure 27 do not correspond to these values, but to the averages of the sample groups indicated at the bottom of the figure.

Row\Sample	TiO_2	S2	S3	N3
a)	(226, 228, 227)	(231, 161, 185)	(170, 214, 217)	(148, 202, 226)
c)	(243, 241, 237)	(235, 175, 202)	(172, 222, 237)	(145, 220, 240)
d)	(225, 226, 222)	(228, 164, 189)	(160, 208, 222)	(135, 199, 224)

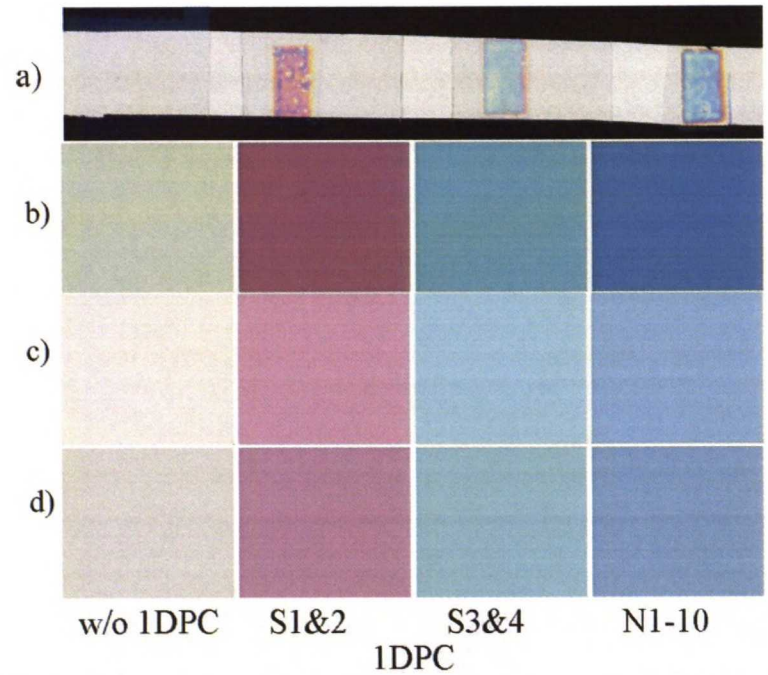

Figure 27: Colors of different PEs and the effect of gamma encoding and color of the lighting. a) Photo of samples in, b) calculated colors without gamma correction, c) gamma corrected colors and d) gamma corrected colors with the correction for the observed brightness of the background in photo. Samples in photo, from left to right: TiO_2 on FTO glass, 1DPCs: S2, S3 and N3.

The gamma encoded RGB values did not exactly match the values extracted from the photo, but the largest error in a single color coordinate was less than 10%, and in general the calculated coordinates seemed to be around 5% larger than determined from the photo (table 2). The unencoded values were too dark by larger margin (data not shown).

The source for differences in RGB values is a bit unclear, but most likely related to how the camera and software do white and color balancing compared to white balancing in calculations. The RGB values of the background in the photo were on average (237, 239, 238). In the calculations (a) – c) in figure 27) the background was assumed to be (255, 255, 255). This difference is caused by the camera and its settings, i.e. how bright it considers some intensity to be. Taking this difference between real and assumed brightness of the background into account improved the accuracy in most cases, but decreased it in a couple of cases. (See table 2 and figure 27.) Some of the error may be related to the fact that the measured transmittance of the samples was not used as such; The transmittance and reflectance of the coupled layers of TiO_2 and 1DPC films were calculated with the knowledge of the average transmittance spectrum of the TiO_2 films. The transmittance of the sample was calculated by multiplying the transmittance of the 1DPCs by the transmittance of the TiO_2 film used in calculations. (This is also how the transmittance of the DSCs was later calculated.) The TiO_2 film used in calculations may have been slightly different from the

one coupled with 1DPC, which might have caused small errors. The difference between the real sRGB encoding and encoding with $\gamma = 1/2.2$ (comparable to L^* and gamma encoding in figure 15) may also explain some of the errors, but most likely less than rounding the calculated values to integers does.

When the R components of S3 and N3 are ignored, the match with the photographs is excellent, when background brightness is taken into account. Therefore the calculation method from transmittance of DSC to the color of the transmitted light seems to be reasonably accurate, when the lighting conditions are known sufficiently well. As rows c) and d) in figure 27 demonstrate, even small differences between real and assumed light intensity in photo will affect the color visibly. In other words, if the lighting conditions can be controlled well enough, the accuracy of predicting the perceived color of DSCs should be limited only by the accuracy of predicting the transmittance spectrum of the solar cell from the optical properties of its components.

To study this in more detail, optical characterization and modeling was carried out for complete DSCs employing different dyes with and without 1DPC and compared with photography at controlled conditions using the same methods as discussed above. The results from this are discussed in the following section.

3.4.2 Color characterization of DSCs

Predicting the transmittance of the DSCs required knowing the spectrum of the absorption coefficient of the dyes that were used. It was not necessary to know the exact concentration or amount of dye compared to some typical amount, so the relative spectrum was sufficient. (See figure 18 for the measured spectra.) Therefore the dye concentration in equation (13) meant only the highest value of the absorption coefficient in the PE in question.

The DSCs were assembled from PEs that were dyed overnight in dye solution. The dye concentration in TiO_2 was not controlled, nor was it measured during dyeing. Two PEs were dyed for each assembled DSC at the same time, because one of them was used to determine the absorptivity of the PE films. The PE chosen for this purpose was dampened with 3MPN and covered with a microscope slide, when its transmittance spectrum was measured. The transmittance of the PE was then compared with predictions about the transmittance of a PE dyed with the dye in question with different peak values ("dye concentration") of the absorption coefficient. The peak values were varied in calculations so that each of them corresponded to some predetermined transparency value (T_{eye} or T_E, equations (41) and (42)) of a complete DSC. The transparency, whose transmittance prediction for the PE best corresponded to the measured transmittance spectrum of the dyed PE, was chosen to be the prediction about the properties of the DSC. The predicted properties of DSCs (transmittance and color) were then compared with the measured properties of the DSCs. In some cases, problems with PEs forced to make the comparisons between DSCs only. In a couple of cases the PE, whose transmittance was measured, was also used to assemble a DSC that could be compared with the predictions.

By scaling the absorption coefficient, a very accurate "prediction" about the measured transmittance spectrum of the PE could be made in the case of most dyes. (D102, D149

and D205, problems with PEs dyed with N719 prevented comparison with PEs. See figures 31, 33 and 34.) The accuracy of the predictions about the DSC with the same absorption coefficient as the best prediction was quite similar with all dyes, but not quite as good as with PEs. For most of the wavelength range the agreement between measurement and prediction was very good, but for some reason the transmittance measured from DSCs at wavelengths between about 530 nm and 650 nm was higher than what was measured from the corresponding PEs. (See figures 31, 33 and 34.) The exact wavelength range and the magnitude of the change depend on the dye, but some kind of change occurred with all dyes. In the case of PEs N8 and N9 (dyed with D205, figure 33) it may seem as if such change did not occur, but the transmittance of the DSC was lower than the transmittance of PE only in the case of predictions. The measured transmittance of the DSC is higher than the measured transmittance of the PE also in this case. The bad fit with the calculated spectrum of PE is most likely caused by the properties of the particular 1DPCs in that case.

In the case of the "standard" Ru dye N719, comparisons to PEs could not be done, so the best matching transparency was decided by comparison to the measured transmittance spectra of the DSCs. The agreement of the best fit and measured spectrum was quite good in all cases, but there was still the mismatch range from about 530 nm to about 650 nm (figures 28 and 30): The wavelength of the local transmittance minimum around 530 nm is different in calculated and measured spectra and the measured transmittance of the slope at longer wavelengths is higher in the case of DSC than in the case of PE. Because comparisons to PEs could not be made, it is impossible to say with absolute certainty that there would have been changes in the spectrum of the absorption coefficient of the dye that would have caused the shift. Such change still seems the most likely explanation, because the possibility of the dye molecules having a similarly anomalous absorption spectrum in only these PE films seems very small. Comparison to a PE film dyed earlier shows that the wavelength of the transmittance minimum near 530 nm appears to have been shifted to shorter wavelengths (figure 30). The change has most likely something to do with the dye-electrolyte interface: If the changed features in the spectrum are caused by some interactions in the DSC, the only new component compared to PEs (and optical samples) is the electrolyte (not 3MPN, but redox couple etc.). The angle of the DSCs with respect to measuring beam would change the transmittance spectrum, but would not shift the position of the local minima and maxima in transmission spectrum (figure 28, DSC18). A comparison of the measured transmittance spectra of DSC18, DSC27 and DSCN2 shows that the DSCs without 1DPC transmit clearly less light in wavelength range between 450 nm and 580 nm. The only difference that could affect this wavelength range enough to explain the difference is the dye concentration, so this clearly indicates that for some reason the 1DPC reduced the amount of dye adsorbed on the TiO_2 film.

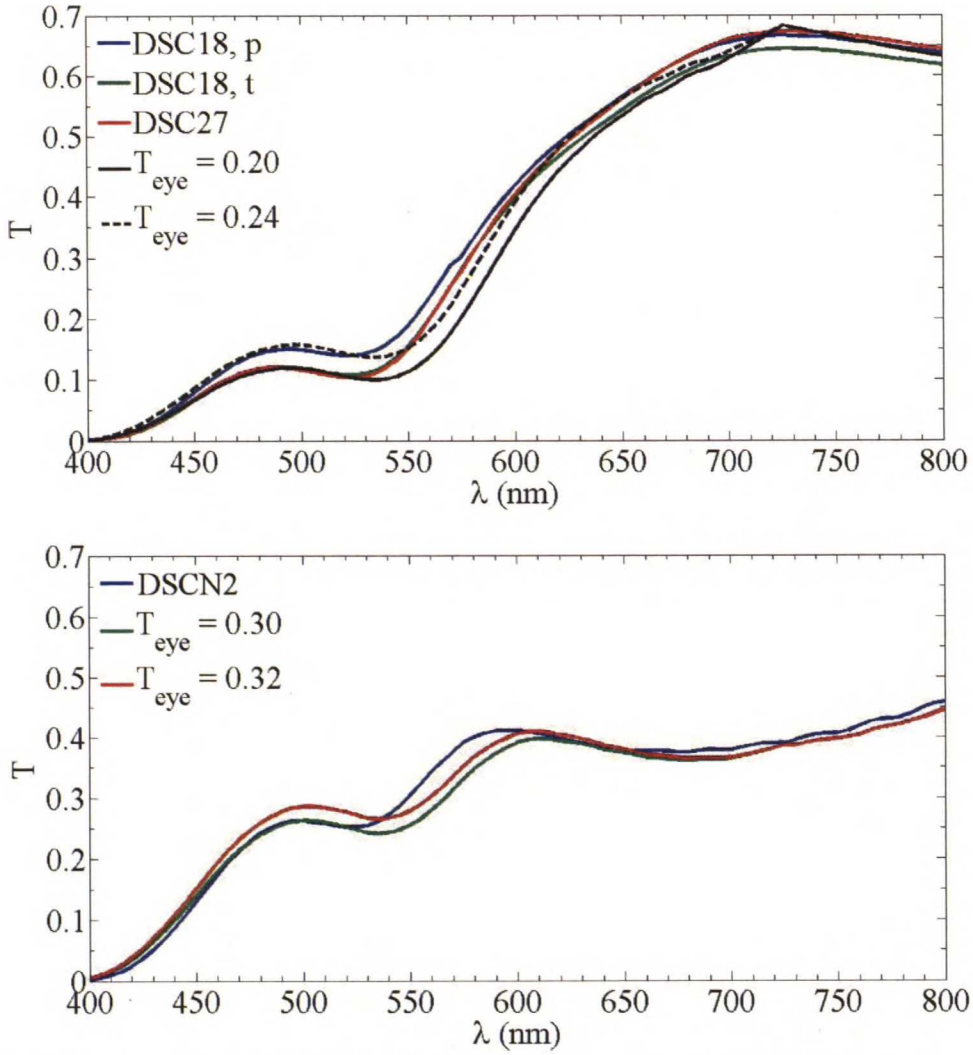

Figure 28: The measured (DSC18, DSC27, DSCN2) and calculated (T_{eye}) transmittance spectra for N719 dye. In upper figure DSC without 1DPC and in lower a DSC with 1DPC. In the case of DSC18 letter "p" means that sample was perpendicular to the beam, "t" in turn means that the sample was tilted and not perpendicular to the measuring light beam. (The latter spectrum does not show well, but it is almost identical to DSC27, when $\lambda < 600\,\text{nm}$.)

Table 3: The RGB values of the samples in the photo (average RGB pixel values over the covered film) and the predicted gamma encoded RGB values, in order (R, G, B) (figure 29).

Sample	(R, G, B)		
DSC18/27/N2	(127, 62, 32)	(103, 48, 28)	(145, 124, 95)
T_{eye}= 0.24/0.20/0.30	(160, 95, 65)	(155, 85, 56)	(143, 113, 85)

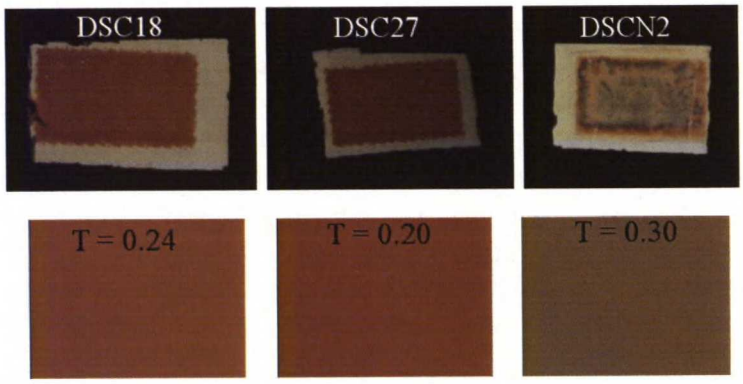

Figure 29: The color of DSC18, DSC27 and DSCN2 and calculated color for T_{eye} = 0.20 and T_{eye} = 0.24 for dyed TiO_2 and T_{eye} = 0.30 for DSC with 1DPC. Note the lighter color of the electrolyte in the case of DSCN2.

Despite these problems, the calculated color corresponding to DSCN2 matches the real color very well and the only significant differences are the higher amount of green and blue in the photo compared to calculated color. (See figure 29 and table 3.) The green could be anticipated from the measured transmittance spectrum (figure 29), but the blue could be due to some degradation that happened between cell assembly and taking the photos. DSCs 18 and 27 did not match the prediction as well, although it can be seen that the predicted color is quite close to the real color and the chromacity has been predicted approximately correct. (Gamma encoding makes direct comparison of values in table 3 less useful, since those values are not linear with respect to light intensity.)

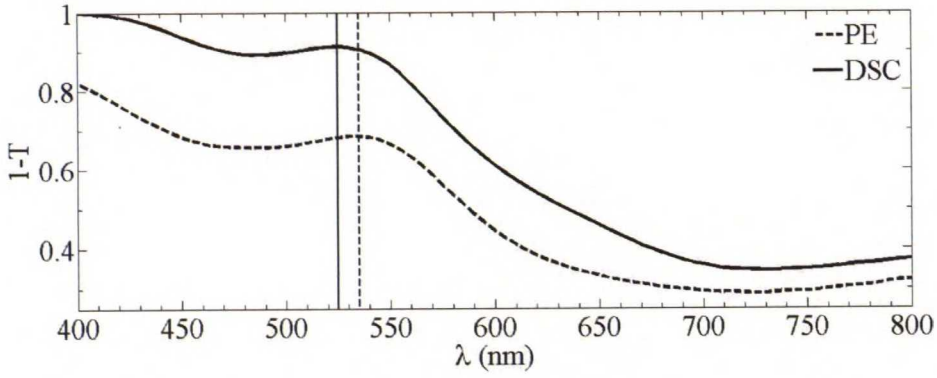

Figure 30: The measured absorptance of a PE and DSC dyed with N719. The vertical lines show the position of the absorption maximum near 530 nm. Note that the films have a different dye concentration, so only the position of the peaks/shoulders is directly comparable.

In the case of D102 the shift of the slope from the transmittance minimum to longer wavelengths occurred similarly to N719: All PEs dyed with D102 (21, 25, N6 and N10) were dyed in same dye solution at the same time, so the transmittance spectra of PEs 21

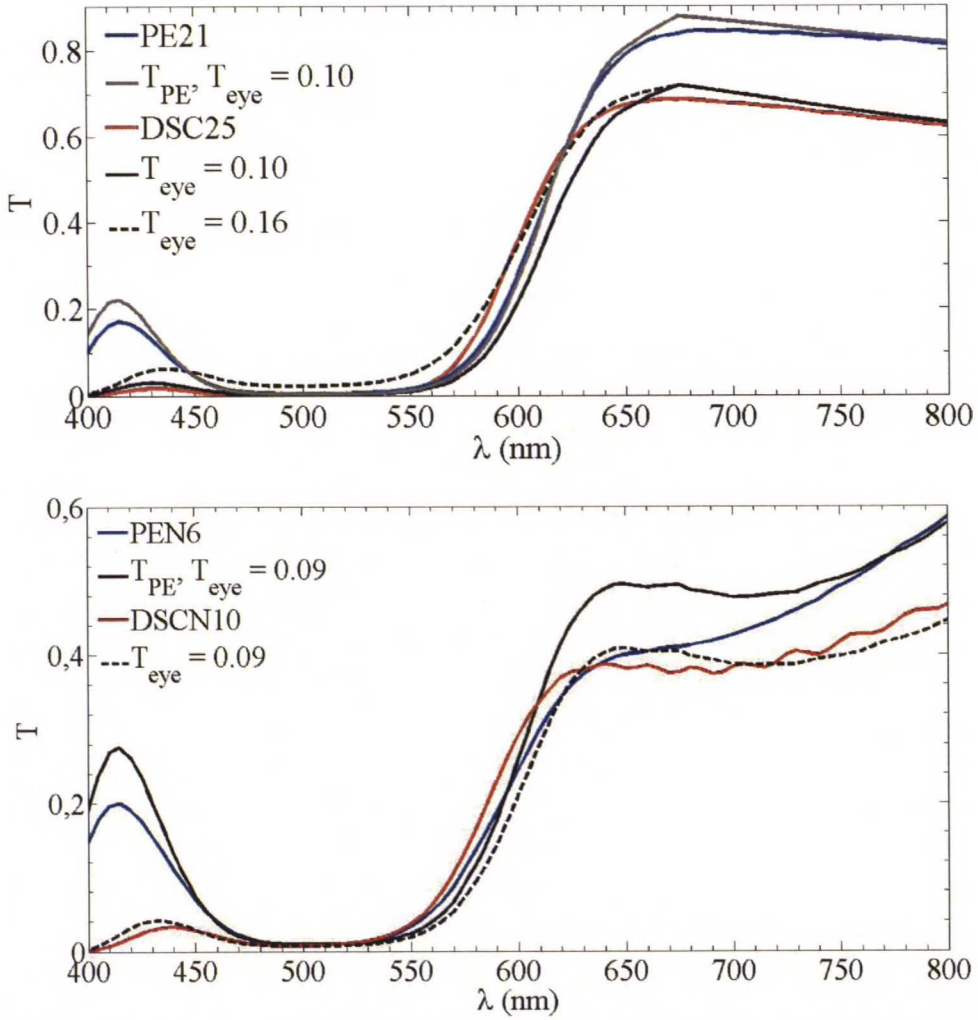

Figure 31: The measured and calculated transmittance spectra for PE and DSC dyed with D102 (top), and for DSC with 1DPC dyed with D102 (bottom).

& 25 and N6 & N10 should be almost identical to each other. It was possible to predict the transmittance spectrum of PE21 almost perfectly by scaling the absorption coefficient of the dye. However, the measured transmittance of DSC25 did not fit the prediction with the absorption coefficient that best fit PE21 (figure 31). Most importantly, its transmittance was higher than that of PE21 at the wavelength range from 550 nm to 620 nm. In the case of N6 no value of the absorption coefficient that predicted the transmittance at wavelengths shorter than 600 nm even close to measured values predicted the transmittance to be even nearly as low as was between 600 nm and 750 nm. The low transmittance at this wavelength range is most likely due to the properties of the 1DPC. In this case the transparency was chosen to be the one that best fit the measured between 450 nm and 600 nm, since the transmittance peak at 420 nm turned out to be impossible to predict accurately, unless clearly too high values of the absorption coefficient were used. This in turn points

to the direction that the 1DPCs may well increase the transmittance near 400 nm. (See figure 17.) The spectrum predicted for DSC fit the measured one as well as in the cases without 1DPC, and the shift between 550 nm and 600 nm also occurred similarly. Also, the comparison of the measured transmittance spectra between 400 nm and 580 nm shows higher transmittances for the DSC with 1DPC, which indicates lower dye concentration.

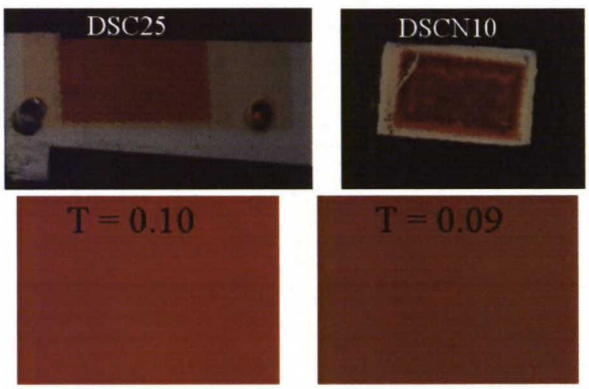

Figure 32: The color of DSC25 and DSCN10 (figure 31) in photo and the calculated color for T_{eye}= 0.09 for DSC with 1DPC and T_{eye}= 0.10 for a DSC without 1DPC.

Table 4: The RGB values of DSC25 and DSCN10 in photo and the predicted gamma encoded RGB values.

Sample	(R, G, B)	
DSC25/N10	(110, 16, 14)	(107, 27, 10)
T_{eye}= 0.10/0.09	(155, 40, 0)	(135, 48, 23)

Similarly to DSCs 18 and 27, the DSCs dyed with D102 were not in the center of the photo, but in the darker areas, and thus their color in the photo is slightly too dark, but the shade is close to same in both photo and prediction. In the case of DSC25 the increased value of blue component may be a sign of slight degradation and increased transmittance at shortest wavelengths.

D149 and D205 were slightly more predictable than N719 and D102: Even though the shift similar to N719 and D102 occurred, the change was smaller and the measured and predicted spectra resembled each other better than with the other two dyes. (Figures 33 and 34.) In the case of N9 it was not possible to make the prediction of the PE fit the measured transmittance by only adjusting the absorption coefficient. Since the problem was at wavelength range from 600 nm to 700 nm, the most likely reason is the properties of that particular 1DPC differing from the average of the 1DPCs. However, the prediction about the transmittance spectrum of the DSC fit the measured spectrum of DSCN8 almost perfectly, even at the wavelength range from 550 nm to 650 nm, where other predictions

failed (figure 33). Also in this case the most likely explanation are the properties of that particular 1DPC being different from the average and cancelling the error caused by the shift in the spectrum of the absorption coefficient. The transmittance of the DSC is higher than the transmittance of the PE at the aforementioned wavelength range once again, so the shift in the spectrum occurs similarly to other cases. Both N8 and N9 reflect shorter wavelengths than N3 that is very similar to the average of the N-1DPCs. (Figures 16 and 17.) This would mean that the transmittance of the measured spectra at precisely the wavelength range 550 nm–650 nm could well be lower than the best fitting prediction.

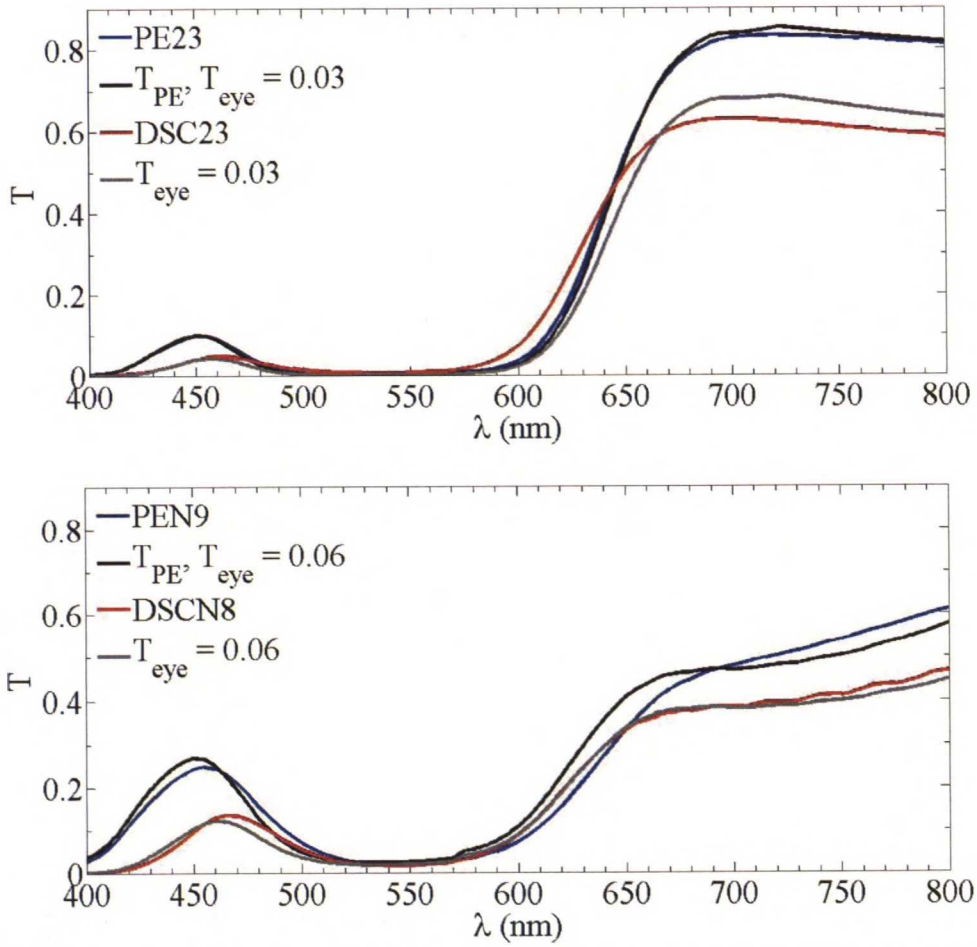

Figure 33: The measured and calculated transmittance spectra for PEs and DSCs dyed with D205.

The colors of the DSCs dyed with D149 and D205 fit the pattern with the ones dyed with N719 and D102: The ones that were in the center, when photos were taken, matched the prediction accurately, but the ones farther from the brightest light were too dark. The difference in background intensity can be seen by comparing the electrolytes in different DSCs: Despite being identical in all DSCs its color in the case of DSCN8 is darker than in the case of DSCs 22 and 23.

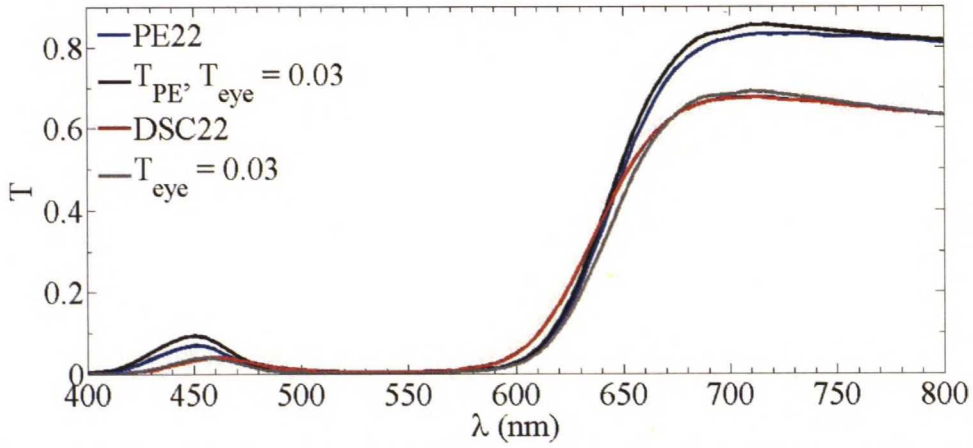

Figure 34: The measured and calculated transmittance spectra for PE and DSC dyed with D149.

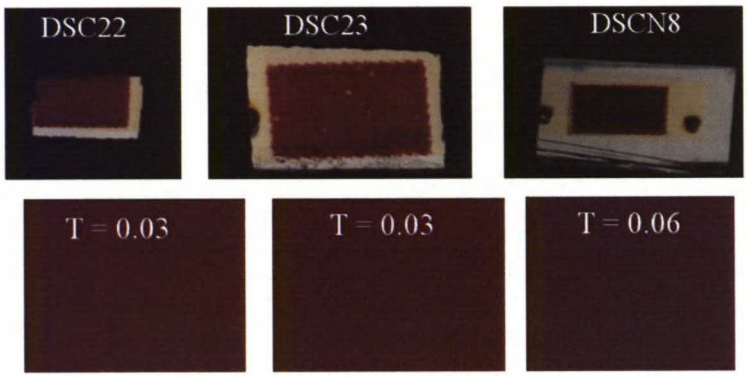

Figure 35: The color of DSC22, DSC23 and DSCN8 photo and color calculated from predicted transmittance spectrum.

Table 5: The RGB values of DSC22, DSC23 and DSCN8 in photo and the predicted gamma encoded RGB values.

Sample	(R, G, B)		
DSC22/23/N8	(84, 3, 18)	(103, 0, 27)	(50, 10, 30)
T_{eye}= 0.03/0.03/0.06	(99, 0, 33)	(99, 0, 36)	(102, 40, 64)

It seems to be possible to predict the transmittance spectrum of a DSC from the transmittance spectrum of the PE quite accurately, when the properties of all other components are known. Also, this predictability does not seem to depend on the dye used in DSCs. At least there were no significant differences in this respect with the dyes used in experiments. The shift seen in the transmittance spectrum repeated quite similarly in all DSCs, so it is

most probably related to some properties common to all measured cells. This limits the possible candidates to electrolyte and CE, electrolyte being the more likely of the two. Unfortunately the exact mechanism behind the change is unknown. Increased transmittance due to properties of the 1DPC layer is not a likely explanation, because the phenomenon was not limited to DSCs with 1DPCs and the wavelengths do not match the wavelengths, where this was observed in measurements. (See figures 17 and e.g. 31.)

The most likely reason for the errors in the darkness of the colors is slightly uneven background illumination: The DSCs that were in the middle of the photos (N2, 22 and 23) were generally predicted very accurately, but the color of the rest was too dark in the photo. (See also figure 23.) The difference in background intensity can easily be seen by comparing the color of the electrolyte, which is lighter in the case of the aforementioned DSCs than in the case of those that were farther from the center, when the photos were taken. The spectral irradiation of the light reflected from the white background was measured from approximately the center of the sample holder, so it corresponds best to the brightest part of the photos, but the relative irradiation spectrum should be the same at every point of the slit in the sample holder. When calculating the colors, it is not the absolute intensity that determines the color of a spectrum, but the intensity compared to the white point. (See also equations (34) and (38).) In this case, the white point was the irradiation coming from behind the DSCs, so its brightness distribution affected the colors in the photos. Because the intensity was assumed to be homogeneous, this shows as predicted colors being too bright. In addition to this, the camera and its settings determine the RGB values that correspond to the brightest light source in the photo, and the rest of the colors will be scaled according to that. Hence the RGB coordinates of the white point had to be adjusted in the calculations to achieve accurate results.

It would be possible to calculate new colors for DSCs in darker areas of the photos, but these results already demonstrate that it appears to be possible to predict the colors accurately, if the transmittance spectrum, lighting conditions and final RGB values of the white point in the photos are known. They also demonstrate effectively the significance of homogeneous light intensity through errors caused by inhomogeneous illumination conditions. In addition to this, the significance of the camera settings can be seen by comparing rows c) and d) in figure 27, where the only difference are the RGB values of the white point. They are determined by the camera and its settings, when taking the photo. These details together make comparing the predicted color to its real life counterpart difficult, since the conditions have to be known and controlled accurately, and even small differences in illumination and camera settings will produce errors that can be seen easily with naked eye. The differences in background intensity can be seen in figure 23. Even if the background intensity seemed almost uniform to naked eye, when taking the photos, there are areas that are clearly brighter than others. This is also visible in the dark colors of the DSCs that were not in the center of the photo. The chromacity of both the photo and predicted color being approximately the same means that the most likely reason for the error is a difference in how bright the light was assumed to be compared to the white point, and how bright it actually was in this comparison. It is naturally possible that there are other errors in predicted colors, but based on the accuracy of the predicted colors in the

case of DSCs in the center of the photos, they are not likely to be very significant. Because it appears that the errors caused by differences in light intensity are significantly larger than those caused by the observed shift in transmittance spectrum, much more attention should be paid to photography in any and all future color testing than was done.

The predictions about the efficiency of the DSCs were not as accurate as the transmittance and color. The IV curve was not measured from any of the DSCs, because the IPCE measurements alone showed that the DSCs could not possibly produce the predicted power: In all measured cases the short circuit current predicted from measured IPCE spectrum ($I_{SC,\ IPCE}$) was at most a bit less than 65% of the predicted value ($I_{SC,\ calc}$, table 6). This is a significant difference, even taking into account that in the calculations the injection efficiency was assumed to be 100%. The predicted short circuit currents are based on the predicted transmittance spectrum, not the measured one, which could explain small differences, but not as large as observed.

Table 6: The short circuit currents (mA/cm^2) of the DSCs. Transmittance of DSC19 is not shown in figures, but it was practically identical to that of DSC22.

Sample (dye)	$I_{SC,\ IPCE}$	$I_{SC,\ calc}$
DSC18 (N719)	5.71	9.18
DSCN2 (N719)	4.49	6.80
DSCN10 (D102)	3.62	10.50
DSC23 (D205)	3.07	13.21
DSC19 (D149)	4.79	13.21

The values predicted from IPCE spectra show that N719 was clearly the best of the dyes: The DSCs dyed with it produced the highest currents and were more transparent than others. The organic dyes seem promising, but produce relatively low currents compared to their transmittance spectra. This may in part be due to coadsorbents not being used, but the effect is not likely to be large, especially because at least D102 has been successfully used with ethanol as solvent without coadsorbents [48, 82].

The cases shown in figures, but not in table, produced practically no current (DSCs 21, 22, 27 and N6) or were not measured, because there were problems with their electric contacts that prevented any current from being extracted from the DSC in question (DSCs 25 and N8). DSC19 is shown in table instead of DSC22. Both were dyed in the same dye solution at the same time and the transmittance spectra of these DSCs are practically identical, but DSC19 produced significantly more current than DSC22.

3.4.3 Controlled dyeing of DSCs

The usefulness of the calculations about the color of the DSCs is based on the assumption that the optical properties of the dyed TiO_2 film could be controlled reliably, and possibly also observed during dyeing process. This assumption was tested in practise with a simple experiment: The dye solution and TiO_2 film were placed in a transparent container that was illuminated with an LED. (See figure 36.) A photodiode converted the transmitted light into current signal that was proportional to the transmittance of the PE film. The effects of other light sources were minimized by placing photodiode, LED and dye container inside a box, whose walls did not transmit visible light. The current signal from photodiode was measured continuously and compared to the measured transmittance of the dyed films after dyeing.

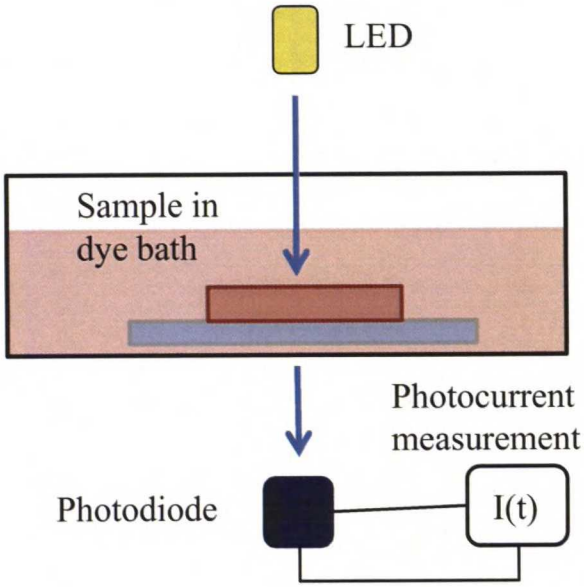

Figure 36: The equipment used in measuring the dye concentration adsorbed in the TiO_2 film.

Assuming that the amount of dye in the solution is much larger than what the TiO_2 film will adsorb, the current signal of the photodiode depends only on the amount of dye adsorbed into the TiO_2 film and the intensity of the LED. With an accurate power source the fluctuations in the intensity of the LED could be reduced and the comparison to photocurrent at the beginning of the dyeing process should tell, when the dye concentration in the TiO_2 film is as high as desired. The current signal coming from the photodiode is

$$I_{\mathrm{PD}}\left(C_{\mathrm{D}}, d_{\mathrm{TiO_2}}\right) = q_{\mathrm{e}} \int_{\lambda_{\min}}^{\lambda_{\max}} \phi_{\mathrm{LED}}\left(\lambda\right) \left(e^{-C_{\mathrm{D}}\epsilon_{\mathrm{D}}(\lambda)d_{\mathrm{TiO_2}}}\right) T_{\mathrm{rest}}\left(\lambda, d_{\mathrm{TiO_2}}\right) \eta_{\mathrm{QE,PD}}\left(\lambda\right) \mathrm{d}\lambda \qquad (43)$$

The photon flux emitted by the LED is $\phi_{\mathrm{LED}}(\lambda)$ and the quantum efficiency of the photodiode is $\eta_{\mathrm{QE,PD}}(\lambda)$. The integrand is integrated over the spectral range, where the LED emits light. The LED used in the measurement configuration had a narrow irradiation spectrum to reduce the uncertainties caused by the unknown transmittance spectrum of the dye container included in T_{rest}, which is the transmittance of the entire dye solution-container-PE substrate package with no dye adsorbed on the TiO_2. (See also figure 18 for the relative absorption coefficient spectra of the dyes.) It also includes the transmittance of the plain TiO_2 film. When the emission spectrum of the LED is narrow, the transmittance of the container can be assumed to be a constant over the integration range. Therefore it can be taken out of the integral and does not affect the ratio of the initial photocurrent ($C_D = 0$) to photocurrent at any nonzero dye concentration. It is assumed that the multiple reflections inside the system can be ignored, so the effect of the dye can be expressed with a single exponential factor, where C_D is the concentration of the dye, $\epsilon_D(\lambda)$ the molar extinction coefficient of the dye adsorbed on TiO_2 and d_{TiO_2} is the thickness of the TiO_2 film. The elementary charge is denoted with q_e. Assuming that the dye does not adsorb on the TiO_2 film too fast, the initial photocurrent ($C_D = 0$) is:

$$I_{\mathrm{PD},0} = I_{\mathrm{PD}}(C_D = 0, d_{TiO_2}) = q_e \int_{\lambda_{\min}}^{\lambda_{\max}} \phi_{\mathrm{LED}}(\lambda)\, T_{\mathrm{rest}}(\lambda, d_{TiO_2})\, \eta_{\mathrm{QE,PD}}(\lambda)\, \mathrm{d}\lambda \tag{44}$$

This method was tested with N719 and D102 dyes. Based on the quality of the dyed films, the feasibility of the method depends on the dye: In the case of D102 the quality of the films that were exposed to LED was poor, whereas the films dyed in dark in otherwise identical conditions were perfectly fine. One film was also dyed so that approximately half of it was illuminated, while the other half was shaded: The shaded half was in good condition after dyeing, whereas the illuminated one was much more transparent. This means that either less dye was adsorbed on the film or the adsorbed dye had been bleached due to exposure to the LED light during the dyeing process. However, these problems did not occur with the N719 dye, indicating that it is more photostable than the organic dye D102, when illuminated in dye bath solution. (See figures 37 and 38.)

In the following the results from the controlled dyeing experiment are analysed only for the N719 dye. The results are from two PE samples dyed with N719 dye: Samples number 10 and 14, TiO_2 deposited by screen printing and sintered in an oven. In both cases the immersion in dye solution lasted for about 2 hours. The photocurrent of the photodiode was recorded for later comparison of measured and calculated transmittance. The photocurrent was not monitored continuously to stop the dyeing at a certain, predetermined transparency, but the calculated transmittance spectra that would be compared to the measured ones were chosen afterwards based on the measured photocurrents. The LED used in experiments was a blue LED, whose maximum photon flux was at about 460 nm with full width at half maximum of about 25 nm.

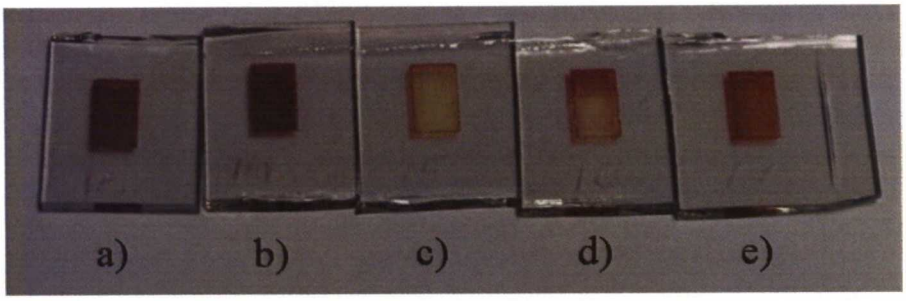

Figure 37: The films dyed with N719 (PE10 and PE14 – a) and b), respectively) and D102 (the rest). Both films dyed with N719 have been continuously illuminated with LED. Film e) was dyed with D102 in dark, whereas c) was continuously illuminated. Film d) was covered so that the top half was in dark and the bottom half was illuminated.

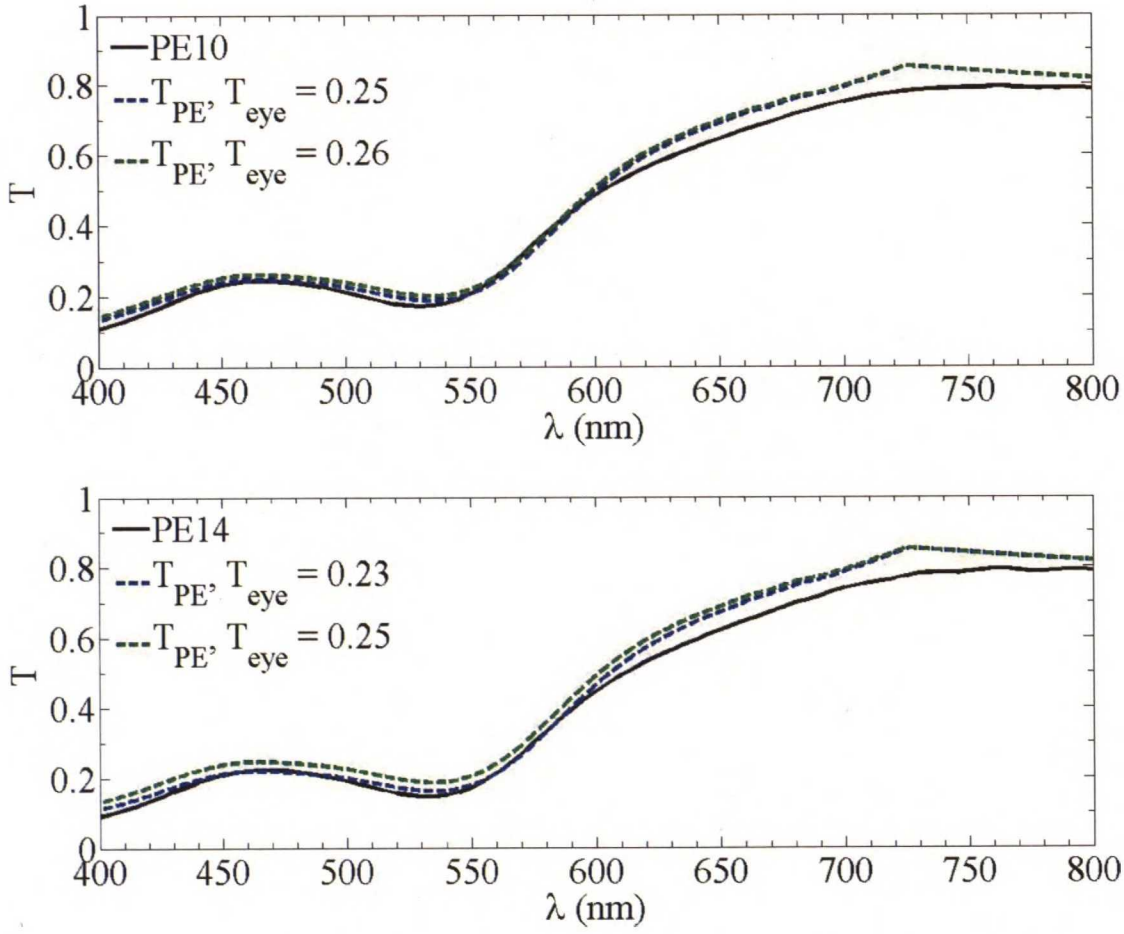

Figure 38: The measured transmittance of films dyed with N719 and the calculated transmittance spectra corresponding to the photocurrent ratio.

The initial photocurrent measured with PE10 was about 0.45 μA and for PE14 about 0.85 μA. At the end of the dyeing the photocurrents were 0.13 μA and 0.23 μA with PE10 and 14, respectively. With the equipment used these photocurrent ratios (0.29 and 0.27 respectively) correspond to transparencies (T_{eye}, see equation (41)) of about 0.26 and 0.245. (See figure 39.) However, transmittance spectra corresponding to slightly lower transparencies of 0.25 and 0.23 fit the spectra measured from dyed films slightly better. (Figure 38.) The values of the photocurrent ratio corresponding to these transparencies are 0.28 and 0.25. Note that the measured photocurrent ratio has been normalized according to the moment, when the PE and LEDs were positioned correctly, which took some time in both cases. Since the PEs were already in the dye solution at that point, their transmittance, and the current from the photodiode, may have been reduced already, and thus the later photocurrent ratio values would likely be slightly higher than equations (43) and (44) predict for the amount of dye adsorbed into the film. This explains at least in part, why the transmittance values of the spectra corresponding to the measured photocurrent ratios were higher then measured, and why the spectra that best fit the measured one corresponded to lower photocurrent ratios (figure 38).

Based on the problems with the D102 dye, it is obvious that the method is not ready to be implemented as such, but the results with N719 dye seem promising. The most logical reason for the degradation with D102 is the continuous illumination. Changing the illumination to the LED being turned on for only short periods of time could significantly reduce the degradation or inhibited adsorption due to illumination. Also, the signal-to-noise –ratio of the measured current was too large for the measured current to be useful as such, but averaging the measured current over time period of one minute significantly reduced the noise. (Figure 39.) Other options for noise reduction were not tested, because this relatively simple solution worked. It is possible that similar signal averaging will be needed in possible future versions of the equipment. The straightforward solution to observed problems would be to illuminate the sample for a short period of time, measure the photocurrent of the photodiode several times and use the average of these values in monitoring the dye concentration in TiO_2. This procedure would be repeated at regular time intervals that would be long enough to let the dye adsorb on the TiO_2 particles.

As can be seen from figure 39, the change in photocurrent appears predictable, except for the strange increase in photocurrent between 60 and 70 minutes in the case of PE10. There is no apparent explanation for this and more experiments would be required to test the repeatability of the process, but at least during the first hour the current ratios of both PEs are remarkably similar. This indicates that, as the intuition would claim, the dyeing process is very repeatable, if the conditions are kept similar. This in turn could be utilized so, that after the initial measurement the dye concentration would not be observed until after a certain period of time that depends on the desired final concentration. Earlier measurements would not be needed, because the dye concentration could not be higher than the wanted final concentration.

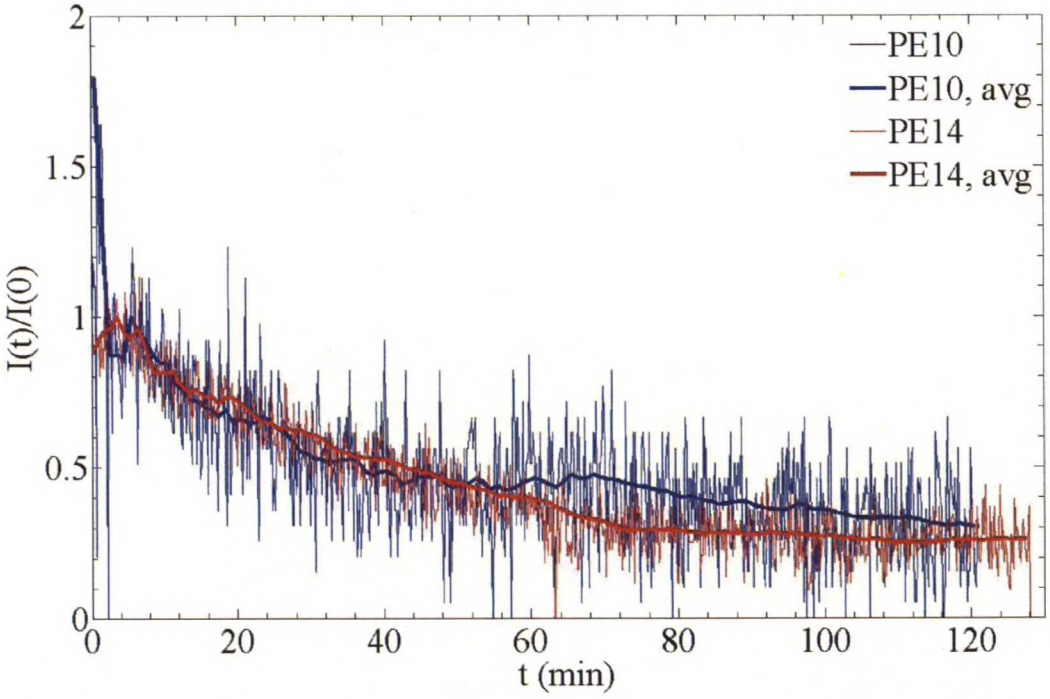

Figure 39: The measured and averaged photocurrent ratios of PE10 and PE14.

There is one important additional detail related to the dyeing of the TiO_2 films and dye concentration that must be taken into account: The dye is not adsorbed on the TiO_2 evenly. The dye concentration saturates at a thin section of the TiO_2 film before the dye molecules reach farther into the film [83]. Therefore a low average concentration means that the concentration near the FTO substrate is almost zero, but may have saturated at areas that dye molecules reach first. In practise this means that instead of dye concentration, the thickness of the TiO_2 film is the property that should be changed to tune the color of the DSC, because the areas without dye may still contribute to recombination, making the collection efficiency lower than in a thinner film with the same amount of dye in it. Therefore the observation of dye concentration might not be needed at all, except for determining the moment the dye concentration has reached its saturation value in order to reduce unnecessary delays in production. The colors and calculations naturally change slightly, because the thickness of the bulk electrolyte changes with the TiO_2 film. Since the dye in TiO_2 has the largest contribution to the changes in the color of DSC and a change in dye concentration or PE thickness affect the optical properties of the DSC similarly, this change would cause only minor adjustments in the calculations. The thickness being the adjustable parameter could also affect the predictions made about the performance of the cells, since the collection efficiency would change with the film thickness and electron collection profile, but that would be relatively easy to take into account in the calculations.

It is possible that DSCs with the lowest transparencies may not be realizable, or at least practical, because the required thickness of the PE film might not fit into limitations set by the sealant thickness. The electron collection from the far edges of the film

could be inefficient, especially considering the small additional amount of photons absorbed compared to thinner films. However, as dyed TiO_2 films show, even thin PE enables low transparencies, so this may not be a relevant consideration in any, but the most extreme cases. (See measured transmittance spectra in sections 3.4.2 and 3.4.3.) Making the TiO_2 film thin enough for high transparencies, especially with the organic dyes, is more likely to be a relevant concern in future manufacturing processes.

3.4.4 Example of DSC design

The appearance of the solar cells is likely to become an important criterion in BIPVs. To demonstrate the possibilities of coupled optical and electrical modeling, selected results from simulations will be shown.

In the example the DSCs may be used for e.g. windows or skylights. In this example scenario the aim is for the luminance transparency to be 0.30. This means that the apparent brightness of the transmitted light will be around 60% of the brightness of the incident light. With available components and data the colors of the transmitted and reflected light would be as shown in figure 40.

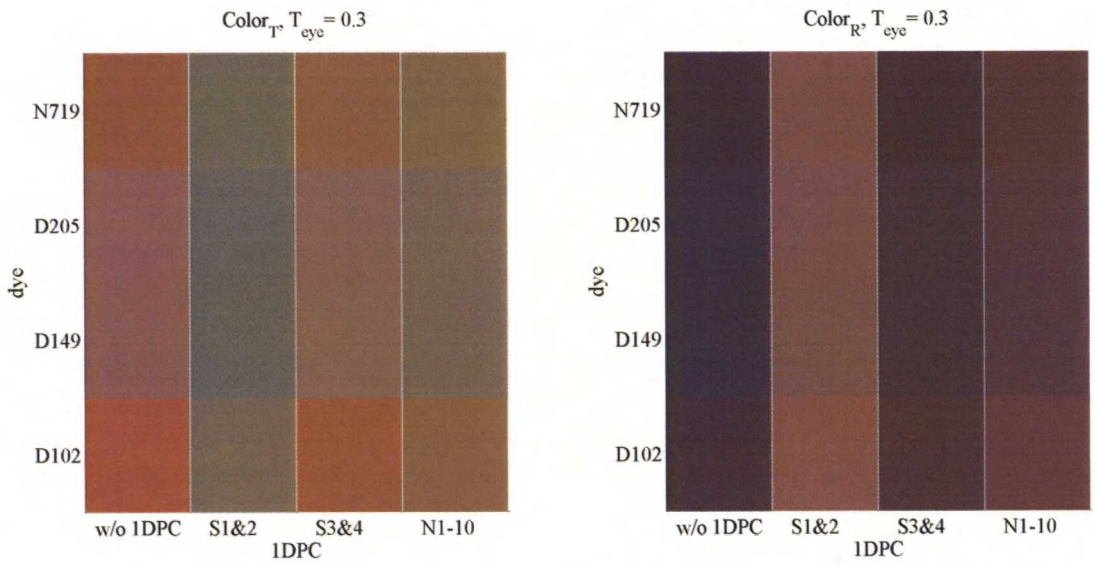

Figure 40: Predicted color of the transmitted (left) and reflected light (right) in AM1.5G illumination, when $T_{eye} = 0.30$.

The color may be an important factor, but without the capability to efficiently produce electricity the DSCs are merely more expensive and glorified alternative for coloured glass. In the case of the presented combinations the efficiencies of the DSCs calculated with $L = 20\,\mu m$ and neglecting losses other than recombination with I_3^- (collection efficiency slightly less than 100%) are presented in table 7. The reason for the similarities between D149 and D205 is their similar absorption spectra: The highest value of the molar absorption

Table 7: The calculated short circuit current (mA/cm^2) and efficiency (%, AM1.5G) of the DSCs shown in figure 40. (I_{SC}, η) The calculations were done using equations (26), (8), (9) and (14a).

Dye\1DPC	w/o 1DPC		S1&2		S3&4		N1–10	
N719	7.89	3.73	4.76	2.13	7.57	3.56	6.98	3.26
D205	6.49	3.00	3.93	1.72	6.21	2.86	5.72	2.61
D149	6.58	3.05	3.99	1.76	6.30	2.91	5.81	2.66
D102	6.84	3.18	3.98	1.75	6.53	3.02	5.95	2.73

coefficient of D205 is higher than that of D149, but the shapes of the spectra are almost identical to each other. (See figure 18.) Therefore, the colors and efficiencies of these dyes, that correspond to same transparency, are very similar. The only difference is that in the case of D149 larger amount of dye is required to absorb as many photons as a film dyed with D205 does. Hence it seems likely that higher light harvesting efficiencies could be achieved with D205 than with D149, if PE thickness is kept the same.

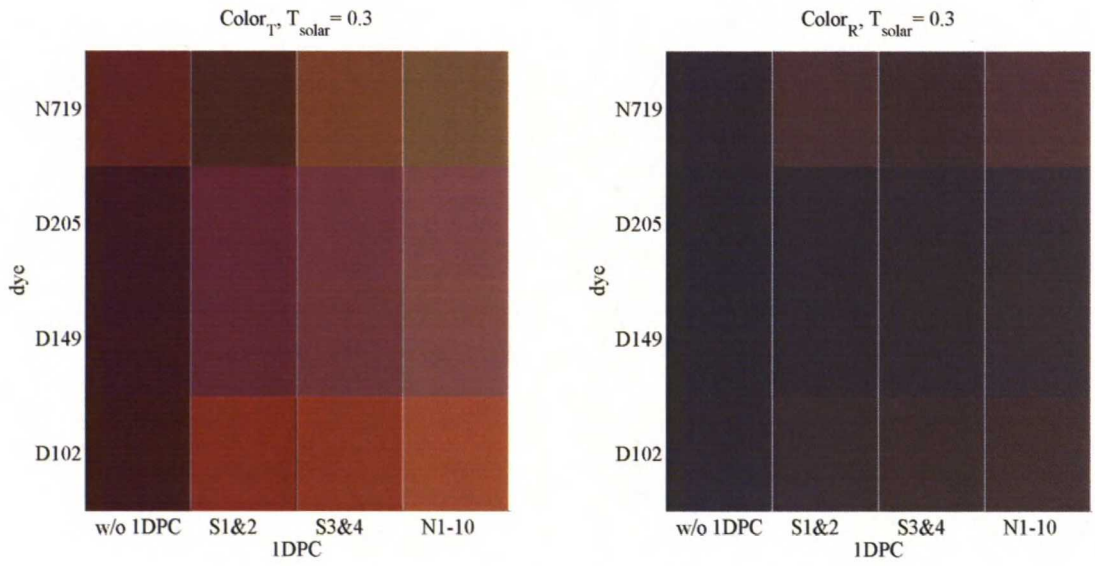

Figure 41: Predicted color of the transmitted (left) and reflected light (right) in AM1.5G illumination, when $T_E = 0.30$.

Had the criterion for transparency been for transmitted intensity of visible light instead of luminance, the dye concentrations would have been different. In this case the dye concentrations would be higher, as comparison between the short circuit currents, efficiencies (tables 7 and 8) and colors of transmitted light (figures 40 and 41) shows. Note that the dye concentrations corresponding to intensity transparency most likely do not correspond

Table 8: The calculated short circuit current (mA/cm^2) and efficiency (%, AM1.5G) of the DSCs shown in figure 41. (I_{SC}, η) The calculations were done using equations (26), (8), (9) and (14a).

Dye\1DPC	w/o 1DPC		S1&2		S3&4		N1–10	
N719	13.20	6.56	10.87	5.30	9.93	4.80	8.37	3.98
D205	13.06	6.49	10.87	5.30	9.42	4.53	7.92	3.74
D149	13.05	6.48	10.84	5.29	9.41	4.52	7.91	3.74
D102	13.49	6.72	10.51	5.11	9.30	4.46	7.56	3.56

to any single luminance transparency, even if only one dye or 1DPC is considered. It is also interesting to notice that there are cases, where different dye-1DPC –combinations (comparison between D149 and D205 excluded) produce very close to same short circuit current and maximum power, but have different appearance caused by different optical properties. By using such DSCs, it might be possible to make solar panels with almost artistic colouration with only little worry about performance differences between different areas of such panels.

When considering the reflected colors, it should be remembered that a bright glass window reflects only few percents of incident light, meaning that the color of that reflection is very dark gray, almost black. Using transparent DSCs could make this reflection slightly reddish or orange mixed with the darker red, purple or green of the transmitted light of indoor lighting.

4 Electrical modeling of DSCs

It has been observed that the small pore size of the 1DPCs is a problem for the diffusion of the redox couple through the 1DPC layer [28]. The porosity of the 1DPCs is comparable to the TiO_2 films, so it should not be the source of the problem[28, 84]. The physical structure parameter behind the diffusion problems is most likely constrictivity that describes the effects of finite-sized particles being diffused through pores, whose dimensions are comparable to the size of the particles [85]. This parameter is often mixed with tortuosity that describes only the effects of the geometric structure of the pore networks, but does not depend on the size of the pores or the particles diffused through them. This section studies the effects of constrictivity with simulations done for different DSCs with different values of constrictivity. The goal of the simulations is to find a value or a range of values, where the constrictivity begins to limit diffusion enough to cause problems for the efficiency of the DSCs in question.

4.1 Theoretical background

4.1.1 Overpotentials at counter electrode

The voltage of the DSCs at any given point of the IV curve is affected by losses related to iodide and tri-iodide concentrations at CE, in addition to recombination at PE. The total effect of the redox couple concentrations on the current flowing through the DSC is given by

$$\frac{i_{\mathrm{CELL}}}{i_{\mathrm{CE},0}} = \sqrt{\frac{C_{\mathrm{I_3^-}} C^*_{\mathrm{I^-}}}{C_{\mathrm{I^-}} C^*_{\mathrm{I_3^-}}}} e^{\frac{\beta q_e V_{\mathrm{CE}}}{k_B T}} - \frac{C_{\mathrm{I^-}}}{C^*_{\mathrm{I^-}}} e^{-\frac{(1-\beta) q_e V_{\mathrm{CE}}}{k_B T}} \tag{45}$$

The exchange current density of the overall reaction at CE is $i_{CE,0}$, and also depends on the iodide concentrations at CE:

$$i_{\mathrm{CE},0} = 2F k^0_{\mathrm{app}} C_{\mathrm{I}}^{*(1-\beta/2)} C_{\mathrm{I^-}}^{*(\beta/2)} \tag{46}$$

The apparent rate constant of the overall reaction is k^0_{app} and F denotes Faraday's constant. The equilibrium concentration of species i at CE is denoted with C_i and C_i^* is its concentration at CE in the operating conditions. The total voltage loss (overpotential) at CE is V_{CE} and β is the symmetry factor of the reaction. Elementary charge is denoted with q_e, k_B is the Boltzmann constant and T temperature. [32]

When diffusion of ions in electrolyte is fast enough to keep the concentrations near their equilibrium values (i.e. $i_{CELL} \ll i_{lim}$) the current overpotential is reduced to

$$\frac{i_{\mathrm{CELL}}}{i_{\mathrm{CE},0}} = e^{\frac{\beta q_e V_{\mathrm{CT,\,CE}}}{k_B T}} - e^{-\frac{(1-\beta) q_e V_{\mathrm{CT,\,CE}}}{k_B T}} \tag{47}$$

In this case the voltage loss is called charge transfer overpotential, $V_{CT,\,CE}$. Equation (47) is also known as Butler-Volmer equation. The charge transfer overpotential can be solved

(analytically) only, when β = 0.5. This assumption is supperted by experiments for Pt catalyst. In this case the overpotential is

$$V_{\mathrm{CT,\,CE}} = \frac{2k_BT}{q_e}\mathrm{arcsinh}\left(\frac{i_{\mathrm{CELL}}}{2\,i_{\mathrm{CE,0}}}\right) \tag{48}$$

The charge transfer resistance at zero polarisation ($V_{CT,\,CE}$= 0), $R_{CT,0}$ is given by

$$R_{\mathrm{CT,0}} = \frac{k_BT}{q_e i_{\mathrm{CE,0}}} \tag{49}$$

Measuring this value then enables estimating the charge transfer overpotential in DSCs. [32]

In the other extreme of the concentrations at CE is the situation, where diffusion in electrolyte is so slow that exchange current density is much larger than current density in cell ($i_{CELL}/i_{CE,0} \approx 0$ and thus $V_{CT,\,CE} \to 0$). Taking this limit in equation (45) (and assuming β = 0.5) enables solving the diffusion overpotential [32]

$$V_{\mathrm{D,\,CE}} = \frac{k_BT}{2q_e}\ln\left[\left(\frac{C^*_{I_3^-}}{C_{I_3^-}}\right)\left(\frac{C_{I^-}}{C^*_{I^-}}\right)^3\right] \tag{50}$$

When the concentrations at given current density are known, it is possible to calculate the total voltage of the DSC

$$V_{\mathrm{tot}} = V_{TiO_2} + V_{\mathrm{CT,\,CE}} + V_{\mathrm{D,\,CE}} \tag{51}$$

Note that $V_{TiO_2} < 0$, whereas the overpotentials are positive.

4.1.2 Charge transfer in electrolyte

The charge transport in the electrolyte is a mass transfer process, where the reduced ions of the redox couple of the electrolyte transfer negative charge to dye cations and then oxidized ions are diffused back to counter electrode to be reduced at the catalyst surface. The most common redox couple is the iodide/tri-iodide couple (I^-/I_3^-).

The first reaction in the dye reduction sequence (5) is the charge transfer reaction that involves the latter two fast chemical reactions that are assumed to be in equilibrium. The charge transfer reaction (5d) is the step that determines the reaction rate with I^- as the reduced and I as the oxidized species. At the CE the charge transfer occurs according to the opposite reaction sequence (7). However, in the presence of high I^- and I_3^- concentrations, some fraction of charge transfer between charge carrier species may occur via Grotthus mechanism [37]:

$$I_3^- + I^- \to I^- \cdots I_2 \cdots I^- \to I^- + I_3^- \tag{52}$$

The contribution of this mechanism may be quite significant especially in ionic liquids and other viscous electrolytes, but most likely negligible in typical liquid electrolytes [37].

The diffusion of the ions of the redox couple in the electrolyte and in the pores of the TiO_2 film is in general described by diffusion equation with the addition of the dye regeneration term that is equal to the profile of excited state forming in dye molecules that can also be expressed as the electron injection profile. The time dependent continuation equation is: [29]

$$\epsilon_{\mathrm{i}} \frac{\partial C_{\mathrm{j,i}}}{\partial t} = D_{\mathrm{j,i}}^{\mathrm{eff}} \nabla^2 C_{\mathrm{j,i}}(x) + a_{\mathrm{j,i}} \left(\nu_{\mathrm{rg}} - \nu_{\mathrm{eer}} \right) \tag{53}$$

Terms ν_{rg} and ν_{eer} are the rate of dye regeneration and electron-electrolyte –recombination respectively. The stoichiometric coefficient $a_{\mathrm{j,i}}$ depends on the charge carrier species and the stoichiometry of the redox couple. In the case of negligible recombination ν_{eer} would be zero. Term $g(\mathrm{x})$ (see also equation (19)) in equations (55) being equal to ν_{rg} is an approximation based on assumption that the iodide concentration differences are small compared to average iodide concentration. A more accurate description of the related mechanism is [29, 61, 86, 87]

$$\nu_{\mathrm{rg}} = k_{\mathrm{rg}} C_{\mathrm{S^+}} C_{\mathrm{I^-}} \tag{54}$$

The concentration of iodide is $C_{\mathrm{I^-}}$ and the concentration of dye cations is $C_{\mathrm{S^+}}$, which is proportional to electron generation rate $g(\mathrm{x})$. The rate constant of the reaction is k_{rg}.

In the case of steady-state operation and I^-/I_3^- redox couple the diffusion equations are [33, 88]:

$$D_{\mathrm{I,i}}^{\mathrm{eff}} \nabla^2 C_{\mathrm{I,i}}(x) - \frac{3}{2} g(x) = 0 \tag{55a}$$

$$D_{\mathrm{I_3,i}}^{\mathrm{eff}} \nabla^2 C_{\mathrm{I_3,i}}(x) + \frac{1}{2} g(x) = 0 \tag{55b}$$

Terms $D_{\mathrm{I,i}}^{\mathrm{eff}}$ and $D_{\mathrm{I_3,i}}^{\mathrm{eff}}$ are the effective diffusion coefficients of the oxidized and reduced ions, respectively. The relationship between the bulk and effective coefficient for both species is: [89, 84]

$$D_{\mathrm{j,i}}^{\mathrm{eff}} = \frac{\epsilon_{\mathrm{i}} \cdot \gamma_{\mathrm{i}}}{\tau_{\mathrm{i}}^2} D_{\mathrm{j}}^{\mathrm{bulk}} \tag{56}$$

The coefficients in this are the porosity ϵ_{i}, constrictivity γ_{i} and tortuosity factor τ_{i} of material i. The bulk value for all these is 1, but for porous media $\epsilon_{\mathrm{i}} < 1, \gamma_{\mathrm{i}} < 1, \tau_{\mathrm{i}} > 1$. In bulk electrolyte all three coefficients equal to unity. When it is assumed that the charge carriers do not chemically react with anything between CE and TiO_2 film (i.e. the effect of Grotthus mechanism is at most negligible), the diffusion equations for the layers between them become:

$$D_{\mathrm{I,i}}^{\mathrm{eff}} \nabla^2 C_{\mathrm{I,i}}(x) = 0 \tag{57a}$$

$$D_{\mathrm{I_3,i}}^{\mathrm{eff}} \nabla^2 C_{\mathrm{I_3,i}}(x) = 0 \tag{57b}$$

The aforementioned link between light absorption and charge carrier concentrations, $g(x)$, is equal to the amount of electrons (moles) successfully injected into TiO_2 per unit time and unit volume. If perfect electron collection is assumed, this equals to the short circuit current that can be extracted from the DSC, if it is smaller than the limiting current density: [33, 88]

$$F \int_0^{d_{PE}} g(x)\, dx = i_{SC} \tag{58}$$

It is assumed that there is no net flux of either iodide or tri-iodide at the PE contact [33, 88]:

$$\left[\frac{dC_j(x)}{dx}\right]_{x=0} = 0 \tag{59}$$

Therefore the current density flowing through the DSC can be expressed with the concentration gradient that is calculated from equations (55), (58) and (59):

$$\left[\frac{dC_{I_3}(x)}{dx}\right]_{x=d_{PE}} = \frac{-i_{SC}}{2\,F\,D_{I_3}^{eff}} \tag{60a}$$

$$\left[\frac{dC_I(x)}{dx}\right]_{x=d_{PE}} = \frac{3\,i_{SC}}{2\,F\,D_I^{eff}} \tag{60b}$$

The flow of both species must be continuous at each interface between DSC components [33, 88]:

$$D_{I_3,i}^{eff}\left[\frac{dC_{I_3}(x)}{dx}\right]_{x=l_i} = D_{I_3,i+1}^{eff}\left[\frac{dC_{I_3}(x)}{dx}\right]_{x=l_i} \tag{61a}$$

$$D_{I,i}^{eff}\left[\frac{dC_I(x)}{dx}\right]_{x=l_i} = D_{I,i+1}^{eff}\left[\frac{dC_I(x)}{dx}\right]_{x=l_i} \tag{61b}$$

Index i denotes the place of the layer in the DSC, value 1 corresponding to the layer in direct contact with PE substrate. The interface of two successive layers (i and i+1) is at $x = l_i$. In addition to continuous fluxes, also the concentrations themselves must be continuous:

$$C_{j,i}(l_i) = C_{j,i+1}(l_i) \tag{62}$$

In addition to previous boundary condition the total amount of both species of a redox couple must be conserved during steady-state operation. When the initial concentration of species j is C_j^*, and the thickness of the layer is given by $d_i = l_i - l_{i-1}$, where l_{i-1} and l_i correspond to the interfaces with previous and next layer, this can be written as

$$C_{\mathrm{j}}^{*} \sum_{i} \epsilon_i \, d_i = \sum_{i} \epsilon_i \int_{l_{i-1}}^{l_i} C_{\mathrm{j,i}}(x) \, dx \tag{63}$$

Equations (55) – (63) enable modeling the charge carrier diffusion in electrolyte together with modeling the light harvesting and photocurrent production at the same time. There are more models that are more detailed and complicated about many things in DSCs, but they still keep the optical part of the simulation relatively simple [29].

Limiting current density (i_{lim}, or limiting current I_{lim}) is one of the most significant consequences of the charge transfer via diffusion: The PE can absorb some wavelength–dependent fraction of the incident light, so in theory it could produce more and more current as the intensity of the light increases. However, the mass transport in the electrolyte sets a limit for the maximum amount of current that can flow from CE to PE. The higher the current flowing through the DSC, the lower the I_3^--concentration at the CE. When the current is high enough, the I_3^--concentration is reduced to zero. In such situation the redox reaction at the CE (reaction (6)) cannot produce more I^- and electrons cannot be transferred from CE to electrolyte. The current at which this occurs is the maximum electric current that can be extracted from the DSC in steady-state operation. However, it is possible to extract higher current densities from the DSC during a very short period of time before the diffusion limitation reduces the current.

4.1.3 Porosity, tortuosity and constrictivity

Diffusion in bulk liquid is described by the diffusion coefficient of the species in liquid. In liquid inside porous material the diffusion in bulk liquid is the starting point, but the properties of the surrounding material set restrictions to how much and how fast the species can be transported through a porous material. Porosity (ϵ, equation (56)) is defined as the volume fraction of the material that is open to transport [90, 91]. It limits the amount of matter that can be transported through the material within certain time, but not directly the time it takes an individual atom, molecule or ion to diffuse through the material, at least as long as the porosity is above the percolation threshold [91].

The factors responsible for increasing the diffusion time of individual particles are tortuosity (τ^2, equation (56)) and constrictivity (γ, equation (56)) of the material. Tortuosity (factor) has several definitions in literature [90]. It is generally considered to be related to the ratio of the true path length between two points in a pore network and the euclidian distance between those points [90, 91, 92, 93, 94]. There are several expressions for tortuosity as a function of porosity in different geometries and systems, but apparently no consensus of the exact definition of tortuosity [90, 91, 93, 95]. The weakness of those formulae is that they merely give an approximation of the tortuosity in some disconnected situations and fail to relate it to its actual source – the microscale geometry of the pore space [90, 92].

The constrictivity is also related to the geometry of the pore space, but also to the size of the diffused particles; it describes the effect of the pore size of the diffusion of particles

of finite size [85]. Hence it is constrictivity that slows large particles or prevents them from being diffused through a material that smaller particles can diffuse through [83, 85, 96].

The macroscopically observable effects of tortuosity and constricitivity to any species of particles are identical to each other, so separating them from each other is difficult and requires measurements in geometry, where the effect of either one is known accurately [85]. Because of this their combined effect is generally presented with one factor, called for example matrix factor, geometric factor or tortuosity term [84, 97].

In the case of DSCs the diffusion through the TiO_2 film must not be restrained to allow efficient regeneration of dye cations. Typically the porosity of the film is considered to be around 0.5, although porosities even up to 0.6 have been observed [84, 98, 99]. Additionally, it has been observed that the adsorption of dye on the TiO_2 can reduce the porosity available for diffusion by up to 30% [100]. The TiO_2 film consists of randomly packed nanoparticles with some size distribution, the average diameter of the particles typically being around 20 nm [83, 99, 100]. The size of the pores in a naked TiO_2 film is almost the same as the size of the TiO_2 nanoparticles [83, 100]. The theoretical values for tortuosity (τ^2, equation (56)) of a film with porosity 0.5 that consists of randomly packed spheres are in the range 1.25–2.0 [89, 90, 91, 93]. The measured values for the matrix factor (combination of tortuosity and constrictivity) of real TiO_2 films range from 1 to 4, the most reliable probably being around 1.3–1.4, which is the tortuosity predicted by theory and simulations for overlapping spheres [84, 90, 91, 95, 98]. Considering the size of the pores (around 20 nm) and tri-iodide (less than 1 nm) it also seems quite unlikely that constrictivity would have a noticeable effect on the diffusion in TiO_2 film [85].

In addition to the light-absorbing PE, also the scattering layers and 1DPCs coupled with it consist of roughly spherical nanoparticles [23, 66]. Due to this structural similarity, the porosity and tortuosity of all three films are likely to be similar, although it is possible to make at least 1DPCs with different porosities [26]. The particles used for 1DPCs are smaller than those in the PE (TiO_2) or approximately the same size (SiO_2), whereas particles in scattering layers are significantly larger [23, 66]. Because the pore size quite likely correlates with the particles size, it seems that constrictivity would not limit diffusion through scattering layers, but could affect diffusion through 1DPCs noticeably [85].

4.2 Simulations

4.2.1 Performed calculations

The simulations were done for a DSC, whose PE was 5.3 μm thick (the measured average thickness of the screen printed TiO_2 films used as a substrate for the 1DPCs). The thickness of the 1DPC was varied between 0.6 μm (average thickness of the 1DPC films) and 1.2 μm. The properties of the scattering layer (SL) were taken from an article by Koo et al. [66]. Since an exact value for the thickness is not given, it is varied in the given range of 3–5 μm. From the available options, film G1 was chosen to represent a typical scattering layer. The total thickness of the DSCs was 25 μm, the thickness of the surlyn 1701 spacer used to seal DSCs. The exact relationship between the reflectance of the 1DPCs and scattering layer

and their thickness was not known, so it was (unrealistically) assumed that the thickness of the layer would not affect the optical properties (figure 42). The reflectance of 1DPC was the measured average of the reflectance spectra of 1DPCs S1 and S2 (when dry) modified similarly to 1DPCs N1–N10 (section 3.3.2) to take into account the effect of liquid in the pores.

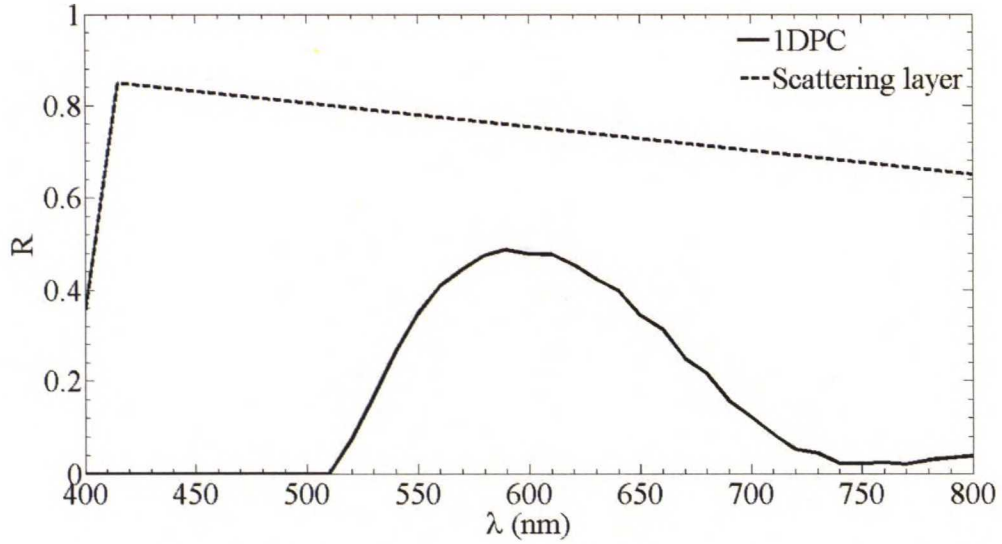

Figure 42: The reflectance spectra of scattering layer and 1DPC used in calculations.

The porosity of all layers was initially 0.5 and the tortuosity (τ^2) 1.37, which was the value measured for the matrix factor of TiO_2 film in [84]. The porosity of 1DPCs has been measured to be about 0.5 ± 0.05 [28]. In the case of scattering layer the porosity was an assumption based on structural similarity with TiO_2 film and 1DPCs. It was assumed that the effect of constrictivity on the diffusion of I^- and I_3^- in TiO_2 would be negligible, but the properties of a complete DSC were calculated for cases, where the constrictivity of 1DPC or scattered layer was varied between 0.01 and 1.

The calculations were performed with two different electrolytes: one with 3MPN as the solvent and an ionic liquid electrolyte. The diffusion coefficients and equilibrium concentrations of I^- and I_3^- in 3MPN were taken from [32]. The ionic liquid electrolyte was chosen to be Z594 from [101], because all necessary information was readily available. The diffusion coefficient used in calculations was the one calculated from measurements at $1000\,W/m^2$ illumination ($5.3{\cdot}10^{-7}\,cm^2s^{-1}$). The absorption coefficient of the 3MPN-based electrolyte was used as a basis for the optical properties of the electrolytes and adjusted linearly with respect to the equilibrium concentration of I_3^-. The local differences from equilibrium concentration were ignored in optical calculations.

The starting point was calculating the limiting current density of the DSC configuration in question. (See figure 43.) In the case of both electrolytes the concentration of I_3^- was the limiting factor, so the limiting current density corresponded to situation, where the I_3^- concentration at CE was zero. The concentration profiles were integrated numerically

with trapezoidal method from the boundary conditions. The DSCs were illuminated with sunlight that had the same relative spectrum as AM1.5G, but the intensity was varied to increase and decrease the photocurrent generation. The photocurrent was calculated according to the model introduced in sections 3.1.1, 3.1.2 and 3.1.4. The IV curve was calculated after the limiting current density was solved: First the IV curve of the PE and then the charge transfer (equation (48)) and diffusion overpotentials (equation (50)) were calculated and added to the IV curve of the PE for the total IV curve. Calculating the diffusion overpotential required knowing the concentrations of I^- and I_3^- at the CE. These concentrations were linear with respect to the generated photocurrent, so they could be calculated from equilibrium concentration and concentration at short circuit conditions. In this short circuit current means the highest photocurrent that the PE could produce in the simulated conditions, so it could be higher than the limiting current density. The concentrations were allowed to be negative for calculating the correct current concentration relationship, but in other calculations (e.g. equation (50)) negative concentrations were considered to be equal to zero.

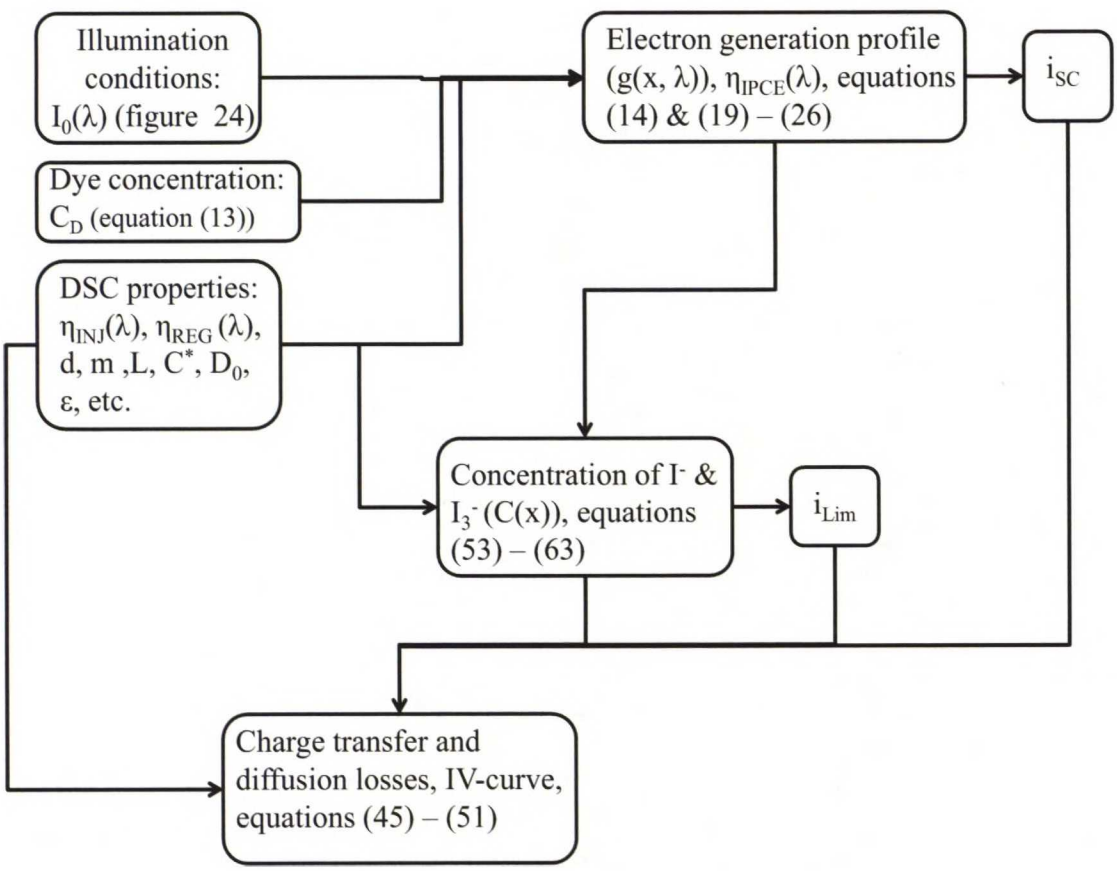

Figure 43: Calculations about the concentration profiles and IV-curve

4.2.2 Simulation parameters

This section includes a list of simulation parameters and variables that were needed for the calculations about diffusion in electrolyte in addition to, or to replace, parameters in section 3.3.4. If the value of any parameter is not given here, it is the same as in calculations about the color of the DSCs and in table 1.

The injection efficiency was estimated by simulating a DSC dyed with N719, whose PE thickness was 13.8 μm and total thickness 25 μm. The calculated short circuit current was compared to measurement results from similar DSCs, and injection efficiency was adjusted to fit the measurement results.

The thickness of the 1DPC was measured to be about 0.6 μm by measuring the thickness of the PEs coupled with 1DPC and similar PEs without 1DPC. The result, 0.6 μm, was used as a lower limit for the thickness of the 1DPC. The thickness of the scattering layer is based on values given in [66]. The reflectance of the 1DPC was measured and then modified to take into account the effect of the electrolyte in the pores as described in section 3.3.2. The spectrum in figure 42 is the result of the fitting.

Table 9: The parameters in simulations about diffusion in electrolyte

Parameter	Symbol	Value	Estimation
Thickness of the 1DPC/scattering layer	d_{1DPC}/d_{SL}	0.6 μm–5.0 μm	Profilometer and [66]
Bulk electrolyte thickness	d_{El}	19.7 μm – d_{1DPC}/d_{SL}	See also table 1
Porosity of TiO_2/1DPC/ scattering layer	ϵ	0.35, 0.50	Assumption, [28, 84, 100]
Tortuosity of TiO_2/ 1DPC/scattering layer	τ^2	1.37	[84], also [90, 91, 93, 95]
Constrictivity of TiO_2 film	γ	1.00	Assumption
Equilibrium concentration of I_3^-	$C_{I_3^-}{}^*$	0.05 M 0.20 M	3MPN, Preparation, [32] Z594, [101]
Equilibrium concentration of I_3^-	$C_{I^-}{}^*$	0.45 M 5.95 M	3MPN, Preparation, [32] Z594, [101]
Tri-iodide bulk diffusion coefficient	D_{0,I_3^-}	$4.85{\cdot}10^{-6}$ cm^2/s $5.3{\cdot}10^{-7}$ cm^2/s	3MPN, [32] Z594 in AM1.5G, [101]
Iodide bulk diffusion coefficient	D_{0,I^-}	$4.85{\cdot}10^{-6}$ cm^2/s $5.3{\cdot}10^{-7}$ cm^2/s	3MPN, assumed equal to D_{0,I_3^-}, [32] Z594, assumed equal to D_{0,I_3^-}, [101]
Electron injection efficiency	η_{Inj}	0.95	Adjusted to i_{SC}
CE charge transfer resistance at zero voltage	$R_{CE,0}$	9.2 Ωcm^2	[32]
Absorption coefficient of N719 dye	α_D	Figure 18	Measured, peak value near 530 nm is $1.3054{\cdot}10^5$ m^{-1}
Absorption coefficient of the electrolyte	α_{El}	Figure 20	Measured, adjusted to $C_{I_3^-}{}^*$ (equation (13))
Reflectance of the 1DPC/SL	R_{1DPC}/R_{SL}	Figure 42	1DPC measured, SL: G1 from [66]

4.3 Results and discussion

The limiting current densities and power conversion efficiencies of the simulated DSCs as a function of constrictivity of the reflecting layer are shown in figure 44. The solid horizontal lines indicate the efficiency and limiting current density without a reflecting layer, different dashed lines the highest photocurrents the configurations can generate in AM1.5G conditions.

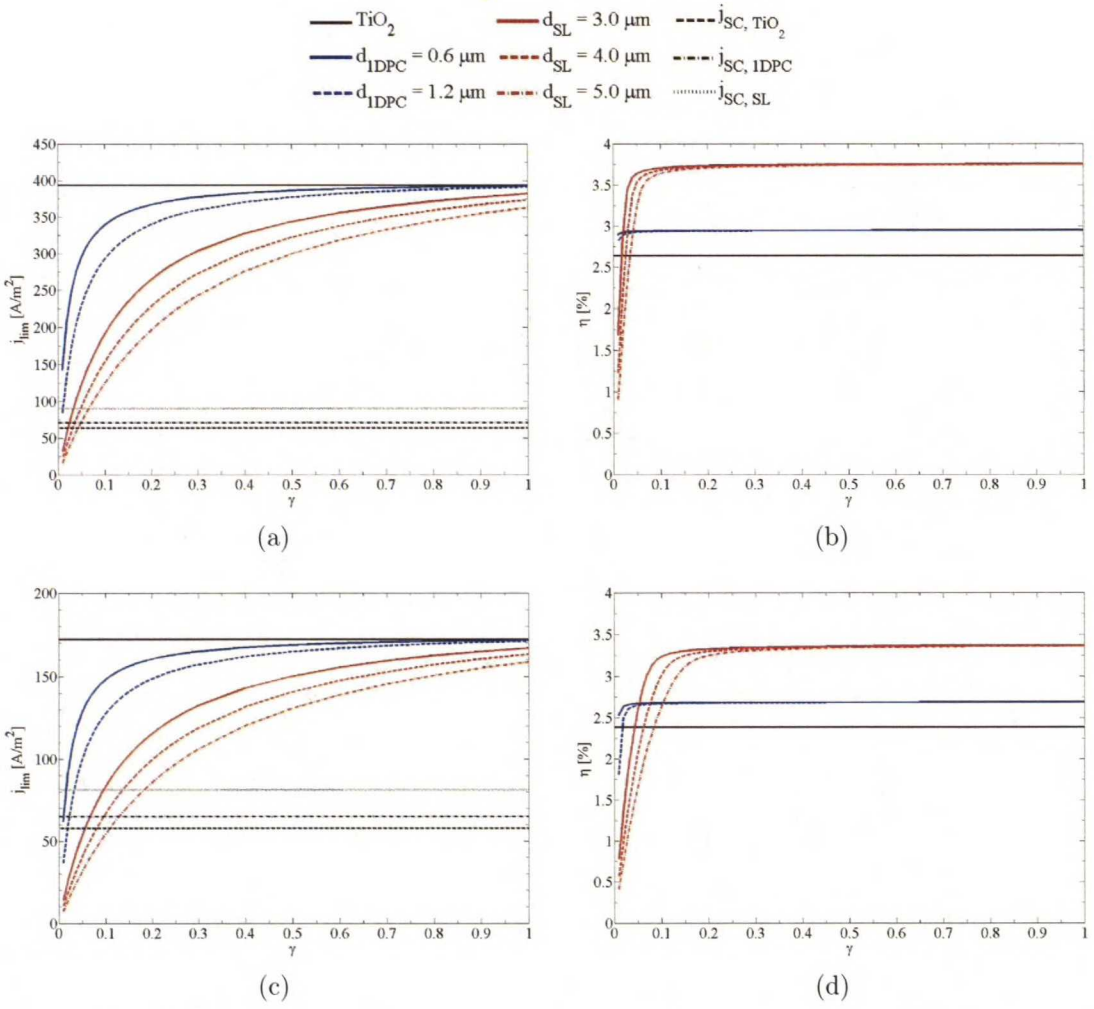

Figure 44: The limiting current densities (a, c) and efficiencies (b, d) of DSCs with 3MPN (a, b) and Z594 (c, d) electrolytes. Note the unit of current densities ($1\,\mathrm{A/m^2} = 0.1\,\mathrm{mA/cm^2}$).

The results show almost nothing that could not be anticipated even without the simulations. Due to higher reflectance, the PEs coupled with scattering layer produce higher photocurrent than the ones coupled with 1DPC. The significance of the thickness of the reflecting layer can be seen by comparing the limiting current densities with scattering layer and 1DPC at different constrictivities: The limiting current density of DSCs with scattering layer is comparable to ones with 1DPC, when both have high constrictivities.

However, when the value of constrictivity is reduced, the limiting current density with 1DPC is almost constant, until constrictivity value becomes very low. In the case of scattering layer, the layer thickness reduces the limiting current density faster than in the case of 1DPC. In the case of the thinner 1DPC, a constrictivity of 0.15 or less is required to reduce the limiting current below the level of scattering layers with $\gamma = 1$. This corresponds to a situation, where the diameter of the diffused molecules is more than one third of the diameter of the pores [85]. Such situation might be possible with a film consisting of very small particles. The average particle size in 1DPCs used in DSCs is around 5 nm, so without a further reduction in pore size at least I^- and I_3^- should be small enough that constrictivity is not a serious problem.

The efficiency of the DSCs with scattering layer is significantly higher than with 1DPCs, except when the constrictivity of both is low. Because of the higher photocurrent generation and lower limiting current density, the efficiency of the DSCs with scattering layer is also reduced notably more with higher constrictivities than in the case of 1DPC. Because the maximum photocurrent of DSCs with 1DPC is lower than limiting current density with almost all constrictivity values, their efficiency is not reduced, until the constrictivity of the 1DPC almost stops the diffusion. Such situation does not seem very likely, even if the pore size in the 1DPC can be very small: The 1DPCs consist of layers of SiO_2 and TiO_2. Some of the dye molecules may be diffused into PE through the 1DPC, so it is possible that they adsorb on the TiO_2 particles of the 1DPC. The size of the TiO_2 particles is small, on average about 5 nm [23]. The pores in TiO_2 layers should be about the same size [28]. The adsorbed dye molecules protrudge from the surface of the particles by up to 1.3 nm [102]. This could reduce the average pore diameter by up to 2.6 nm, which is a significant amount in a pore, whose diameter is around 5 nm. Hence the addition of dye in the 1DPC could significantly reduce the available pore volume of the TiO_2 layers. Considering that the size of I_3^- is around 0.6 nm, this might reduce the constrictivity from 0.6 to even 0.3 [85]. Such constrictivity would affect the diffusion, but based on the simulations, its effect on the limiting current density and efficiency seem negligible. However, the simulations do not take into account the effects of I^- and I_3^- concentrations on e.g. recombination and regeneration in PE. The reduced constrictivity values could have a significant effect on those via charge carrier depletion and accumulation in the pores of the TiO_2 film.

The shading effect of I_3^- can be seen by comparing the short circuit currents in figure 44: The higher I_3^- concentration of Z594 electrolyte absorbs more light than the I_3^- in 3MPN-based electrolyte. Because of this, the short circuit current of DSCs with Z594 is lower than the short circuit current of similar DSCs with 3MPN-based electrolyte. The change in light harvesting efficiency also changes the electron generation profile, which may contribute slightly to efficiency through collection efficiency.

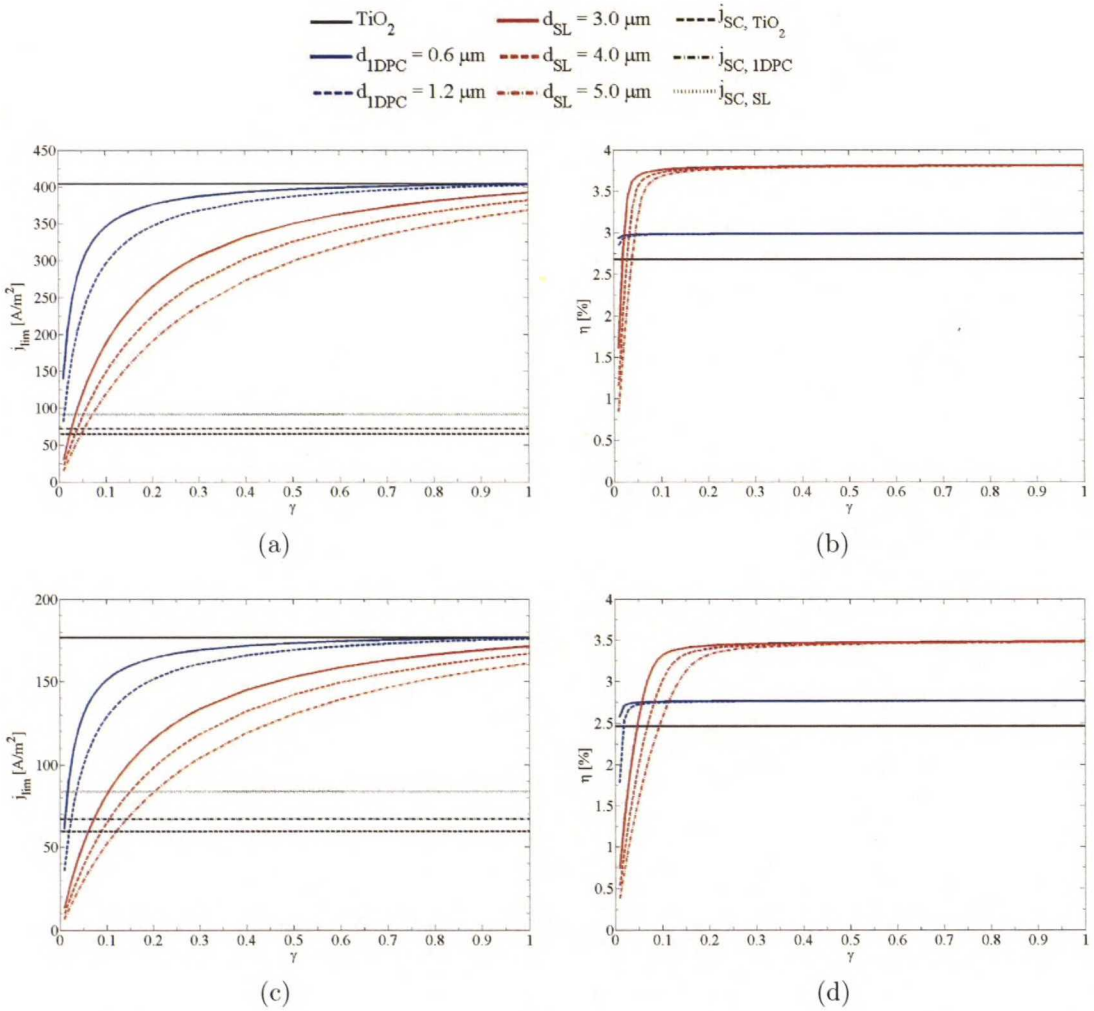

Figure 45: The limiting current densities (a, c) and efficiencies (b, d) of DSCs with 3MPN (a, b) and Z594 (c, d) electrolytes, when porosity of all layers is reduced to 0.35. Note the unit of current densities ($1\,\mathrm{A/m^2} = 0.1\,\mathrm{mA/cm^2}$).

It has been shown that the dye adsorption can reduce the pore volume of TiO_2 films by up to 30% [100]. The effects of such drastic reduction in porosity were tested by doing the simulations again with $\epsilon = 0.35$ in all layers (PE, 1DPC, scattering layer). In the 1DPCs the volume reduction could be more significant due to smaller pore size, and correspondingly less significant in scattering layers due to larger particles and pores. The short circuit and limiting current densities along with efficiencies are shown in figure 45. The reduced porosity also reduces the optical shading of electrolyte (in equilibrium), which slightly increased the short circuit currents of all DSC configurations. It is interesting that also the limiting current densities were slightly increased. Some part of this may be explained with the reduced optical shading and changed electron generation profile, but apparently reducing porosity may actually increase the limiting current density, if the PE is thinner than the bulk electrolyte. The curves in figure 46 were calculated according to an analytical

solution for limiting current density in a DSC with a PE consisting of only dyed TiO_2 under monochromatic illumination and Beer-Lambert light absorption (deduced in [33]):

$$i_{\mathrm{lim,PE}} = \frac{6\epsilon q_{\mathrm{e}} N_{\mathrm{A}} D_0 C^*_{I_3^-}}{d_{\mathrm{PE}}} \frac{1 + \frac{d_{\mathrm{El}}}{\epsilon d_{\mathrm{PE}}}}{\frac{1}{f_{\mathrm{PE}}(A_\lambda)} + 3\epsilon \frac{d_{\mathrm{EL}}}{d_{\mathrm{PE}}} + \frac{3}{2}\left(\frac{d_{\mathrm{EL}}}{d_{\mathrm{PE}}}\right)^2} \tag{64a}$$

$$f_{\mathrm{PE}}(A_\lambda) = \frac{2}{3} \frac{A_\lambda^2 \ln(10)^2 \left(10^{A_\lambda} - 1\right)}{A_\lambda^2 \ln(10)^2 10^{A_\lambda} + 2A_\lambda \ln(10) - 2\left(10^{A_\lambda} - 1\right)} \tag{64b}$$

The bulk liquid diffusion constant of I_3^- is D_0 and its equilibrium concentration is $C_{I_3^-}{}^*$. The optical thickness of the PEs in figure 46 is $A_\lambda = 1$, which corresponds to transmittance $T = 10^{-A_\lambda} = 0.1$. The limiting current densities of the analytical solution depend on the optical thickness of the PE, which is not taken into account in figure 46. This dependency would only decrease the limiting currents of thick PEs with respect to thinner PEs with same porosity. The largest changes would occur with low porosities, while high porosities would be less affected, which would only increase the differences in figure 46. When the TiO_2 film is thin enough, correctly chosen monochromatic illumination approximates the electron generation under AM1.5G illumination quite accurately [29]. The results corresponding to thicker PEs are thus somewhat more inaccurate than the results about thin PEs. The total thickness of the DSC was kept constant at 25 μm. This scenario approximately corresponds to "TiO_2" in figures 44 and 45, where $d_{\mathrm{El}}/d_{\mathrm{PE}} \approx 3.8$. Values corresponding to 3MPN-based electrolyte were used in calculations for figure 46.

The presented analytical solution supports the possibility that a small decrease in porosity may increase the limiting current density of a DSC, when the bulk electrolyte is thicker than the PE. It does not offer any physical explanation for this phenomenon, but neither do the simulation results. In the article, where the solution was given, it was used to study the effects of changing the thickness of the bulk electrolyte layer with a constant PE thickness instead of changing the PE thickness with constant DSC thickness, as was done here [33]. Therefore the behaviour observed here may not have been noticed by the authors, which explains the lack of explanation for this behaviour. In the absence of an explanation, this behaviour remains a mystery.

The increased short circuit currents were also based on the assumption that the reduced porosity would not affect the surface area that the dye molecules can adsorb on. The reason for the simulations with reduced porosity was essentially to study the effect of the volume taken by the dye molecules. Thus in this case the situation can be considered as a comparison of the simulation accuracy between a situation with dye molecules of finite size and a situation, where the volume taken by the dye is ignored. Otherwise the assumption of unchanged surface area may hold with small changes in porosity, but in the case 30% reduction it would be at least questionable. Especially against this background it seems very interesting that the reduced pore volume would actually increase both limiting current density and efficiency of the DSCs, when intuition would suggest a completely opposite effect: In the case of both electrolytes the efficiency was increased in most cases, when

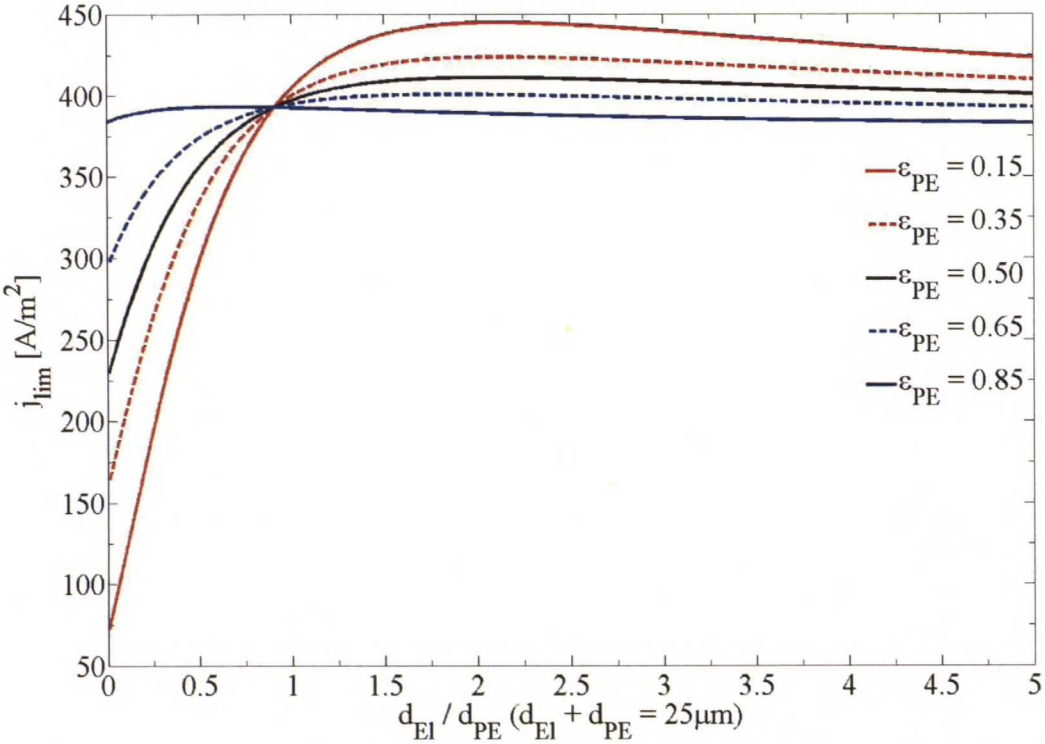

Figure 46: The limiting current densities of DSCs with dyed TiO_2 as PE as a function of the ratio of d_{El} and d_{PE}. The comparison of different PE porosities illustrates, how the limiting current density behaves differently as a function of porosity in the case of thin and thick PEs.

porosity was reduced from 0.50 to 0.35. The increase was caused by increased limiting current density and reduced optical shadowing. In the case of the scattering layers the efficiency was slightly reduced, when constrictivity values were very low, most likely because no electrons were generated in the layer, but it significantly impeded diffusion.

The results in figures 44 and 45 show only, how the structure of the DSC affects the limiting current density and how this affects the efficiency via charge transfer and diffusion overpotentials. Since the efficiencies appear to be almost unaffected by the constrictivity of the reflecting layer, the CE overpotential is not likely to be the main problem with reflecting layers and slow diffusion through them. A more likely candidate for possible observed losses in real-life DSCs are the reduction in dye regeneration and increase in recombination with conduction band electrons in PE, which were not taken into account in the model. Both regeneration and recombination rates depend linearly on the concentration of the redox species taking part in the reaction in question [29]. In the worst case a very constrictive 1DPC can increase the I_3^- level to several times the equilibrium concentration and deplete the PE of I^- almost completely. It might even be possible that the true current density limitation is not set by the I_3^- concentration at CE, but the lack of regeneration and increased recombination and optical shadowing in PE. The connection between the concentrations of the redox couple and these phenomena strongly suggests that a decrease in constrictivity value of the reflecting layer should affect the short circuit current and

efficiency of the DSC more than predicted by the calculations. The lack of regeneration and recombination effects in the model also seems likely to be the reason for the counter-intuitive increase in efficiency, when the pore volume available to electrolyte was decreased from 0.50 to 0.35. However, estimating the losses caused by regeneration, recombination and shadowing issues, and the efficiency, would require more detailed models.

The particle size in the scattering films is large enough that constrictivity is not likely to a problem with them, so simulation results about them and DSCs with only dyed TiO_2 as the PE, when $\gamma \approx 1$ should be relatively accurate estimations about the performance of the simulated DSC configurations, at least with 3MPN-based electrolyte. Otherwise the lack of changes in efficiency shows that the CE overpotential is not likely to be a very significant loss factor in these DSCs. In the case of 1DPCs it is difficult to say, how constrictive the films are. The particle size, and hence the pore size, are known to be small, but thay may still be large enough that the charge carriers can diffuse through the pore network quite freely [23, 28, 85]. Therefore it is impossible to say with certainty anything about the possible performance limitations caused by 1DPCs, except that they are not likely to be a caused by charge transfer or diffusion overpotentials, but rather some other effect of accumulation of I_3^- and lack of I^- in PE.

5 Conclusions

5.1 Optical model and color predictions

The optical model turned out to give quite accurate predictions about the optical properties of the DSCs. The shift in the measured transmittance spectrum of DSCs compared to that of PEs with same dye concentration was most likely caused by some reaction. As this was assumed not to happen in the model, it seems that the model does not take all necessary phenomena into account, but is otherwise capable of accurate predictions.

The color of the samples could be calculated accurately, when the optical properties and lighting conditions were known accurately enough. Small differences in optical properties did not have as large effects on the results as the lighting conditions. Differences in light intensity, that were almost invisible to naked eye, clearly affected the predicted colors. Similarly to this, the settings of the camera can affect the results, mostly by making the photos either overexposed or severely underexposed.

Despite the inaccuracies in predicting the optical properties, the method used to calculate the color of the 1DPCs/DSCs seems to be very accurate, when the lighting conditions are known. Based on this, it seems possible to predict the appearance of a DSC with any dye-1DPC combination. The performance predictions will require additional information about the charge transfer and diffusion losses. Additionally, more detailed information about e.g. the recombination with the used dyes and electrolytes may be needed in some cases that significantly differ from typical situations. Otherwise the calculation method could well be used to predict the appearance and performance potential of different DSC configurations with given transparency requirements.

5.2 Diffusion model and overpotentials

Modeling the diffusion in electrolyte improves the accuracy of the performance predictions about the DSCs. Based on them it may seem initially that the diffusion through the 1DPCs would not be a performance limiting factor alone, unless the electrolyte is very viscous.

It seems likely that the most significant losses caused by the 1DPCs are not a consequence of reduced limiting current density that increases diffusion losses, but caused by the optical shadowing, reduced dye regeneration and increased recombination due to very low I^- and high I_3^- concentrations in the TiO_2 film. Since these phenomena were not accounted for in the model used in the calculations, determining their effect would require more detailed simulations about the DSC configurations. Moreover, since they may well cause more losses than the CE overpotential, more detailed simulations may well be required for simulating the effects of especially 1DPCs on the efficiency of the DSCs. Because of these unanswered questions the picture of the 1DPCs as reflecting films that do not obstruct diffusion enough to cause significant losses may yet change significantly, if more accurate simulations about diffusion and its effect on recombination and regeneration will be done. To some extent this applies also for scattering layers, but in their case the pore size is significantly larger. Hence the most significant factor for concentrations is not the constrictivity, but the thickness of the layer.

The simulation results may not have been as accurate as could be hoped for, because the effect of the concentrations of I_3^- and I^- on regeneration and recombination was not considered, but at least they clearly indicate that the CE overpotential should not be a significant loss factor with simulated DSC configurations. This removes these overpotentials from the list of the most significant problems, if real DSCs with coupled reflective layer have significantly lower efficiency than predicted here. Additionally the results show that the DSCs that have a reflective layer coupled with their PE could in theory achieve significant efficiency improvements, if the potential problems with recombination and regeneration can be solved. The magnitude of these problems would have to be calculated with more detailed models. Comparisons with experiments and more detailed models would show, whether the model used here would be accurate enough for characterising diffusion related problems in DSCs or not. Until that is done, it seems that the results for high constrictivity values may well be accurate, but the others are more or less questionable and should be used with caution.

References

[1] International Energy Agency, "Key world energy statistics 2011." http://www.iea.org/textbase/nppdf/free/2011/key_world_energy_stats.pdf, Oct. 2011.

[2] B. Kavalov and S. D. Petens, "The future of coal," Feb. 2007. ISBN 978-92-79-05531-7.

[3] U.S. Energy Information Administration, "International energy outlook 2011," Sept. 2011. DOE/EIA-0484(2011).

[4] W. Zittel and J. Schindler, "Coal: Resources and future production." EWG-Series No 1/2007, Mar. 2007.

[5] B. Parida, S. Iniyan, and R. Goic, "A review of solar photovoltaic technologies," *Renewable and Sustainable Energy Reviews*, vol. 15, no. 3, pp. 1625–1636, 2011.

[6] R. Laleman, J. Albrecht, and J. Dewulf, "Life cycle analysis to estimate the environmental impact of residential photovoltaic systems in regions with a low solar irradiation," *Renewable and Sustainable Energy Reviews*, vol. 15, no. 1, pp. 267–281, 2011.

[7] M. Oliver and T. Jackson, "Energy and economic evaluation of building-integrated photovoltaics," *Energy*, vol. 26, no. 4, pp. 431–439, 2001.

[8] "Building-integrated photovoltaics." http://en.wikipedia.org/wiki/Building-integrated_photovoltaics, Nov. 2011.

[9] M. Pagliaro, R. Ciriminna, and G. Palmisano, "BIPV: merging the photovoltaic with the construction industry," *Progress in Photovoltaics: Research and Applications*, vol. 18, no. 1, pp. 61–72, 2010.

[10] "2010 Solar prize for klein Matterhorn restaurant." http://www.zimbio.com/Zermatt+Travel+Itinerary/articles/MuFUItiniDQ/2010+Solar+Prize+Klein+Matterhorn+Restaurant, Nov. 2011.

[11] "2010 European solar prize for Zermatt Bergbahnen." http://www.zermatt.ch/en/page.cfm/contact/presscorner/pc_press_releases/pm_solarpreis_eu, Nov. 2011.

[12] M. Raugei and P. Frankl, "Life cycle impacts and costs of photovoltaic systems: Current state of the art and future outlooks," *Energy*, vol. 34, no. 3, pp. 392–399, 2009.

[13] G. Bizzarri, M. Gillott, and V. Belpoliti, "The potential of semitransparent photovoltaic devices for architectural integration," *Sustainable Cities and Society*, vol. 1, no. 3, pp. 178–185, 2011.

[14] T. Miyazaki, A. Akisawa, and T. Kashiwagi, "Energy savings of office buildings by the use of semi-transparent solar cells for windows," *Renewable Energy*, vol. 30, no. 3, pp. 281–304, 2005.

[15] T.-T. Chow, Z. Qiu, and C. Li, "Potential application of "see-through" solar cells in ventilated glazing in hong kong," *Solar Energy Materials and Solar Cells*, vol. 93, no. 2, pp. 230–238, 2009.

[16] T. Y. Y. Fung and H. Yang, "Study on thermal performance of semi-transparent building-integrated photovoltaic glazings," *Energy and Buildings*, vol. 40, no. 3, pp. 341–350, 2008.

[17] W. Tian, Y. Wang, J. Ren, and L. Zhu, "Effect of urban climate on building integrated photovoltaics performance," *Energy Conversion and Management*, vol. 48, no. 1, pp. 1–8, 2007.

[18] M. Grätzel and B. C. O'Regan, "A low-cost, high-efficiency solar cell based on dye sensitized colloidal TiO_2 films," *Nature*, vol. 353, pp. 737–740, 1991.

[19] L. M. Peter, "Dye-sensitized nanocrystalline solar cells," *Physical Chemistry Chemical Physics*, vol. 9, no. 21, pp. 2630–2642, 2007.

[20] "Long-term stability of dye solar cells." `http://reginnovations.com/key-scientific-articles/long-term-stability-of-dye-solar-cells/`, Nov. 2011.

[21] A. Mihi, M. E. Calvo, J. A. Anta, and H. Miguez, "Spectral response of opal-based dye-sensitized solar cells," *Journal of Physical Chemistry C*, vol. 112, no. 1, pp. 13–17, 2008.

[22] S. Guldin, S. Hüttner, M. Kolle, M. E. Welland, P. Müller-Buschbaum, R. H. Friend, U. Steiner, and N. Tétreault, "Dye-sensitized solar cells based on three-dimensional photonic crystal," *Nano Letters*, vol. 10, no. 7, pp. 2303–2309, 2010.

[23] S. Colodrero, A. Mihi, L. Häggman, M. Ocaña, G. Boschloo, A. Hagfeldt, and H. Míguez, "Porous one-dimensional photonic crystals improve the power-conversion efficiency of dye-sensitized solar cells," *Advanced Materials*, vol. 21, no. 7, pp. 764–770, 2009.

[24] G. Lozano, S. Colodrero, O. Caulier, M. E. Calvo, and H. Míguez, "Theoretical analysis of the performance of one-dimensional photonic crystal-based dye-sensitized solar cells," *Journal of Physical Chemistry C*, vol. 114, no. 8, pp. 3681–3687, 2010.

[25] M. E. Calvo and H. Míguez, "Flexible, adhesive, and biocompatible bragg mirrors based on polymethylsiloxane infiltrated nanoparticle multilayers," *Chemistry of Materials*, vol. 22, no. 13, pp. 3909–3915, 2010.

[26] L. González-García, G. Lozano, A. Barranco, H. Míguez, and A. R. González-Elipe, "TiO_2–SiO_2 one-dimensional photonic crystals of controlled porosity by glancing angle physical vapour deposition," *Journal of Materials Chemistry*, vol. 20, no. 31, pp. 6408–6412, 2010.

[27] N. Hidalge, M. E. Calco, S. Colodrero, and H. Míguez, "Porous one-dimensional photonic crystal coatings for gas detection," *IEEE Sensors Journal*, vol. 10, no. 7, pp. 1206–1212, 2010.

[28] C. López-López, S. Colodrero, S. R. Raga, H. Lindström, F. Fabregat-Santiago, J. Bisquert, and H. Míguez, "Enhanced diffusion through porous nanoparticle optical multilayers," *Journal of Materials Chemistry*, vol. 22, no. 5, pp. 1751–1757, 2012.

[29] P. R. F. Barnes, A. Y. Anderson, J. R. Durrant, and B. C. O'Regan, "Simulation and measurement of complete dye sensitised solar cells: including the influence of trapping, electrolyte, oxidised dyes and light intensity on steady state and transient device behaviour," *Phys.Chem.Chem.Phys.*, vol. 13, pp. 5798–5816, 2011.

[30] T. L. Bahers, F. Labat, T. Pauporte, P. P. Laine, and I. Ciofini, "Theoretical procedure for optimizing dye-sensitized solar cells: From electronic structure to photovoltaic efficiency," *Journal of the American Chemical Society*, vol. 133, pp. 8005–8013, 2011.

[31] S. Södergren, A. Hagfeldt, J. Olsson, and S. E. Lindquist, "Theoretical models for the action spectrum and the current-voltage characteristics of microporous semiconductor films in photoelectrochemical," *Journal of Physical Chemistry*, vol. 98, p. 5552, 1994.

[32] J. Halme, P. Vahermaa, K. Miettunen, and P. Lund, "Device physics of dye solar cells," *Advanced Energy materials*, vol. 22, no. 35, pp. E210–E234, 2010.

[33] N. Papageorgiou, M. Grätzel, and P. P. Infelta, "On the relevance of mass transport in thin layer nanocrystalline photoelectrochemical solar cells," *Solar Energy Materials and Solar Cells*, vol. 44, no. 4, pp. 405–438, 1996.

[34] T. Ameri, G. Dennler, C. Waldauf, H. Azimi, A. Seemann, K. Forberich, J. Hauch, M. Scharber, K. Hingerl, and C. J. Brabec, "Fabrication, optical modeling, and color characterization of semitransparent bulk-heterojunction organic solar cells in an inverted structure," *Advanced Functional Materials*, vol. 20, pp. 1592–1598, 04-21 2010.

[35] Y. Chiba, A. Islam, Y. Watanabe, R. Komiya, N. Koide, and L. Han, "Dye-sensitized solar cells with conversion efficiency of 11.1%," *Japanese Journal of Applied Physics*, vol. 45, no. 25, pp. L638–L640, 2006.

[36] "Dyes for organic solar cells." http://www.uni-ulm.de/en/nawi/institute-of-organic-chemistry-ii-and-advanced-materials/research/research-groups-rg/dyes-for-organic-solar-cells.html, Dec. 2011.

[37] A. Hagfeldt, G. Boschloo, L. Sun, L. Kloo, and H. Pettersson, "Dye-sensitized solar cells," *Chemical reviews*, vol. 110, pp. 6595–6663, 2010.

[38] K. Hara and H. Arakawa, *Dye-sensitized Solar Cells*, ch. 15, pp. 665–682. John Wiley & Sons Ltd., 2003.

[39] B. C. O'Regan and J. R. Durrant, "Kinetic and energetic paradigms for dye-sensitized solar cells: Moving from the ideal to the real," *Accounts of Chemical Research*, vol. 42, pp. 1799–1808, 2009.

[40] L. M. Peter, ""Sticky electrons" transport and interfacial transfer of electrons in the dye-sensitized solar cell," *Accounts of Chemical Research*, vol. 42, no. 11, pp. 1839–1847, 2009.

[41] Y. Suzuki, S. Ngamsinlapasathian, R. Yoshida, and S. Yoshikawa, "Partially nanowire-structured TiO_2 electrode for dye-sensitized solar cells," *Central European Journal of Chemistry*, vol. 4, no. 3, pp. 476–488, 2006.

[42] K. Jung, J. S. Hong, R. Vittal, and K.-J. Kim, "Enhanced photocurrent of dye-sensitized solar cells by modification of TiO_2 with carbon nanotubes," *Chemistry Letters*, vol. 31, no. 8, pp. 864–865, 2002.

[43] K. Jung, S.-R. Jang, R. Vittal, D. Kim, and K.-J. Kim, "Photocurrent improvement by incorporation of single-wall carbon nanotubes in TiO_2 film of dye-sensitized solar cells," *Bulletin of Korean Chemical Society*, vol. 24, no. 10, pp. 1501–1504, 2003.

[44] S.-R. Jang, R. Vittal, and K.-J. Kim, "Incorporation of functionalized single-wall carbon nanotubes in dye-sensitized TiO_2 solar cells," *Langmuir*, vol. 20, no. 22, pp. 9807–9810, 2004.

[45] C.-Y. Yen, Y.-F. Lin, S.-H. Liao, C.-C. Weng, C.-C. Huang, Y.-H. Hsiao, C.-C. M. Ma, M.-C. Chang, H. Shao, M.-C. Tsai, C.-K. Hsieh, C.-H. Tsai, and F.-B. Weng, "Preparation and properties of a carbon nanotube-based nanocomposite photoanode for dye-sensitized solar cells," *Nanotechnology*, vol. 19, no. 37, p. 375305, 2008.

[46] T. Sawatsuk, A. Chindaduang, C. Sae-kung, S. Pratontep, and G. Tumcharern, "Dye-sensitized solar cells based on TiO_2-MWCNTs composite electrodes: Performance improvement and their mechanisms," *Diamond & Related Materials*, vol. 18, no. 2-3, pp. 524–527, 2009.

[47] K.-M. Lee, C.-W. Hu, H.-W. Chen, and K.-C. Ho, "Incorporating carbon nanotube in a low-temperature fabrication process for dye-sensitized TiO_2 solar cells," *Solar Energy Materials & Solar Cells*, vol. 92, no. 12, pp. 1628–1633, 2008.

[48] T. Horiuchi, "Highly efficient metal-free organic dyes for dye-sensitized solar cells," *Journal of Photochemistry and Photobiology A: Chemistry*, vol. 164, no. 1-3, pp. 29–32, 2004.

[49] T. Horiuchi, H. Miura, K. Sumioka, and S. Uchida, "High efficiency of dye-sensitized solar cells based on metal-free indoline dyes," *Journal of the American Chemical Society*, vol. 126, no. 39, pp. 12218–12219, 2004.

[50] T. Horiuchi, H. Miura, and S. Uchida, "Highly-efficient metal-free organic dyes for dye-sensitized solar cells," *Chemical Communications*, no. 24, p. 3036, 2003.

[51] L. Schmidt-Mende, U. Bach, R. Humphry-Baker, T. Horiuchi, H. Miura, S. Ito, S. Uchida, and M. Grätzel, "Organic dye for highly efficient solid-state dye-sensitized solar cells," *Advanced Materials*, vol. 17, no. 7, pp. 813–815, 2005.

[52] S. Ito, S. M. Zakeeruddin, R. Humphry-Baker, P. Liska, R. Charvet, P. Comte, M. K. Nazeeruddin, P. Péchy, M. Takata, H. Miura, S. Uchida, and M. Grätzel, "High-efficiency organic-dye-sensitized solar cells controlled by nanocrystalline-TiO_2 electrode thickness," *Advanced Materials*, vol. 18, no. 9, pp. 1202–1205, 2006.

[53] A. Ehret, L. Stuhl, and M. T. Spitler, "Spectral sensitization of TiO_2 nanocrystalline electrodes with aggregated cyanine dyes," *The Journal of Physical Chemistry B*, vol. 105, no. 41, pp. 9960–9965, 2001.

[54] R. Y. Ogura, S. Nakane, M. Morooka, M. Orihashi, Y. Suzuki, and K. Noda, "High-performance dye-sensitized solar cell with a multiple dye system," *Applied Physics Letters*, vol. 94, no. 7, p. 073308, 2009.

[55] M. A. Green, K. Emery, Y. Hishikawa, W. Warta, and E. D. Dunlop, "Solar cell efficiency tables (Version 38)," *Progress in Photovoltaics: Research and Applications*, vol. 19, pp. 565–572, 2011.

[56] H. N. Tsao, C. Yi, T. Moehl, J.-H. Yum, S. M. Zakeeruddin, M. K. Nazeeruddin, and M. Grätzel, "Cyclopentadithiophene bridged donor-acceptor dyes achieve high power conversion efficiencies in dye-sensitized solar cells based on the tris-cobalt bipyridine redox couple," *ChemSusChem*, vol. 4, no. 5, pp. 591–594, 2011.

[57] S. M. Feldt, E. A. Gibson, E. Gabrielsson, L. Sun, G. Boschloo, and A. Hagfeldt, "Design of organic dyes and cobalt polypyridine redox mediators for high-efficiency dye-sensitized solar cells," *Journal of the American Chemical Society*, vol. 132, no. 26, pp. 16714–16724, 2010.

[58] G. Boschloo and A. Hagfeldt, "Characteristics of the iodide/triiodide redox mediator in dye-sensitized solar cells," *Accounts of Chemical Research*, vol. 42, no. 11, pp. 1819–1826, 2009.

[59] P. Wang, B. Wenger, R. Humphry-Baker, J.-E. Moser, J. Teuscher, W. Kantlehner, J. Mezger, E. V. Stoyanov, S. M. Zakeeruddin, and M. Grätzel, "Charge separation and efficient light energy conversion in sensitized mesoscopic solar cells based on binary ionic liquids," *Journal of the American Chemical Society*, vol. 127, no. 18, pp. 6850–6856, 2005.

[60] S. E. Koops, B. C. O'Regan, P. R. Barnes, and J. R. Durrant, "Parameters influencing the efficiency of electron injection in dye-sensitized solar cells," *Journal of the American Chemical Society*, vol. 131, no. 13, pp. 4808–4818, 2009.

[61] A. Y. Anderson, P. R. F. Barnes, J. R. Durrant, and B. C. O'Regan, "Quantifying regeneration in dye-sensitized solar cells," *The Journal of Physical Chemistry C*, vol. 115, no. 5, pp. 2439–2447, 2011.

[62] J. Halme, G. Boschloo, A. Hagfeldt, and P. Lund, "Spectral characteristics of light harvesting, electron injection, and steady-state charge collection in pressed TiO_2 dye solar cells," *Journal of Physical Chemistry C*, vol. 112, no. 14, pp. 5623–5637, 2008.

[63] K. Miettunen, I. Asghar, X. Ruan, J. Halme, T. Saukkonen, and P. Lund, "Stabilization of metal counter electrodes for dye solar cells," *Journal of Electroanalytical Chemistry*, vol. 653, no. 1-2, pp. 93–99, 2011.

[64] S. Inoue and Y. Aoyagi, "Design and fabrication of two-dimensional photonic crystals with predetermined nonlinear optical properties," *Physical Review Letters*, vol. 94, no. 10, 2005.

[65] A. Bauer, M. Müller, T. Lehnhardt, K. Rößner, M. Hümmer, H. Hofmann, M. Kamp, S. Höfling, and A. Forchel, "Discretely tunable single-mode lasers on GaSb using two-dimensional photonic crystal intracavity mirrors," *Nanotechnology*, vol. 19, no. 23, p. 235202, 2008.

[66] H.-J. Koo, J. Park, B. Yoo, K. Yoo, K. Kim, and N.-G. Park, "Size-dependent scattering efficiency in dye-sensitized solar cell," *Inorganica Chimica Acta*, vol. 361, no. 3, pp. 677–683, 2008.

[67] J. Bisquert and I. Mora-Sero, "Simulation of steady-state characteristics of dye-sensitized solar cells and the interpretation of the diffusion length," *The Journal of Physical Chemistry Letters*, vol. 1, pp. 450–456, 2010.

[68] J. Villanueva-Cab, H. Wang, G. Oskam, and L. M. Peter, "Electron diffusion and back reaction in dye-sensitized solar cells: The effect of nonlinear recombination kinetics," *The Journal of Physical Chemistry Letters*, vol. 1, no. 4, pp. 748–751, 2010.

[69] J. R. Jennings, A. Ghicov, L. M. Peter, P. Schmuki, and A. B. Walker, "Dye-sensitized solar cells based on oriented TiO_2 nanotube arrays: Transport, trapping, and transfer of electrons," *Journal of the American Chemical Society*, vol. 130, no. 40, pp. 13364–13372, 2008.

[70] C. A. Poynton, "'Gamma" and its disguises: The nonlinear mappings of intensity in perception, CRTs, film and video," *SMPTE Journal*, vol. 102, no. 12, pp. 1099–1108, 1993.

[71] "Cone cell." `http://en.wikipedia.org/wiki/Cone_cell`, Oct. 2011.

[72] K. A. Jameson, S. M. Highnote, and L. M. Wasserman, "Richer color experience in observers with multiple photopigment opsin genes," *Psychonomic Bulletin & Review*, vol. 8, no. 2, pp. 244–261, 2001.

[73] J. L. Schnapf, T. W. Kraft, and D. A. Baylor, "Spectral sensitivity of human cone photoreceptors," *Nature*, vol. 325, no. 6103, pp. 439–441, 1987.

[74] J. Nathans, D. Thomas, and D. Hogness, "Molecular genetics of human color vision: the genes encoding blue, green, and red pigments," *Science*, vol. 232, no. 4747, pp. 193–202, 1986.

[75] C. Oleari and M. Pavesi, "Grassmann's laws and individual color-matching functions for non-spectral primaries evaluated by maximum saturation technique in foveal vision," *Color Research & Application*, vol. 33, no. 4, pp. 271–281, 2008.

[76] "RGB color model." `http://en.wikipedia.org/wiki/RGB_color_model`, Oct. 2011.

[77] "CIE 1931 color space." `http://en.wikipedia.org/wiki/CIE_1931_color_space`, Oct. 2011.

[78] H. S. Fairman, M. H. Brill, and H. Hemmendinger, "How the CIE 1931 color-matching functions were derived from Wright-Guild data," *Color Research & Application*, vol. 22, no. 1, pp. 11–23, 1997.

[79] "Specification of sRGB. (Specified in IEC 61966-2-1:1999)." `http://www.color.org/sRGB.pdf`, Nov. 2011.

[80] J. Schanda, ed., *Colorimetry: Understanding the CIE system.* Wiley-Interscience, 2007. ISBN 9780470049044.

[81] "What colour is the sun?." `http://casa.colorado.edu/~ajsh/colour/Tspectrum.html`, Nov. 2011.

[82] T. Miyasaka, "Toward printable sensitized mesoscopic solar cells: Light-harvesting management with thin TiO_2 films," *The Journal of Physical Chemistry Letters*, vol. 2, no. 3, pp. 262–269, 2011.

[83] M. Dürr, A. Schmid, M. Obermaier, A. Yasuda, and G. Nelles, "Diffusion properties of dye molecules in nanoporous TiO_2 networks," *The Journal of Physical Chemistry A*, vol. 109, no. 17, pp. 3967–3970, 2005.

[84] G. Kron, U. Rau, M. Dürr, T. Miteva, G. Nelles, A. Yasuda, and J. H. Werner, "Diffusion limitations to I_3^-/I^- electrolyte transport through nanoporous TiO_2 networks," *Electrochemical and Solid-State Letters*, vol. 6, no. 6, pp. E11–E14, 2003.

[85] R. E. Beck and J. S. Schultz, "Hindered diffusion in microporous membranes with known pore geometry," *Science*, vol. 170, no. 3964, pp. 1302–1305, 1970.

[86] I. Montanari, J. Nelson, and J. R. Durrant, "Iodide electron transfer kinetics in dye-sensitized nanocrystalline TiO_2 films," *The Journal of Physical Chemistry B*, vol. 106, no. 47, pp. 12203–12210, 2002.

[87] C. Nasr, S. Hotchandani, and P. V. Kamat, "Role of iodide in photoelectrochemical solar cells. Electron transfer between iodide ions and ruthenium polypyridyl complex anchored on nanocrystalline SiO_2 and SnO_2 films," *The Journal of Physical Chemistry B*, vol. 102, no. 25, pp. 4944–4951, 1998.

[88] N. Papageorgiou, P. Liska, A. Kay, and M. Grätzel, "Mediator transport in multilayer nanocrystalline photoelectrochemical cell configurations," *Journal of the Electrochemical Society*, vol. 146, no. 3, p. 898, 1999.

[89] N. Epstein, "On tortuosity and the tortuosity factor in flow and diffusion through porous media," *Chemical Engineering Science*, vol. 44, no. 3, pp. 777–779, 1989.

[90] F. J. Valdés-Parada, M. L. Porter, and B. D. Wood, "The role of tortuosity in upscaling," *Transport in Porous Media*, vol. 88, no. 1, pp. 1–30, 2010.

[91] L. Shen and Z. Chen, "Critical review of the impact of tortuosity on diffusion," *Chemical Engineering Science*, vol. 62, no. 14, pp. 3748–3755, 2007.

[92] M. Cieszko, "Description of anisotropic pore space structure of permeable materials based on Minkowski metric space," *Arch. Mech.*, vol. 61, no. 6, pp. 425–444, 2009.

[93] L. Pisani, "Simple expression for the tortuosity of porous media," *Transport in Porous Media*, vol. 88, pp. 193–203, 2011.

[94] K. P. Saripalli, R. J. Serne, P. D. Meyer, and B. P. McGrail, "Prediction of diffusion coefficients in porous media using tortuosity factors based on interfacial areas," *Ground Water*, vol. 40, no. 4, pp. 346–352, 2002.

[95] S. Khirevich, A. Holtzel, A. Daneyko, A. Seidel-Morgenstern, and U. Tallarek, "Structure-transport correlation for the diffusive tortuosity of bulk, monodisperse, random sphere packings," *Journal of Chromatography A*, vol. 1218, no. 37, pp. 6489–6497, 2011.

[96] F. Chen, R. Mourhatch, T. T. Tsotsis, and M. Sahimi, "Pore network model of transport and separation of binary gas mixtures in nanoporous membranes," *Journal of Membrane Science*, vol. 315, no. 1-2, pp. 48–57, 2008.

[97] S. V. Churakov and T. Gimmi, "Up-scaling of molecular diffusion coefficients in clays: A two-step approach," *The Journal of Physical Chemistry C*, vol. 115, no. 14, pp. 6703–6714, 2011.

[98] Z. Kebede and S.-E. Lindquist, "The obstructed diffusion of the I_3^- ion in mesoscopic TiO_2 membranes," *Solar Energy Materials and Solar Cells*, vol. 51, no. 3-4, pp. 291–303, 1998.

[99] D. Vargas-Florencia, T. Edvinsson, A. Hagfeldt, and I. Furo, "Pores in nanostructured TiO_2 films. size distribution and pore permeability," *Journal of Physical Chemistry C*, vol. 111, no. 21, pp. 7605–7611, 2007.

[100] N. Papageorgiou, C. Barbé, and M. Grätzel, "Morphology and adsorbate dependence of ionic transport in dye sensitized mesoporous TiO_2 films," *The Journal of Physical Chemistry B*, vol. 102, no. 21, pp. 4156–4164, 1998.

[101] F. Fabregat-Santiago, J. Bisquert, E. Palomares, L. Otero, D. Kuang, S. M. Zakeeruddin, and M. Gratzel, "Correlation between photovoltaic performance and impedance spectroscopy of dye-sensitized solar cells based on ionic liquids," *Journal of Physical Chemistry C*, vol. 111, no. 17, pp. 6550–6560, 2007.

[102] A. Sasahara, C. L. Pang, and H. Onishi, "STM Observation of a ruthenium dye adsorbed on a $TiO_2(110)$ surface," *The Journal of Physical Chemistry B*, vol. 110, no. 10, pp. 4751–4755, 2006.